EXPLICIT FINITE ELEMENT ANALYSIS OF WEB-ROLLER INTERACTION IN WEB PROCESS MACHINERY

By

SIDDHARTH S. VAIJAPURKAR

Bachelor of Civil Engineering
University of Pune
Pune, India
2003

Master of Technology in Structural Engineering
National Institute of Technology
Surat, India
2005

Submitted to the Faculty of the
Graduate College of the
Oklahoma State University
in partial fulfillment of
the requirements for
the Degree of
DOCTOR OF PHILOSOPHY
May, 2013

EXPLICIT FINITE ELEMENT ANALYSIS OF

WEB-ROLLER INTERACTION IN WEB

PROCESS MACHINERY

Dissertation Approved:

Dr. J. K. Good

Dissertation Adviser

Dr. Jay C. Hanan

Dr. Raman P. Singh

Dr. Bruce W. Russell

Outside Committee Member

ACKNOWLEDGEMENTS

With a great sense of gratitude I take this opportunity to thank all those who helped me in accomplishing this dream called ‘Ph D’ for which I came to the United States. During my time here, many people have inspired me through their ideas, assistance and support for which I am obliged.

First and foremost, I offer humble appreciation to my advisor Dr. J. K. Good for allowing me to be a part of his research group and introducing me to the world of Web Mechanics and the Finite Elements. His tremendous faith in my abilities and unwavering support has guided me towards the scientific truth and excellence. He granted me a comfortable amount of freedom and his measured criticism has always been invaluable in my research endeavors. Over the past few years, I have realized how great a privilege it is to work under his magnificent command. His encouragement combined with the knowledge and experience in mechanics has led me towards successful completion of this work. The basis of this research work is mainly derived from the scholarly accomplishments of Dr. Good and the eminent members of his research group. I am indebted being in the company of such brilliant folks.

I convey sincere gratitude towards my committee members for their guidance, suggestions and help. During the courses which I studied from them, I got the opportunity to learn interesting Engineering. I would like to thank each committee member for their time and effort necessary to conduct exams required for this degree.

I would like to extend my appreciation to Mr. Ron Markum for his guidance during my lab-work. I also thank my team-mates and colleagues from WHRC for their friendship and for all the great discussions we have had. The support from sponsors of WHRC for their funding and help is greatly appreciated. IWEB conferences and IAB meetings have been a great opportunity to learn and interact with experienced researchers from the industry and institutes around the globe.

Of course, I must also thank all my friends here in Stillwater and around. I consider myself very lucky to have all these cheerful and caring folks in my life. You guys are the reason for my happiness.

For my beloved parents, Aai and Baba, dear brother Salil and my entire family I don't have enough words of gratitude. Throughout my life, they have never ceased to convey absolute confidence in my abilities and faith which encourages me in all my accomplishments. Though I will try to live up to their expectations, I hope this work serves as a small token of my appreciation towards their generous love for me.

Name: SIDDHARTH SHRIRAM VAIJAPURKAR

Date of Degree: MAY, 2013

Title of Study: EXPLICIT FINITE ELEMENT ANALYSIS OF WEB-ROLLER INTERACTION IN WEB PROCESS MACHINERY

Major Field: MECHANICAL AND AEROSPACE ENGINEERING

Abstract: A *web* can be defined as thin material manufactured and processed in continuous flexible strip form. A web is usually supported, guided and propelled by rollers. In order to make it travel through the process machine line, sufficient external machine direction force and velocity must be applied to web. The work presented here studies the mechanics and associated instabilities of webs running over the rollers which are not perfectly cylindrical in shape. Lateral and longitudinal behavior of web on concave, crown and tapered roller is studied. The exact boundary conditions are established. Several roller geometries, web materials and webline conditions are modeled using explicit finite element method for analyzing web-roller interaction. Instabilities in the form of troughs and wrinkles induced as a result of imperfection such as roller crown and taper are also studied. The simulation results are compared with available closed form solutions and experiments documented by previous researchers. A satisfactory agreement is observed for deflection, stress and overall behavior of web on such contoured (non cylindrical) rollers. This study revealed that normal entry condition is valid at the entry of web to a contoured roller. It is also found that web does not slip over its wrap on roller surface till the very exit from roller surface. These findings were then used to formulate computer code that predicts web behavior quite satisfactorily utilizing very few computational resources and time.

TABLE OF CONTENTS

Chapter Page

I. INTRODUCTION 1

II. LITERATURE REVIEW 7

2.1 Lateral Mechanics / Dynamics of Web 7
2.2 Web Instability and Wrinkling 15
2.3 Shear and Moment Interaction in Web Spans 17
2.4 Web Encountering Contoured Rollers 19
2.5 Summary of Current State of Knowledge 24
2.6 Research Objective 27

III. FINITE ELEMENT OF WEBS IN TRANSIT THROUGH WEB PROCESS MACHINERY 28

3.1 Explicit Finite Element Analysis 29
3.2 General Setup and Aspects of Explicit Modeling 32
3.2.1 Contact Formulation 33
3.2.3 Resolving Excessive Overclosures 34
3.3 Computational Cost and Accuracy 35
3.4 Elements in ABAQUS® 37
3.4.1 Shell Elements 37
3.4.2 Membrane Elements 38

IV. ANALYSIS OF WEBS APPROACHING MISALIGNED ROLLER 40

4.1 Webs Approaching Misaligned Roller 41
4.2 Experimental Procedure and Simulation 44
4.2.1 Convergence Analysis 45
4.3 Results and Discussion 47

Chapter Page

V. FINITE ELEMENT ANALYSIS OF WEBS ON CONCAVE ROLLER.....52

5.1 Spreading of Web by Concave Roller 53
5.2 Finite Element Modeling and Simulation of Narrow Web.....56
5.2.1 Convergence Analysis 58
5.2.2 Narrow Web Model Results and Discussion 60
5.2.3 MD and CMD Stresses in Narrow Web 62
5.2.4 Study of Negative CMD Stresses and Troughs in Exit Span.....67
5.2.5 Friction and Slippage on Roller Surface.....70
5.3 Finite Element Modeling and Simulation of Wide Webs.....73
5.3.1 Wide Web Model.....73
5.3.2 Wide Web Model Results and Discussion.....76
5.3.3 Study of Boundary Conditions.....77
5.4 Development of Static Model for Webs on Concave Roller 80
5.4.1 Web Coupon with Parabolic End-Loading due to Concave Roller 80
5.4.2 Results of Static Analysis of Web Entering Concave Roller.....84

VI. FINITE ELEMENT ANALYSIS OF WEBS ON CROWNED ROLLER 87

6.1 Web Behavior on Crowned Roller.....89
6.1.1 Strain Energy Method for Analysis of Webs on Crowned Roller 90
6.1.2 Matrix Structural Analysis of Webs on Crowned Roller.....91
6.2 Modeling of Adjustable Crowned Roller.....96
6.2.1 Trough Formation due to Roller Crown 97
6.2.2 Mesh Convergence Study 99
6.3 Trough Model Results and Discussion 106
6.4 Wrinkles due to Roller Crown 112
6.4.1 Modeling Wrinkle on Crowned Roller 113
6.5 Static Analysis of Web Instabilities due to Crowned Roller 118
6.5.1 Parabolic Loading at the end of Static Coupon 118
6.5.2 Prediction of Troughs using Static Crowned Roller Model.....121
6.5.3 Prediction of Wrinkles using Static Crowned Roller Model 123

VII. ANALYSIS OF WEBS ON TAPERED ROLLER.....127

7.1 Theory and Experimentation of Webs on Tapered Roller 128
7.2 Modeling of Tapered Rollers 133
7.3 Lateral Behavior of Web on Tapered Roller.....135
7.4 Troughs due to Roller Taper 139

Chapter Page

VIII. CONCLUSION AND REMARKS 141

8.1 Web Behavior on Concave Roller 142
8.2 Web Behavior due to Roller Crown.....144
8.3 Web Approaching a Tapered Roller 146
8.4 Recommendation for Future Study 147

BIBLIOGRAPHY 148

APPENDICES 152

LIST OF TABLES

Table Page

4.1 Misaligned Roller Experiment and Simulation Parameters....44
4.2 Computational Details of 0.006 Rad Misaligned Roller Model....46

5.1 Geometrical Properties of Concave Rollers....57
5.2 Concave Roller Model Parameter Values for Narrow Webs....58
5.3 Computational Details for ρ = 800" Concave Roller Model....59
5.4 Concave Roller Model Parameter Values for Wide Webs....74

6.1 Parameter Values of Trough Formation Model for Adjustable Crown Roller...99
6.2 Computational Details of Shell Elements in Crowned Roller Model....102

7.1 Tapered Roller Model Parameter Values....133

LIST OF FIGURES

Figure Page

1.1 Assumed Boundary Conditions for Web–Misaligned Roller Interaction.....2
1.2 Interaction of Web and Contoured Roller: Boundary Conditions 4

2.1 General setup of Roller and Web Arrangement with Tram Error (θj).....9

4.1 Web on Downstream Misaligned Roller: Moment Interaction.....41
4.2 Boundary Conditions of Web on Downstream Misaligned Roller.....43
4.3 Convergence Study for Lateral Deformation (v_j) on Misaligned Roller 46
4.4 Comparison of Lateral Behavior of Web on Misaligned Roller.....47
4.5 Slope of Web (θ_j) at Entry of Downstream Roller (*R3*) 49
4.6 Slope of web (θ_i) at Exit of Upstream Roller (*R2*) 50

5.1 Nominal Geometry and Configuration of Concave Roller.....53
5.2 Spreading Mechanism of Concave Roller by Classical Theories.....54
5.3 Narrow Web Model and MD Stress in Web on Concave Roller.....56
5.4 Amplitude Variation for Boundary Conditions of Narrow Web Model.....58
5.5 Convergence Study for MD Stress in Web on Concave Roller.....60
5.6 MD Stress Induced by Concave Roller of Varying Curvature Radius 61
5.7 MD Stress as a Function of Curvature at Entry and Exit of Roller 63
5.8 MD Stresses on Edge and Center of Web Transiting a Concave Roller 64
5.9 CMD Stresses on Edge and Center of Web Transiting a Concave Roller.....66
5.10 CMD Stresses across the Width of Concave Roller 68
5.11 Trough Formation due to CMD Surface Stresses for Concave Roller 70
5.12 Slippage of Web Edge on Concave Roller 71
5.13 Amplitude Variation for Boundary Condition of Wide Webs.....74
5.14 Convergence of MD and CMD Stresses in Wide Webs.....75
5.15 Stresses in Wide Web at Entry- Exit of Roller and Entry-Exit Spans.....76
5.16 Comparison of Slope of Lateral Deformation of Wide Webs 78
5.17 Web Approaching a Concave Roller: Static Analysis 80
5.18 Discrepancies in Web Coupon Study of Concave Roller Analysis 81
5.19 Actual and Proposed Closed Form Shear force Stress Distribution 82
5.20 Flowchart for Static Code of Web on a Concave Roller 84
5.21 Web Approaching a Concave Roller: Enforcing Normal Entry 84
5.22 Static Analysis results for L 18” T 6 lb case.....85
5.23 Comparative Study of MD and CMD Stresses.....86

Figure Page

6.1 Nominal Geometry and Configuration of Crowned roller.....89
6.2 Rectangular Plate Subjected to Parabolic Edge Loading 90
6.3 Crowned Roller as a Web-Gathering Device.....92
6.4 Mathematical Conversions of Adjustable Crowned Roller Profiles.....96
6.5 Beisel's Crowned Roller Data for Troughs Generated due to Roller Crown 97
6.6 Crown Roller Model Setup and Trough Formation in Entering Span.....98
6.7 MD Stress and Out of Plane Deformation of Web: Membrane Elements.....100
6.8 MD Stress and Out of Plane Deformation of Web *Shell* Elements 102
6.9 Convergence of MD Stress and CMD Deformation on Crowned Roller.....103
6.10 MD and CMD Stress Convergence through Execution Time 104
6.11 Comparison of MD Stress at Entry and Exit of Crowned Roller 105
6.12 CMD Stress in Web Crowned Roller at Various Tension Levels 107
6.13 Out of Plane Deformation of Web for 800psi Profile.....109
6.14 Out of Plane Deformation of Web for 900psi Profile.....109
6.15 Out of Plane Deformation for Various Tension and Pressure Levels 110
6.16 Troughs Generated at various Roller Crowns and Webline Tensions.....111
6.17 Beisel's Crowned Roller Data: Wrinkles Generated due to Roller Crown 113
6.18 Negative CMD Stresses on Crowned Roller for different Web Tension.....115
6.19 Prediction of Critical Stress to form a Wrinkle on Crowned Roller.....116
6.20 Prediction of Wrinkle for Webline Conditions and Roller Crown 117
6.21 Web Approaching a Crowned Roller: Static Analysis 118
6.22 Static Analysis Results of Web on Crowned Roller: L 20in T 20 lb.....120
6.23 Flowchart of Static Analysis of web on Crowned Roller 121
6.24 Troughs generated on Crowned Roller 123
6.25 Boundary Conditions and Loading for Wrinkling due to Roller Crown 124
6.26 Critical CMD Stresses in Wrinkling Model of Roller Crown 125
6.27 Wrinkles generated by Roller Crown 126

7.1 Tapered Roller Profile and Coordinates 128
7.2 Low Taper Roller Profiles from Beisel Plots and Abaqus.....134
7.3 Web Deflection due to Taper for various Web spans and Tension values 135
7.4 Web Deflection due to Taper for various Web spans and Tension values 136
7.5 Lateral Behavior of Web on 0.00075"/in Tapered Roller (L20in_T 20 lb) 137
7.6 Imitation of Beisel's Trough Test for (m= 0.00056"/in, L = 10").....139
7.7 Formation of Trough due to Tapered Roller, L = 10".....140

NOMENCLATURE

a_0	Parabolic roller profile coefficient *(in)*
a_1	Parabolic roller profile coefficient *(1/in)*
A_s	Shear area of web *(in^2)*
$A_{(t)}$	Amplitude at time *'t'*
$A_{(s)}$	Initial amplitude
$A_{(f)}$	Final amplitude
c	Depression at the roller center *(in)*
E	Machine direction modulus of elasticity *(Psi)*
G	Shear modulus *(Psi)*
h	Web thickness *(in)*
I	Moment of inertia *(in^4)*
L	Web span length *(in)*
L_a	Entering web span length *(in)*
L_b	Exiting web span length *(in)*
p	Contact pressure *(psi)*
r	Roller radius *(in)*
R	Radius of cylindrical shell *(in)*
R_0	Average roller radius *(in)*
T	Web tension *(lb)*
u	Displacement *(in)*
$\mathring{u}$, $\ddot{u}$	Velocity*(ft/s)* and acceleration *(ft/s^2)*
v	Lateral deflection *(in)*
V_{avg}	Average velocity of the web *(ft/s)*
$V_{(y)}$	Velocity of the web as a function of *y* location *(ft/s)*
W	Web width *(in)*

y	Distance from center of the web *(in)*
y_c	Distance from ½ web centroid in the cross machine direction *(in)*
δ	Deflection *(in)*
Δt	Stable time increment *(sec)*
$\varepsilon_{(y)}$	Strain as a function of y location
λ	Lame's constant
μ	Coefficient of friction
ϕ	Shear parameter
ρ	Equivalent radius of curvature *(in)*
σ_{cr}	Stress required to buckle the web *(Psi)*
σ_{md}	Machine direction stress *(Psi)*
σ_{cmd}	Cross machine direction Stress *(Psi)*
σ_x	Stress in web due to tension *(Psi)*
θ	Roller misalignment *(rad)*
θ_{cr}	Critical roller misalignment *(rad)*
θ_{trough}	Misalignment required to develop trough *(rad)*
$\theta_{wrinkle}$	Misalignment required to develop wrinkle *(rad)*
v	Poisson's ratio
ω	Angular velocity of the roller *(rad/s)*

CHAPTER I

INTRODUCTION

An understanding of the static behavior of a web is necessary for realizing the dynamics of web transit. Determining the boundary conditions associated with the static analysis of webs is the foundation for determining the boundary conditions with the dynamics of webs. To date, there have been several theories presented on modeling the behavior of web on rollers in web handling. The basics of web handling are explained in Appendix A. All of these theories rely on the elementary beam theory and its assumptions for their basic analysis. Successful results from these theories rely on the assumption of correct boundary conditions. These boundary conditions may be kinematic such as the normal entry law, kinetic boundary conditions such as no slip of the web on the roller or yet other conditions such as Brown's conservation of mass and normal strain rule.

Shelton [35] successfully modeled the case of web steering effects due to a misaligned downstream roller. He derived the boundary conditions for his analysis considering web as a cantilever beam system supported on rollers. According to him boundary conditions for this problem are:

$$\theta_i = 0, \;\; v_i = 0 \text{ and } \theta_j = \theta_{Misaligned\_roller}$$

Further, a fourth boundary condition is that the moment just upstream of misaligned roller, $M_j = 0$. This was based on Shelton's experimentation on a versatile web guiding test machine. With the

help of experiments measuring the raceway angle and slider displacement on a roller, he proved that under steady state conditions, moment in the web just before its entry to misaligned roller is zero. Shelton further discussed the concept of normal entry of a web to a roller that he first attributed to Lorig [23]. An earlier reference from Swift [41] is also found where he mentions the concept of normal entry of belt (web) to a pulley (roller). Fu *et al*[10] and Good [12] demonstrated that the assumptions made for the analysis of single span web systems may not be valid while analyzing multiple span web systems. A simple example for this would be that the cantilever support assumed by Shelton at the upstream roller in a single span would require infinite friction between the web and the upstream roller, at the exit of upstream roller. Since the infinite friction is not possible, web is bound to slip over the roller which was never accounted.

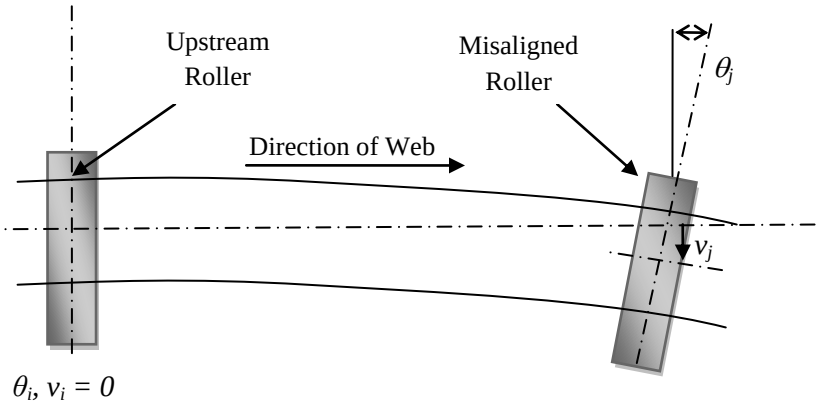

Figure 1.1 Assumed Boundary Conditions for Web – Roller Interaction

Beisel [1] succeeded in modeling the lateral deformations of webs approaching tapered and misaligned rollers and several other conditions. While studying boundary conditions, Beisel keeps the location of web entry to the span with a downstream tapered roller constant. This leads to the first boundary condition $v_i = 0$. Here, v_i is arbitrarily set to zero without affecting the relative lateral displacements of the web that may be due to misaligned rollers, tapered rollers, or other disturbances in upstream spans. Beisel's work attempts to account for shear deformation in addition to bending deformations in web. So the total deformation becomes $v = v_b + v_s$ and the

slope now has two components $\frac{dv}{dx} = \frac{dv_b}{dx} + \frac{dv_s}{dx}$. Hence for the tapered roller, the boundary conditions can be stated as follows:

$$v_i = 0 \qquad \ldots \text{Arbitrary}$$

We assume that the friction between the web and roller is sufficient to prevent any bending deformation of the web and thus, $\left.\frac{dv_b}{dx}\right|_{x=i} = 0$. However the slope $\left.\frac{dv_s}{dx}\right|_{x=i}$ is the shear strain becomes non-zero immediately as the web enters the span. This is due to the shear induced by the tapered roller, which is equal to f_{yj}, the member end force. Thus we can write:

$$\theta_i = \underbrace{\left.\frac{dv_b}{dx}\right|_{x=i}}_{0} + \left.\frac{dv_s}{dx}\right|_{x=i} = \frac{f_{yj}}{GA_s} = \gamma$$

where G is Shear Modulus and A_s is the area reacting shear, i.e. $A_s = (5A/6) = (5\ t.W/6)$. At the downstream roller *j*,

$$\theta_j = \left.\frac{dv}{dx}\right|_{x=j} = \left.\frac{dv_b}{dx}\right|_{x=j} + \left.\frac{dv_s}{dx}\right|_{x=j} = 0$$

This is due to the low of normal entry. The deformations and slopes defined as degrees of freedom have both bending and shear contribution. The fourth boundary condition is derived assuming that the web achieves a matching velocity to that of the tapered roller at the tangent entry point. Since the tapered roller has a linear variation in tangential velocity over its width we assume the web now has that same velocity variation. This results in a linear variation in strain and MD stress across the web width and results in a moment boundary condition for the web as

$$M_j = \frac{mE_{MD}tW^3}{12R_o}$$

where m is the slope that defines the taper of the roller and R_o is the nominal roller radius at the CMD center of the roller. With four boundary conditions described, elementary beam theory can be applied and the lateral deformation of the web can be determined for all points in the web span.

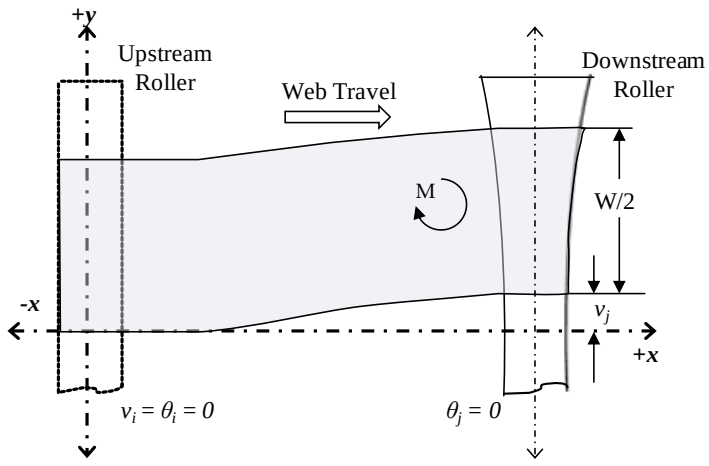

Figure 1.2 Interaction of Web and Contoured Roller: Boundary Conditions

For the analysis of web on a contoured roller such as a concave or crowned roller surface also, the web is treated as a beam. Since the web and roller are assumed symmetrical about the longitudinal center line of web, only one half of the width of the web is considered as shown in Figure 1.2. The coordinate system could be assumed originated at the center of upstream roller extending x axis in the direction of web travel. As per the previous attempts of modeling webs as a beam, the web exit at the upstream roller is regarded fix point giving the first condition as $v_i = 0$. The no slip boundary condition between roller and the web imparts sufficient friction so the web exits upstream roller with zero slope and hence $\theta_i = 0$. Given sufficient friction, the web material will be oriented normal to the downstream contoured roller at the initial point of contact

with the roller, providing $\theta_j = 0$. Further, the Moment boundary conditions could be established as $M_j = \Sigma \sigma_{md}.y.dA$.

Though above boundary conditions and analysis will help understanding behavior of half web width over contoured rollers, the exact conditions and mechanics of centered web on a concave or crowned roller is still unknown. Though Swanson [40] and Markum *et al* [25] have given theories on spreading devices, the literature is in dearth of the web behavior on a concave roller. We still do not have closed form solutions that will dictate the ability of centered web to be spread by a spreader. We still lack guidelines that link the spreading of web with roller concavity and other webline parameters such as material properties and span lengths. Similarly, the amount of crown required to destabilize given web in terms of trough and wrinkle is also unknown.

In the above cases considered there is a basic assumption that webs are homogeneous and uniform. These theories also rely on the premise that a web can be modeled as a beam and plane sections of web would remain plane before and after deformation and bending. These assumptions are never ultimately correct but are often partly true. Instability is a common phenomenon in transported webs. The thickness of the web is typically small and thus only small compressive stresses are required to induce instability in web spans. After instability occurs a cross section of the deformed web may no longer be planar. The boundary conditions for webs encountering rollers of different profiles (than a plane cylinder of uniform section) or for non-uniform webs encountering aligned and misaligned cylindrical rollers are yet to be explored.

The analyses presented in this study have employed the explicit finite element method for solving problems of webs encountering misaligned, contoured and tapered rollers. It can efficiently solve both transient and quasi-static problems. The contact algorithms are capable of modeling the friction forces between web and rollers and determining when stick or slip will occur. No direct boundary conditions will be set in these analyses that will affect the web

behavior in the given test span. The web velocity and tension at the web ends, the web/roller friction coefficient, and the web elastic properties are the only conditions prescribed. If the traction between a web and roller is sufficient normal entry may be observable in the output. When stick and slip occurs between the web and a roller will be governed by Coulomb's Friction Model. The web properties and roller geometries are set to represent cases that have been reported in the literature. One of the advantages of these codes is that they allow us to explore boundary conditions associated with the cases such as contoured rollers where boundary conditions are currently unknown. The suitability of explicit finite element pertaining to web handling has been shown in the reports [46] and publications such as [48] , [10]. Kandadai and Good [19] have already successfully analyzed problems of wound rolls using this method.

CHAPTER II

LITERATURE REVIEW

2.1 Lateral Mechanics/Dynamics of Web

The origin of studies about interaction between webs and rollers can be traced back to the steering of drive belts on pulleys. The need of power transmission in various capabilities during time of industrial revolution was one of the main reasons to study basic principles of Belt-Pulley interaction. Various classical references were studied by this author to trace the origin of such analysis. The oldest mention was found in the 1896 book authored by Robinson [32] where he notes the tendency of a belt to rise towards the crown of pulley. He considers the edgewise stiffness variation in the belt due to crown as the responsible factor of the centering action. He further suggests applying this knowledge to carry *narrow* belts at an angle to avoid any obstacle in the path of belt. He does not give any guidelines for amount of crown and angle. He further suggests the use of a crowned pulley as a guide-pulley to provide turns to belt.

Another book [33] was published by Schwamb, Merrill and James in 1921, where they talk about various mechanisms used in industries. In the chapter on belt, ropes and chains they give a detailed description of crowned pulleys and its centering action for the belt. This is probably the first time a fundamental principle governing running of all belts was given. It states that a plane through the center of the receiving pulley, perpendicular to the pulley axis must

include the delivering point of the pulley from which the belt is running. Though they specifically do not mention *normal entry*, it inclines towards it. Moreover, they give preliminary guidelines on pulley crown based on the width of pulley. They describe two different types of crown, and various configurations of belt-pulley systems for various industrial needs. The case of shafts not being parallel is also considered where they seem to understand belt-pulley interaction for misaligned pulley system.

'The belt must be delivered from each pulley in the plane of pulley on to which it is running' is given in the 1909 book on Machine Design by Unwin [45]. He also talks about the rounding of pulleys which is nothing but crown so as to center belt on pulley. He suggests that the problem of flat belt running off the pulley can be rectified by use of crown. He gives some guidelines on values of crown per the width of pulley.

Swift has authored some significant publications where he successfully formulated the fundamentals of power transmission by belts and pulleys. His 1928 paper [42] mainly deals with investigation of fundamentals of power transmission. He investigated effects of factors such as creep and slip, Tension variation, material of belts on power transmission. He supported his work by experiments carried out in lab.

Swift also authored a very important paper [41] in 1932 where he explained the centering action of a crowned pulley for belts for the first time. This is probably the first ever evidence of introducing the most important concept of *Normal Entry*. He states that given it is in steady state of velocity, the belt over the pulley must enter the pulley perpendicular to its axis of rotation. He studied various geometrical imperfections in drive and pulley system such as oblique and twisted drives, crooked belts and staggered shafts carrying pulleys. He developed guidelines and templates for the amount of crown or taper required on the pulleys (*rollers*), to control the stresses induced in the belt (*web*). The effect of pulley camber on belt was also studied. He also

gave various closed form expressions for moment developed in the belt due to crown or taper of pulley. He gave experimental results to support the corrections he suggested.

Lorig [23] in 1950 discussed steering action of webs on cylindrical, convex, concave and jointed rollers. Though he was unable to deduce any closed form solutions or models, he seems to have correctly understood the lateral behavior of belt (web). His work does not include quantitative analysis and explanation of boundary conditions used. The effect of degree of curvature on web-roller interaction is not discussed in the light of parameter such as velocity.

Shelton [35] in his 1968 thesis, studied various cases of the lateral behavior of webs on rollers. This is perhaps the first attempt of modeling various aspects of web steering due to numerous forms of web guides. Shelton starts with listing of common forms of web guidance systems with their working details and principles. He summarizes the necessity for knowledge of the lateral static and dynamic behavior of web. He then establishes a model for web deflection based on assumptions of the web being treated as a beam. He presented the boundary conditions of a web span encountering a downstream misaligned roller. He demonstrated that a moving web will align itself perpendicular to the axis of ration

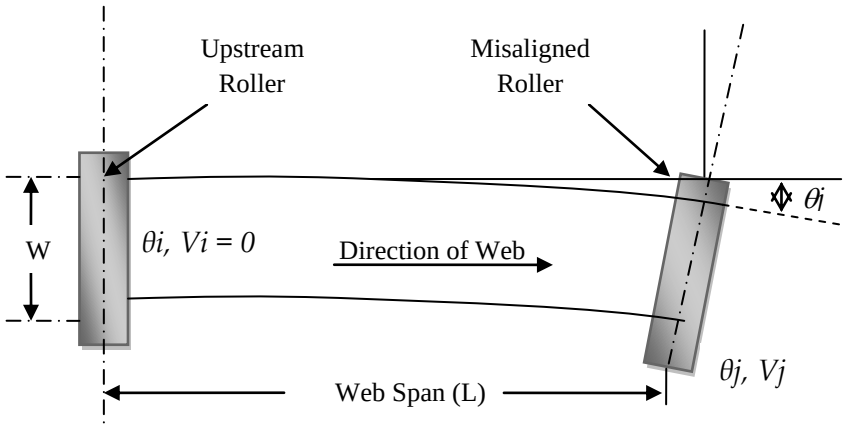

Figure 2.1 General Setup of Roller and Web Arrangement with Tram Error *θj*

of a given roller and uniformly distribute its tension across the web width immediately upstream to the roller. Shelton discussed the normal entry rule for web approaching a roller. The misalignment of downstream roller causes the web to enter normal to misaligned axis. The Moment in the entering span increases linearly from zero at the misaligned roller to the maximum value at upstream roller. With the help of experiments measuring the raceway angle and slider displacement on a roller, Shelton proved that under steady state conditions, moment in the web just before entering the misaligned roller is zero. He designed and built a versatile web guiding test machine. This machine went under several modifications and is still used at WHRC lab. While testing webs on his machine, Shelton also described experimentation went in deriving the material properties of various materials and coefficient of friction of various surfaces.

In 1971, Shelton authored two publications [36, 37] based on his thesis giving method for deriving approximate dynamic relations for lateral behavior of a moving web. He explained relations of lateral dynamics of a web at a downstream roller due to longitudinal web velocity, amount of misalignment, induced web curvature and web dynamics.

Shelton [34] in 1993 studied buckling of web due to generation of lateral compressive forces in free span. He compared experimental value of wavelengths of troughs and corrugations predicted with classical buckling theory given by Timoshenko. The simplified equation for wavelength of buckled web was given as:

$$\lambda = 1.95\sqrt{LT}\left(E/\sigma_x\right)^{1/4} \qquad (2.1)$$

He suggested expressions for lateral slippage on a roller and extended the theory he derived to explain lateral compression caused by change in tension across a roller, changes in temperature and moisture, viscoelastic memory, bending of a wound roll, and finally the roller deflection. Expression for maximum value of strain caused by roller deflection was also derived. Shelton suggested some ways to avoid wrinkles such as uniform tension and dimensionally stable web.

Good and Beisel [13], presented their work in 2003 IWEB, concerning troughs and wrinkles on *orthotropic webs* due to downstream misaligned roller. They modified the deflection equation for an orthotropic plate including membrane forces and derived concise expressions calculating half wave number *(n)* and CMD stress *(σ_{ycr})* required to buckle a web to form troughs:

$$n = b\sqrt{\frac{2}{\pi Lh}}\sqrt[4]{\frac{3(1-\nu_{xy}\nu_{yx})\sigma_{md}}{E_y}} \quad \text{and} \quad \sigma_{ycr} = \frac{\pi h}{\sqrt{3}L}\sqrt{\frac{\sigma_{md}E_y}{1-\nu_{xy}\nu_{yx}}} \qquad \textit{(2.3; 2.4)}$$

Then they altered constitutive expressions for buckling of cylindrical shell to derive half wave number and critical stress required to buckle an orthotropic cylinder to form a wrinkle on a roller as:

$$\frac{n\pi}{b} = \sqrt{\frac{2}{Rh}}\sqrt[4]{\frac{3E_x(1-\nu_{xy}\nu_{yx})}{E_y}} \quad \text{and}\, \sigma_{ycr} = \frac{h}{R}\sqrt{\frac{E_xE_y}{3(1-\nu_{xy}\nu_{yx})}} \qquad \textit{(2.5; 2.6)}$$

Starting with beam theory and stiffness matrix, the critical rotation required to induce a trough in given orthotropic web was derived. Then they verified the trough model with the help of numerous experiments considering wide range of span ratios, enabling them to see influences of both shear and tension stiffening. They concluded that the effect of shear stiffening is important in short span while tension effects were more critical in the longer spans. One of the important outcomes of this work is the fact that the web orthotropy has very little change in MD tension required to sustain a wrinkle upon a roller surface.

Webb, [49] in 2004 studied the relations between critical angle of roller misalignment for wrinkle formation and trough formation, for a large number of materials. He experimentally verified relation in lateral deflection due misalignment angle from an initially straight moving

web. When a cantilever beam is subjected to an end load, the lateral deformation is related to the end rotation by equation *(2.7)*.

$$v_j = \left(\frac{2}{3} \cdot L + \frac{2}{5} \cdot \frac{b^2 \cdot (1+\nu)}{L} \right) \cdot \theta_j \qquad (2.7)$$

This relationship was tested for a 92 gage polyester web with a span length of 18 in. When conducting experiments to measure θ_{trough} and $\theta_{wrinkle}$, the following procedure was performed. The downstream roller was adjusted so that there were no troughs present in the web span. The roller was then gradually misaligned until a trough first became visible. This misalignment angle was recorded. The roller was then misaligned until a wrinkle formed. Then the roller was misaligned the other direction and again both trough and wrinkle data were recorded. This cycle was performed three times so that an average could be obtained for each data point. Also, misaligning the downstream roller in both directions and averaging the results negated the effects of camber in the web. He found a linear relationship amongst these inputs. He developed a FE model in COSMOS® using membrane elements to help develop the understanding of this relation. One of the conclusions in his study 'width reduction in the web span due to trough formation is responsible for the compressive stress that develops in the web that wraps around the downstream roller and ultimately results in wrinkle' sounds a logical reason why troughs are predecessor of wrinkles.

Brown [4] suggested a new method for analyzing lateral behavior of web on rollers of various profiles such as misaligned, tapered, crowned, and concave. He founded his new method on two basic boundary conditions namely the normal entry rule and the other, which he presented for the first time was based on principle of conservation of mass. Based on this theory he compared his results with Shelton's model and test parameters by Markum and Good. He claimed that 'the controlling conditions at the entry of roller are fundamentally geometric with stresses

only controlling the relationship between strains that govern particle path and mass flow'. This paper lacks independent experimental verification of models so as to prove its worth. He uses partial differential equation solver to solve nonlinear plain stress equations, results of which are compared with models developed by others.

In 2006, Beisel in his PhD thesis [1] extensively studied troughs and wrinkles as a result of various roller defects such as misalignment, taper and roller curvature. He starts with modeling webs as beam element considering the deflection as a result of roller taper, and develops closed form solutions for shear force and deflection of web on these rollers. He then develops models predicting troughs and wrinkles as a result of roller misalignment. He then considers a unique case of misaligned-tapered roller. All these above models were verified experimentally in labs. FE modeling with computer codes was also studied. He designed a dynamically variable crowned roller to experiment webs encountering various geometries of crowned roller. He considered cases of orthotropic web properties over misaligned and tapered roller. For the first time the shear and tension effect was accommodated in the expressions calculating critical angle for troughs and wrinkles.

In 2006 Good and Beisel [14] presented their pioneered work of orthotropic web buckling due to roller misalignment in TAPPI® journal. They give acceptable levels of roller misalignment for give web material. They highlight the applications part of these theories stating the wide variety of industrial applications. They state the suitability of their models in various changed situations such as increase web-speed.

The Explicit Finite Element was used for the first time in studying web handling problems for analysis of wound rolls by Kandadai and Good [19], in 2007. They developed model for stresses developed in the center of wound rolls for both the cases of with and without a nip roller. They explained various aspects of modeling such as element library, material

constitutive behavior, surface interaction and contact modeling with commercial FE code, Abaqus®. The modeling techniques of amplitude rates, solution accuracy are also explained. The proportional relationship of Nip Induced Tension to that of friction between web layers and Nip load was given.

In 2009, Good *et al* [15] presented their work for the prediction of troughs and wrinkles in a web line. This paper is important for the study of web instability since it combines theory, experiments and FE modeling. It gave various expressions modeling the troughs in free spans due to instability caused by misaligned and tapered rollers. It was also followed by wrinkle analysis. They showed that existence of trough in free span is a necessary condition for wrinkle to form on roller. Non linear FE analysis was presented using the membrane element to model compressive CMD stresses due to roller imperfections. Expressions were given and verified by experiments for critical misalignment and taper for generating troughs and then wrinkles in web.

Explicit FE was used [47] to study problems due to roller misalignment in 2010. The web-roller geometries studied were exactly similar to the experimental setup by Webb [49]. Though previous analysis used various assumptions in terms of boundary conditions, the explicit analysis used has very few assumptions such as the web tension and velocity. It was shown that Explicit FE can produce results that compare well with literature and experiments for the case of roller misalignment. Various aspect of explicit finite element is also explained giving the procedural layout of the method.

2.2 Web Instability and Wrinkling

Gehlbach et al [11] in 1989 studied shear wrinkles in free web spans. Here they applied plate buckling theory to generate a model that predicts appearance of shear wrinkles in isotropic webs. They came up with basic equations for failure criteria used to indicate if troughing has occurred in web. A Closed form solution to determine the maximum shear stress which can be applied to the web prior to wrinkling $(\sigma_{y,cr})$ was computed. Expressions were then derived to relate this critical shear stress to degree of misalignment in the web line. The proposed model was then verified experimentally. Authors suggest two different approaches to be adopted while applying failure criteria based on whether moment transfer between the rollers is occurring or not.

In 1991, Gopal and Kedl [17] presented their work in first IWEB conference where they gave a finite element model that was claimed successful in prediction of troughs and shear wrinkles formation in plastic webs due to misalignment of downstream roller. They extended previous analysis of troughs by plate buckling theory to include slack web and troughs of various shapes other than sine wave. They tried modeling webs in two different software environments with different element types. The first approach was employing 2D membrane element in ANSYS®. Here, membrane elements did not have any capacity to resist compressive stresses. This approach was unsuccessful since exact shape of membrane after wrinkling was not definable. Unless the exact deformation was known, tram error was not predicted. Hence they concluded that 2D membrane element failed to predict wrinkles. In second approach, 3D triangular plate elements of ABAQUS® code were used to model web, allowing out of plane deformation. Analysis was carried out in two different phases. First being the application of tension in MD and the second, shear force depicting roller with tram error and out of plane deformation. The formation of wrinkle was predicted by raising shear stress incrementally until instability is reached. They simulated web by agitating several random nodes in out of plane direction by the amount of web thickness. Then, shearing load was increased and displacements

were calculated for various tram errors. They have listed results of FE code experimental analysis and close form solutions in tabular form. Those results have a wide range of errors. The roller was not modeled, where wrinkles are actually formed on web.

In 1997, Good et al [16] applied the classical instability theory to web wrinkling. They designated Regime 1 wrinkles as independent of velocity and that of Regime 2 as velocity dependent. Authors suggest successful models starting with very basic buckling theories to predict half wave number *i* and critical stresses *(σ_{ycr})* in CMD causing wrinkle on the web. Then they modify expressions for second principal stresses to yield a critical rotation of the misaligned roller to generate regime 1 wrinkles in web, which is then verified experimentally.

$$\text{Critical Rotation } \theta_{cr} = \frac{6\tau_{cr} L^2}{Eb^2} \qquad (2.8)$$

$$\text{where } \tau_{cr} = \sqrt{\sigma_{ycr}{}^2 - \sigma_x \sigma_{ycr}} \qquad (2.9)$$

Then they recognize very important phenomena where wrinkles which were trying to form in the web spans, are seen to be disappearing as the web enters the roller as a function of absence of proper friction. Hence they develop a traction algorithm to calculate traction between web and roller as a function of air film thickness. Both theories about regime 1 and regime 2 wrinkles are elaborately supported by experimental work.

Jacques et al [18a] in 2007 conducted finite element simulations using Abaqus to study post buckled wrinkling of metal strips (webs) on continuous processing lines. Though they seem to recognize the phenomena of wrinkle formation on a crowned roller, they fall short in explaining reasons for wrinkles formation. They did not explain exactly when a buckle (trough) would convert into a wrinkle. Simulation results were not validated. General conclusions are drawn such as frictions being an important factor n wrinkling without quantifying the claim.

2.3 Shear and Moment Interaction in Web Spans

Good [12] in 1997 IWEB explained models predicting the shear in multiple web spans as a result of roller misalignment. He explains how shear can be affected by traction in web-roller interaction and web edge slackness. He uses the stiffness matrix developed by Przemieniecki to obtain moment shear and lateral deformations in second (span B) of multispan system with conditions of no moment transfer between spans and no slack edge formation. Then he modifies these expressions for moment transfer and slack edge. The taut web edge is modeled as tapered beam and expressions are derived for critical misalignment required to cause the tapered beam (web) to become slack. Good then verified these expressions by showing agreement with experiments carried on polyester webs.

Shelton [38] in 2005 revisited the case of interaction of two web spans with a misaligned downstream roller. He introduces velocity slippage ratio Ks to facilitate analysis. Then he forms different fourth order differential equations for two (entering and pre-entering) spans depending upon ratio (L/W) and simultaneously solves it with iterative methods. He compares the result of his theory with tests reported by Good [12]. Based on this study, he gives some suggestions and tolerable values to avoid problems due to misalignment.

The problem of moment interaction of webspans is extensively studied in [10] by Fu *et al.* This 2011 paper studies the much studied roller misalignment problem where the misalignment of the roller is increased so that it generates moments beyond the value the upstream roller could resist. This causes the moment to transfer in upstream span. The slippage at the upstream roller becomes large enough to transfer the lateral deformation of web in upstream span. The observations were verified on a test rig developed for experiment in lab. This paper uses explicit Finite Element for studying the simulations based on exactly same geometries that of the experiments and theories. The explicit FE has no assumptions in terms of boundary

conditions and hence the interaction is entirely governed by the roller and web friction. It was observed that though the assumption of normal entry is true, the normal exit is not exact. It was showed that the line of zero moment, which assumed at the entry of misaligned roller, exists after the web contacted roller. It was shown for the first time that non-contact method of studying web deformations, the LDVs can be successfully employed in web handling.

2.4 Webs Encountering Contoured Rollers

Credit of being the first to analyze behavior of web on contoured rollers goes to Swift [41]. In 1932, as discussed in earlier section, he was the first to discuss defects in web due to the geometric non-uniformity of rollers. He developed model treating web (belt) as a beam bent due to applied couple. He recognized that due to (web) tension, the strain profile of the belt conforms to the geometry of pulley. This strain profile gives the effect of spreading for concave roller and gathering for crowned. He gave expressions for the lateral rate of travel of belt across the pulley (while forming helices around pulley) when it enters the pulley at some angle.

Shelton [35], explained the principle of web transport based on the idea of idle arc as given by Swift. He is responsible for founding the base of web handling in his thesis, which is discussed earlier.

In 1977 Pfeiffer [27], discussed some elementary concepts about web handling with context of narrow and wide webs. Starting with the velocity ration, he explains the normal entry rule and slippage over ordinary rollers. He states that the narrow webs are not susceptible for stress generation in CMD due to roller profiles. He further explains behavior of wide webs such as web shear and diagonal straining, CMD web stiffening and air entrainment. He then talks about some applications of these concepts such as spreading action, slitting and misalignment. This paper is an introduction to web handling concepts and so, lacks some mathematical expressions and detail analysis of web behavior. One important conclusion is that the web behavior is more complex than mere intuitions.

Feiertag [9], in 1981 studied wrinkle prevention for paper and plastic webs on curved axis rollers. He developed initial mathematical model for spreading of web on curved axis rollers. Then he used this model to develop recommendations for design to prevent wrinkle. His study was focused on bow magnitude and entry spans.

Butler [6] in 1985, wrote an article where he explained some applications of concave roller to fabric industry. He discussed how a concave roller can be used to remove 'bow' *(MD shifting of CMD fibers due to high web tension in fabric disrupting the design or texture)* from fabric. He gave some guidelines about ideal location of concave rollers in a web line, appropriate concavity.

Leport [22] in his MS thesis in 1987 studied the mechanics of concave roller using finite element method. He developed a FE model to investigate effects of spreading on entry and exit spans and on the roller surface. He compared various parameters of concave roller and linear taper profile roller. This work recommends experimentation verification and further work on accuracy of model suggested.

Leport's work was continued further by Kliewer [21] in 1988 as his MS thesis. He was successful to add new parameters such as strain redistribution to provide more flexibility to previous model. He then tried a range of FE runs of the model changing various parameters. He concludes 'increasing the radius of curvature, angle of wrap, web tension, and coefficient of friction induced increased spreading of the web. Conversely, increases in the modulus of elasticity, Poisson's ratio and thickness of web resulted in decrease in the spreading response.'

In 1993 IWEB, Delahoussaye and Good presented analysis of web encountering concave roller [7] and curved axis roller [8]. This work aims in studying the effects of variations in geometry, material properties and operating conditions on the spreading behavior of the system. They developed a FE model predicting elastic deformation and stresses in web crossing these types of rollers. They developed a pre-processor to compute material properties of web, roller geometry and boundary conditions. These outputs are then used for modeling purpose. They assumed that sufficient friction is present between web and roller to avoid slippage. This made the model to transform the displacement at the entrance of the roller till exit. There are very

interesting observations noted in this paper which are of specific importance for work of this study. One of the findings recorded is that MD stresses are greatest near edge of roller and smallest near center. They noted a surprising large region of compressive CD stresses in the exit span, which is very consistent to the findings of this work. They conclude with one surprising remark of requirement of high coefficient of friction to prevent slippage on roller.

Roisum [31] in 1993 studied mechanics of various types of spreaders such as bowed, concave, expanders and D-bars. In this paper, he first lists out elementary web handling principles related to traction and spreading. Then he explains behavior of various types of spreaders and rollers those can be used in a web line. This publication lacks in closed form solutions presenting analysis and experimental verification of study.

Stack *et al* [39], 1997 presented a nonlinear FE model for study of web behavior on straight, bowed in plane and bowed out of plane rollers (D bar). They start with explaining importance and suitability of Eulerian modeling technique over Lagrangian. They adopt the later technique since it gives user the freedom to adjust mesh density in a particular area in domain according to importance of location. Authors state that 'necking' is a result of Poisson's contraction and will cause spreading on straight bar. Then they demonstrate the ability of their model to predict changes in web behavior and stresses when one of the parameters like Poisson's ratio or coefficient of friction is altered. They conclude with results showing D-bar as most efficient spreader, friction being the most important factor. Experimental verification or support is not provided.

In 1997, Swanson [40] presented various cases of testing and analysis of ten spreading devices. He suggested simple models based on cantilever beam theory and belt equations followed by extensive experimental work. Aluminum roller was the standard by which all other rollers (such as outward/inward spiral grove, tape bumpers, reverse crown, curved axis etc) were

tested. All the spreading devices were checked on three different types of tests namely drag test, wrinkle regime test and slit test. His analysis approved and in some cases disproved commonly held beliefs about spreading devices. He found that only four of ten (tape bumpers, reverse crown, curved axis and expanding surface) rollers actually spread the web.

In 6th IWEB in 2001, Markum and Good [25] presented their work giving mathematical derivations to be used to calculate spreading ability of concave and 'bow tie' roller. They derived these equations treating web as beam and used classical matrix structural analysis. They derived strain of the web in terms of web velocity assuming that the web remains in traction with the roller and moves with the same velocity as that of roller.

$$\sigma_{md} = E\varepsilon_{md} \quad \text{Where} \quad \varepsilon_{md} = \frac{V_{(y)} - V_{avg}}{V_{avg}} \qquad \textit{(2.10; 2.11)}$$

The equation given for calculation of bending moment *($M_{centroid}$)* and lateral deformation *(v)* for concave roller are as follows:

$$M_{centroid} = \frac{Ea_1tW^4}{16(12a_0 + a_1W^2)} \text{ and } v = \frac{5a_1EL^2tW^4}{(12a_0 + a_1W^2)(4L^2T + 5EtW^3)} \qquad \textit{(2.12; 2.13)}$$

Authors then derived equations representing sufficient web tension so as to ensure the web remain in contact with roller surface. This gives an engineer the ability to design concave rollers for specific amount of slackness to be removed and vice-versa. They supported their work by extensive experiments on both the devices where they tested theories by comparing amount of separation generated by spreader on a slit web. This deflection is then used to validate results of shear force given by closed form solutions.

Brown [4] presented a new method for analysis of concave and curved axis rollers in 2005. He, with normal entry rule introduced additional boundary condition called normal strain

rule. He compared results obtained by his theory for two different types of rollers. He developed a new beam theory model for cambered webs. Validation of these theories with independent experiments is not considered.

Markum and Good [26] in 2007 studied mechanics of flexible grooved spreader rolls and determined the principle these devices employ spreading. They explained the three basic rules by which spreading occurs namely normal entry, sliding and moment induction. Then they studied the flexible grooved rollers with detailed experimental analysis and developed closed form solutions for lateral deformation of web on these rollers. They found that the normal entry rule is the base of spreading in this case. FE model and guidelines about installation of grooved spreaders was also presented. They studied effect of various aspects of grooved rollers such as the slope and rotation of rubber lands, wrap angle, web tension on spreading.

The explicit finite element method was used [48] to study the lateral mechanics and web behavior on concave rollers. It was shown that the concave roller is a local spreader that might induce troughs in exit spans. Several roller concavities, web widths, materials were presented. The cases studied by other researchers were also analyzed and results seem to be agreeing. Various new conclusions regarding the state of stress in web around a concave roller were made.

2.5 Summary of the Current State of Knowledge:

All the literature referred here exhibits the great deal of effort that has been expent by various authors and researchers so as to understand web behavior on rollers. The focus of the work on lateral mechanics/dynamics is important because the ability to be able to predict where a web is located laterally in a process machine is very important especially in printing and precision coating processes. We also see the efforts that have been expent to study web instability. Web instability must be minimized to maximize profits. Of the works on lateral mechanics and instability that focus on modeling, boundary conditions have been assumed. These boundary conditions may be kinematic such as the normal entry law or they can be kinetic such as Shelton's zero moment conditions just upstream of a misaligned roller. Other authors have claimed yet other boundary conditions such as Brown and his conservation of mass condition. Are there limits of applicability of these boundary conditions? Of course the answer is Yes, and evidence has been given for the case of the web approaching a misaligned roller in the papers on moment interaction by Good *et al* [16]. For low levels of misalignment of a roller, web moments may be confined to the span with the downstream misaligned roller. The boundary conditions for such a web include $v_i = 0$, $\theta_i = 0$ or $\theta_i = \frac{f_{yj}}{GA_s}$ (If shear deformation is included), the misalignment of the roller $\theta_j = \theta_c$ and $M_j = 0$

As soon as the roller is misaligned, θ_c has become non zero and a moment *Mi* is generated at the upstream roller. This moment will result in slippage of the web at the exit of upstream roller and hence $\theta_i \neq 0$! So we see that our disturbance θ_c is responsible for affecting θ_i which we were attempting to set to zero! Thus we cannot set one boundary condition (θ_c) without affecting the other boundary condition (θ_i). This is probably the simplest case of web behavior to attempt to model yet we see the complexity of the boundary conditions.

Contoured rollers have a profile other than cylinder as their surface. Two typical examples are Concave and Crowned roller. A concave roller also called as a *spreader*, will have depression at the center making its diameter smaller at center than edges. Crowned rollers have exactly opposite geometry than concave roller. Increased diameter at center gives it a profile raised at roller center compared to edges. Due to its geometry, crown roller will impart a compressive force on the web and hence is known as a *gatherer*. Both of these types of rollers are used for various purposes in web handling industry. Concave rollers can be solutions to various web handling problems that result from widthwise web contraction. Troughs, wrinkles and baggy lanes can be visual identifiers of such problems but in some cases like that of nonwovens the width reduction may be absorbed by the web but the loss of width may still be unacceptable. Concave rollers have been employed with various levels of success. Several sources such as [18, 24] warn that too much concavity should be avoided. They further provide guidelines for limiting the diameter variation. These limits are provided because the sources are aware that devices such as concave rollers are capable of creating web problems. Potential problems can include inducing nonuniform inelastic deformation in the web and lateral dynamic instability.

Crowned rollers are traditionally been used as a stabilizers. Though originated for the purpose of stabilizing the belt on a pulley in power transmission, they frequently are used in web handling industry. Unlike belts, webs are much thinner and have very less buckling resistance to compressive CMD stresses. Whenever a web is made to run over crowned roller, the crowned profile generates shear force in web resulting in compressive CMD stresses. If these compressive stresses pass beyond critical stress value σ_{ycr}, instabilities in the form of troughs and wrinkles may be generated in web. We do not have a closed form solution yet developed that will link the roller crown with webline parameters and web material properties. We lack a guideline as to how much roller crown could be tolerated by a certain webline and web material before troughing or even wrinkling.

The interaction between the web and the contoured rollers is not fully understood. Although the devices are useful, there is yet much to be explored about their working and design before they can be designed for particular applications. Experimentation is difficult since most accurate means of strain and stress measurement are interfering methods when applied to thin webs. Still though there is a great time and efforts spent on concave rollers, the literature lacks a robust design model that the engineer can use to specify the parameters or spreading or gathering of web due to these rollers.

2.6 Research Objective

The purpose of this effort is to qualify the following topics for final defense and dissertation:

To certify the method of explicit finite element through commercial codes such as Abaqus®, for analyzing web-roller interaction of misaligned and tapered roller cases already studied and experimented in the literature. After modeling these cases I will examine what boundary conditions exist.

To model the case of concave roller, where less is known concerning boundary conditions. To review the simulation output so as to determine if the normal entry rule is applicable. To examine the stresses and strains in the web in contact with the concave roller to determine if any kinetic boundary conditions apply in this case.

To model the cases from literature for both trough and wrinkle formation due to a downstream crowned roller. To inspect stress and strain output revealing the related boundary conditions at the web roller interaction.

Formulate computationally economical, fast and easy static code for the study and behavior of parameters related to contoured rollers based on the knowledge of boundary conditions from the explicit simulations.

CHAPTER III

FINITE ELEMENT OF WEBS IN TRANSIT THROUGH WEB PROCESS MACHINERY

The explicit method of analysis is based on the central difference approximation of time derivatives of displacements (i.e. velocity and acceleration). Taking constant time steps designated as Δt the central difference expressions for velocity and acceleration at time i are calculated. We use Explicit Finite Element for modeling of webs since it can efficiently solve both transient and quasi-static problems. The presented research involves transient solutions through time for the behavior of web travelling through web process machinery. Kandadai [19] have already successfully analyzed problems of wound rolls using Explicit FE method. In his PhD thesis, Kandadai [20] has explained basic concepts such as material constitutive behavior, interface modeling, contact formulation, loading rates & damping and other computational aspects of this technique pertaining to web handling problems. A brief overview of modeling process of the commercial FE code ABAQUS® is explained here. Additional topics are covered in this chapter so as to explain explicit finite element modeling of webs through process machines.

3.1 Explicit Finite Element Analysis

An explicit dynamic analysis is computationally efficient analysis tool which can analyze large models with relatively short dynamic response times and extremely discontinuous processes. The explicit analysis is computationally inexpensive because there is no solution procedure involved for a set of simultaneous equations. The method can be computationally expensive because the time increment must be chosen to be small enough to yield a stable solution. The explicit central-difference operator satisfies the dynamic equilibrium equations at the beginning of the increment *t;* the accelerations calculated at time *t* are used to advance the velocity solution to time $(t + \Delta t/2)$ and the displacement solution to time $(t + \Delta t)$.

Explicit analysis is suitable to study webs in transit in web process machinery because of the greater ease with which it resolves complicated contact problems. It explicitly advances the kinematic state from the previous increment. Even though it requires larger number of increments, the analysis is more efficient than standard methods. Explicit methods consume fewer system resources for large-scale models as compared to implicit methods. ABAQUS/Explicit integrates the equations of motion explicitly through time, using the kinematic conditions at one increment to calculate the kinematic conditions at the next increment. At the beginning of the increment the program solves for dynamic equilibrium, which states that the nodal mass matrix ***M***, times the nodal accelerations $\ddot{\boldsymbol{u}}$, equals the total nodal forces (the difference between the external applied force ***P***, and internal element forces, ***I***) which can be expressed as

$$M\ddot{u} = P - I \qquad (3.1)$$

The accelerations at the beginning of the current increment (time t) are given as

$$\ddot{u}\big|_{(t)} = (M)^{-1}.(P - I)\big|_{(t)} \qquad (3.2)$$

Since the explicit procedure always uses a diagonal or lumped mass matrix, there are no simultaneous equations to solve. The acceleration at any node is determined by its mass and the net force acting on it. This makes the nodal calculations very fast and economical in terms of computational cost. The accelerations are integrated through time using the central difference rule, which calculates the change in velocity assuming that the acceleration is constant. This change in velocity is added to the velocity from the middle of the previous increment to determine the velocities at the middle of the current increment as

$$\dot{u}\big|_{(t+\frac{\Delta t}{2})} = \dot{u}\big|_{(t-\frac{\Delta t}{2})} + \frac{(\Delta t\big|_{(t+\Delta t)} + \Delta t\big|_{(t)})}{2}\ddot{u}\big|_{(t)} \qquad (3.3)$$

The displacement at the end of the increment is determined by adding the velocities integrated through time to the displacement at the beginning of the increment.

$$u\big|_{(t+\Delta t)} = u\big|_{(t)} + \Delta t\big|_{(t+\Delta t)}\dot{u}\big|_{(t+\frac{\Delta t}{2})} \qquad (3.4)$$

This satisfies the dynamic equilibrium at the beginning of the increment, which leads to acceleration. Once the acceleration is calculated, velocities and displacements incremented through time. For this method to produce accurate results, time increments must be very small so that the accelerations are essentially constant during increment. The small time increments results in large number of steps, but it does not hurt the overall efficiency of the system since most of the computation expense lies in the calculation of internal forces acting on the elements. The element stresses and forces are calculated based on element strains and constitutive relationships. The steps of any explicit dynamic algorithm are given as follows:

1. Nodal calculations.

   a. Dynamic equilibrium. $\ddot{u}_{(t)} = M^{-1}(P_{(t)} - I_{(t)})$ *(3.5)*

   b. Integrate explicitly through time.

$$\dot{u}\big|_{(t+\frac{\Delta t}{2})} = \dot{u}\big|_{(t-\frac{\Delta t}{2})} + \frac{(\Delta t\big|_{(t+\Delta t)} + \Delta t\big|_{(t)})}{2}\ddot{u}\big|_{(t)} \qquad \text{...Velocity} \qquad (3.6)$$

$$u\big|_{(t+\Delta t)} = u\big|_{(t)} + \Delta t_{(t+\Delta t)}\dot{u}_{(t+\frac{\Delta t}{2})} \qquad \text{...Displacement} \qquad (3.7)$$

2. Element calculations.

   a. Compute element strain increments dε, from the strain rate $\dot{\varepsilon}$.

   b. Compute stresses from constitutive equations.

$$\sigma_{(t+\Delta t)} = f(\sigma_{(t)}, d\varepsilon) \qquad (3.8)$$

   c. Assemble nodal internal forces $I_{(t+\Delta t)}$

3. Set *(t + Δt)* to *t* and return to Step 1.

3.2 General Setup and Aspects of Explicit Modeling

The Finite Element method requires a complete description of the geometric and elastic properties of the system being modeled and the boundary conditions to be applied. Webs are modeled as isotropic materials in models. The actual in-plane moduli of material to be modeled were measured using the stretch test method in the lab. In a stretch test, a 50 ft sample of the web is stretched and the load versus deformation is recorded. The modulus is calculated from the slope of the stress-strain curve. Width-wise contraction and thinning of web material is governed by Poisson's ratio along principle axes. Static and kinetic coefficient of friction were measured by previous researchers through experiments as documented by Kandadai[20] and Reddy[29]. ABAQUS/Explicit® employs Coulomb's friction law to model surfaces with given friction-coefficient ($\boldsymbol{\mu}$) value. This law relates the maximum allowable frictional shear stress ($\boldsymbol{\tau_{crit}}$) across an interface to the contact pressure ($\mathbf{p_{(x)}}$) between the contacting bodies. This relation is given as

$$\tau_{crit} = \pm \mu p_{(x)} \qquad (3.9)$$

Since friction is involved, the contact status may be open ($\boldsymbol{p_{(x)} = 0}$), sticking ($\boldsymbol{\tau < \tau_{crit}}$) or slipping ($\boldsymbol{\tau \geq \tau_{crit}}$) depending upon the values of parameters explained before. The surface to surface contact phenomenon is handled by contact algorithms in Abaqus. These are divided into groups of general contact algorithms and contact-pair algorithms. The general contact algorithm imparts a very simple association of contact and has few limitations on types of surfaces involved. Whereas the contact pair algorithm has more restriction on types of surfaces and its association needs detailed definition of contact. The choice of suitable algorithm greatly depends upon nature, behavior and mechanics of the problem to be modeled. Considering requirement for contact formulation of web-roller interaction, the contact-pair algorithm was selected for modeling. The modeling consists of combinations of constraints, boundary conditions and loads. For better accuracy and efficiency, these constraints should be applied as slow as possible to

minimize transient effects. This was achieved by selecting various amplitude curves for each application. The details about calculating the amplitudes to ramp up desired boundary conditions and load are given for specific cases later.

3.2.1 Contact Formulation

The contact formulation in ABAQUS/Explicit includes constraint enforcement, surface weighting and sliding formation. Kinematic contact algorithm and Penalty contact algorithm are two types of constraint enforcement methods. By default, ABAQUS® enforces a predictor/corrector algorithm which is the Kinematic method. It has no effect on the stable time increment. In kinematic enforcement, during each increment the kinematic state is advanced into a predicted configuration without considering the contact conditions. It then determines which slave nodes in the predicted configuration penetrate the master surfaces. The depth of slave node's penetration, mass associated with it and the time increment are used to calculate resisting force required to oppose penetration. Further step is distribution of resisting forces and masses of all slave nodes to the nodes on master surface. These forces and masses are used to calculate acceleration correction for the master and further for slave surface nodes. The acceleration correction so calculated gives a corrected configuration for next increment. For the case where analytical rigid master surface is used, the resisting forces of all slave nodes are applied as generalized forces on the concerned rigid body.

The penalty contact algorithm has less precise enforcement of contact constraints compared to kinematic algorithm. It therefore has more freedom on types of surfaces used in contacting. This method introduces additional stiffness into model and so, might affect stable time increment value as explained in Δt calculations. The spring stiffness relating the contact force to the penetration distance is chosen automatically by ABAQUS/Explicit such that the effect on the time increment typically is an order of magnitude greater than the parent element's

elastic deformation normal to the surface. The default penalty stiffness values can be scaled with user defined factor. This scaling may affect automatic time incrementation. Use of larger factor might increase number of increments by reducing the Δt value. The Penalty contact algorithm has fewer restrictions and so can model types of contacts where kinematic algorithms fail.

3.2.2 Resolving Excessive Overclosures

The initial excessive overclosure that exists due to various reasons such as insufficient mesh density in a contact pair during initial steps are automatically adjusted in analysis. The adjustments are made with strain-free initial displacements to the slave nodes on the surfaces. Initial penetration is detected only when a slave node lies within the thickness of the underlying element and the initial penetration is resolved by moving the slave node to the nearest surface of element. If an adjustment of amount p_o is made for an initial overclosure, the penetration up to ε p_o could still exist in the first increment, where ε is 'machine epsilon' of the computer. The machine epsilon of a given computer is the smallest positive number that can be added to 1 with the computed result being greater than 1. For most common types of the systems ε is at least approximately 1×10^{-16} with double precision used in job module. With this kind of accuracy, the overclosure problems could be neglected. Above numbers strengthen the use of double precision and signify the level of geometrical precision that could be achieved with this analysis technique.

3.3 Computational Cost and Accuracy

The total computational time taken for running a simulation using explicit time integration with a given mesh is proportional to the time period of the event. The time increment is given by

$$\Delta t \leq \min\left(L_e \sqrt{\frac{\rho}{\lambda + 2\mu}} \right) \qquad (3.10)$$

Where, *Le* = Characteristic length of element, ρ = Material density, λ and μ are Lame's constants given by

$$\lambda = \frac{Ev}{(1+v)(1-2v)} \text{ and } \mu = \frac{E}{2(1+v)} \qquad (3.11)$$

The number of increments is $n = T / \Delta t$ and hence it can be approximated to previous expression as

$$n \approx T \max\left(\frac{1}{L_e} \sqrt{\frac{\lambda + 2\mu}{\rho}} \right) \qquad (3.12)$$

In a 2D analysis refining mesh by a factor of two in each direction will increase the run time in the explicit procedure by a factor of eight i.e. four times as many elements and half the original time increment size.

Reduction in computational cost can be achieved by artificially reducing the time required for the event *T*. It may involve some problems such as increased inertial forces or changed behavior of rate dependent materials. Another effective way is called 'Mass Scaling'. It is nothing but artificially increasing the material density, ρ by a factor f^2 reduces *n* to *n/f* reducing *T* to *T/f*. Mass scaling has exactly the same effect on inertia forces as speeding up the time of

simulation, but it is more suitable since it can be used in rate-dependent problems. It is very important to judge the limit to restrict values of mass scaling factor since increase of mass would result increase in inertia, density and might lead to ineffective modeling. Further reduction in number of time increments could be achieved by changing the smallest element dimension ($\boldsymbol{L_e}$). Since increase in element size can reduce accuracy affecting contact definition, a suitable value could be finalized by mesh convergence analysis.

3.4 Elements in ABAQUS®

The selection of appropriate element from a vast variety of element library available in ABAQUS is based on certain aspects such as type of structure to be modeled, degrees of freedom required, number of nodes necessary to model given problem per element, formulation and integration over element. Shell and Membrane elements are suitable to model structures such as webs where one dimension (the thickness) is significantly smaller than the other dimensions and in which the stresses in the thickness direction are negligible. Explicit analysis uses the Lagrangian analysis for description of behavior. This means the element will deform with the material. The other type of analysis is Eulerian where, the material 'flows' through elements that are fixed in space. Numerical techniques are used to integrate various quantities over the volume of each element following material behavior. Mostly ABAQUS uses Gaussian quadrature to calculate material response at each integration point in given element. There is a choice of full or reduced integration during analysis.

3.4.1 Shell Elements

Conventional shell elements were used to model the web since they have both displacement and rotational degrees of freedom. For the shell, thickness is defined as a shell section property unlike the Continuum elements where thickness is defined by nodal geometry. For shells the positive normal is given by the right-hand rule going around the nodes of element in the order that they are specified in the element definition. The top surface in positive normal direction is referred as positive face (SPOS) and bottom surface is negative face (SNEG). We use reduced integration for reducing computational time without losing accuracy of results. We can specify any odd number of section points through the shell thickness when the properties are integrated during the analysis. By default, Abaqus uses five section points through the thickness of a homogeneous shell, which is sufficient for most nonlinear design problems. Moreover, by

selecting the section integration during analysis we use numerical integration through thickness of shell to calculate section properties. This type of shell should be used for non-linear material behavior in the section. Finite-strain elements and small-strain elements are the two kinds of shell elements available for modeling. The former account for finite membrane strains and arbitrarily large rotations and therefore are used for large-strain analysis whereas the later is better for modeling small membrane strains and arbitrarily large rotation and so they are both good for large rotations. The transverse shear stiffness is computed by matching the shear response for the shell to that of a three-dimensional solid for the case of bending about one axis using the parabolic variation of transverse shear stress in each layer. The shell elements used in analysis for this study are S4R (4-node doubly curved general-purpose shell, reduced integration with hourglass control, finite membrane strains) elements.

3.4.2 Membrane Elements

The Membrane element library in Abaqus is limited compared to Shell elements. These elements are surface elements that transmit only in-plane forces and hence, no moments. As a result of this behavior they do not have bending stiffness. These elements are also suitable to model web behavior since they offer in-plane strength but have no bending stiffness. We use general purpose membrane since the deformation of the structure can evolve in three dimensions. The element normal definitions are very similar as explained before in shell. We use M3D4R (4-node quadrilateral, reduced integration, hourglass control) element for this study.

A comparison of results obtained by both, the membrane and shell element will be presented separately to show that both types of elements yield very similar results. The MD and CMD stress profiles show exactly the same behavior. The stress, strain, and other selected output variables for Shell elements are available at three section points through the depth of the element including the bottom and top surfaces and the mid-plane. A potential benefit of shell elements

over the membrane elements is that with 6 defined degrees of freedom per node the out-of-plane deformation within the domain of an element can be more complex than the membrane elements. The benefit lies in that the contact between the web and surfaces of complex geometry can be described with greater accuracy for a given mesh density. Membrane elements are computationally more economical than shells since they have fewer degrees of freedom per node to resolve.

CHAPTER IV

ANALYSIS OF WEBS APPROACHING MISALIGNED ROLLERS

Considerable amount of work is being done in the area of roller misalignment. We chose this problem to verify quality of ABAQUS® codes since the problem of roller misalignment is being studied very carefully and precisely by previous researchers as discussed earlier. In any web line, the web is guided by rollers which are placed with their axes parallel to each other in order to steer the web in MD. Many a times in web handling industry, the axes of rollers driving the web are not perfectly parallel to one another. A small misalignment of roller may cause development of instabilities such as troughs or wrinkles on the web which are a disaster in production. Roller alignment is a challenging and time consuming process. The web handling industry has a constant need for improved guidelines and tolerances of misalignment to prevent troughs and wrinkles.

4.1 Web Approaching Misaligned Roller

The web on a misaligned roller is modeled as a beam. The problem was first studied by Shelton [35] where he modeled web as a cantilever beam over rollers. Good *et al* [15] suggested successful models to predict trough and wrinkle on misaligned roller. They conducted experiments to verify their models and comparison is well documented. Good and Beisel [12] also developed closed form solutions including shear and tension effect for orthotropic webs. Webb has carried out experiments at WHRC and is documented in his MS thesis [49].

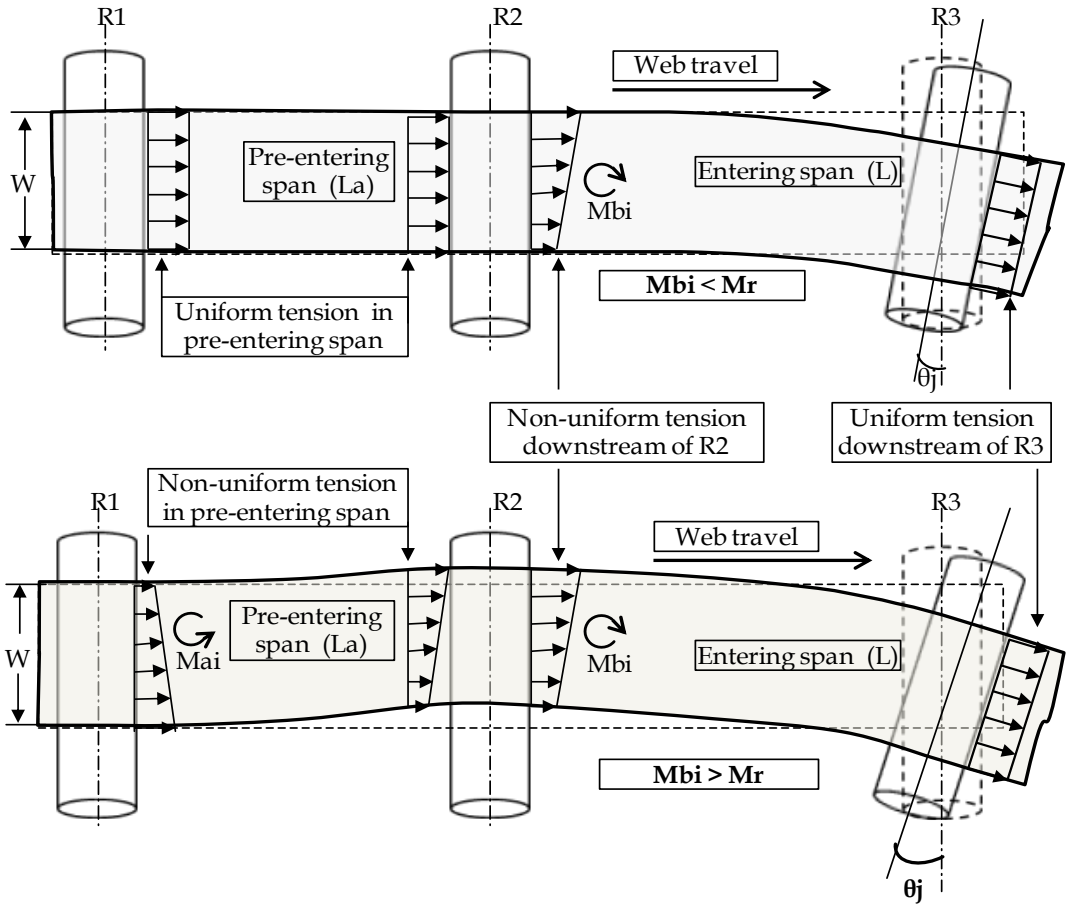

Figure 4.1 Web on Downstream Misaligned Roller: without (*top*) and with (*bottom*) Moment Interaction

The cases of roller misalignment considered here are chosen such that it does not involve *moment interaction*. Moment interaction occurs when the moment induced at the upstream roller because of the downstream roller misalignment exceeds the moment that could be resisted by friction between upstream roller and web. As shown in Figure 4.1, whenever the downstream roller *R3* is misaligned by θj a bending moment (M_{bi}) is generated in the entering span (L). This moment is highest at the exit of upstream roller *R2* and diminishes linearly to zero as it approaches *R3*. There is more moment generated at *R2* for increased misalignment of *R3*. This moment M_{bi} is to be reacted by friction μ_{R2} between *R2* roller-surface and web. For smaller values of misalignment, M_{bi} will be lesser than that could be reacted by μ_{R2}. There is a limit to the moment that could be sustained by μ_{R2} and is called *critical moment* M_r. This critical moment can be calculated by expressions given by Good [12]. Whenever there is a moment higher than M_r generated at *R2* the phenomena of moment interaction takes place where in the moment is transferred from entering span L into upstream pre-entering span L_a. This results in induction of moment (M_{ai}) and deformation (v_i) in pre-entering span. Moment interaction is studied in detail and is documented in [10]. It is a separate topic for research in itself and hence for the cases considered here, the levels of misaligning roller *R3* are confined so as to avoid moment interaction.

For the case of downstream misaligned roller, the boundary conditions used in previous analysis are as follows: The lateral deflection of web on upstream roller *R2* is set to zero giving fixed point of exit of web on *R2* as

$$v_i = 0 \qquad (4.1)$$

The slope of web at this upstream roller is given by

$$\theta i = \frac{f_{yj}}{GA_s} \qquad (4.2)$$

Where, f_{yj} is shear in a web span due to misaligned downstream roller, G is the shear modulus and As is the area reacting shear. Shelton [35] formulated third condition as the moment boundary condition giving the entry of downstream misaligned roller is zero and hence

$$M_j = 0 \tag{4.3}$$

The slope of web at the entry of misaligned roller which is nothing but the amount of misalignment

$$\theta_j = \theta_{Misaligned\_roller} \tag{4.4}$$

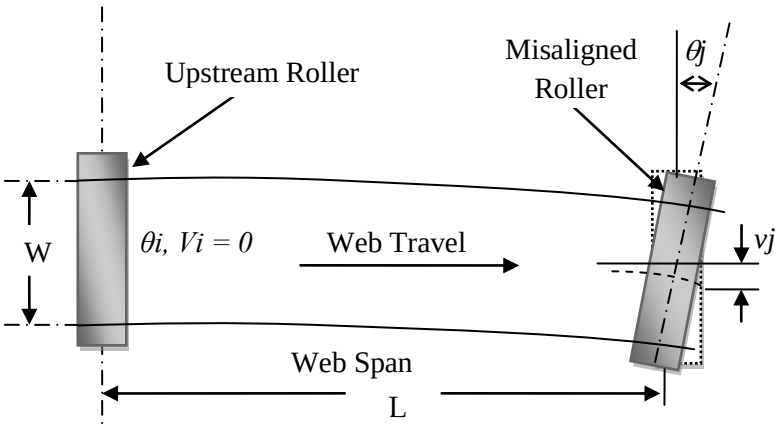

Figure 4.2 Boundary Conditions of Web on Downstream Misaligned Roller

The web is steered laterally (v_j) as shown in Figure 4.1 as a result of roller misalignment θ_j. As this misalignment is increased further, troughs are seem to be appeared in the span, which results in wrinkles formed in the web material on roller if the θ_j is further increased.

4.2 Experimental Procedure and Simulations

The model geometry, dimensions, material properties and loading conditions simulated in this work are exactly similar as that of Webb's set up documented in his MS thesis [49]. He conducted his experiments on a closed loop web transport system at WHRC. The web was unwound at a controlled tension and velocity, made to enter the test span after it passed a web steering unit so as to keep the upstream web edge at a constant set point. The downstream roller was mounted such that it could be pivoted horizontally about its center and the angle of misalignment could be adjusted to any desired values. Webb ensured the web did not slip on the rollers in the test section by covering the upstream and downstream rollers with a high coefficient of friction tape. Keyence 3060 Laser Micrometers were used to record the deflection as the web moved laterally. The output of these sensors was recorded using an analog LabVIEW® setup. These sensors could not monitor web deflection on roller *R3* located at the very end of the web span due to their physical size. This problem was tackled by placing sensors on the web span that followed the test span. Doing this made it possible to determine the deflection at the end of the web span after subtracting the radius of the downstream roll multiplied by the sine of the

Property	Value
Web Width *(W)*	6 inch
Web Thickness *(h)*	0.00092 inch
Young's Modulus *(E)*	580000 psi
Poisson's Ratio *(υ)*	0.3
Entering Span to concave roller *(L)*	18 inch
Pre-entering span *(L_a)*	6 inch
Web Tension *(T)*	12.3lb
Web Velocity *(v)*	1 inch/second
Coefficient of Friction *(μ)*	4

Table 4.1: Misaligned Roller Experiment and Simulation Parameters Values

misalignment angle. The web properties and other related parameters are enlisted in table 4.1. We modeled a setup which has 6 inch of pre-entering span and 18 inches of entering span with a misaligned downstream roller. It was assured during the simulations that enough length of web is passed over the rollers so as to attain dynamic equilibrium and steady state of lateral behavior of web on roller. The values of web tension and velocity were ramped to their final value linearly through time using the amplitude variation tool available in modeling techniques in ABAQUS®. Conventional shell (S4R) elements were used to model web. Rollers were discrete rigid shell structures. The misaligned roller was setup in cylindrical coordinate geometry so as to facilitate exact amount of roller misalignment and to restrict vertical or any tangential movement of roller due to web tension.

4.2.1 Convergence Analysis

The mesh refinement is a major factor controlling computational resources needed for executing every successful simulation. Reduction in the size of smallest element increases number of elements to be handled during given analysis causing additional time for job execution. Sufficiently small element size is needed to accurately define contact mechanics underlying the interacting surfaces. This is particularly important when cylindrical objects such as rollers or shells such as web on roller are being modeled. Finalizing optimum mesh size involves correct dimensioning and types of elements, suitable computational cost analysis and material properties. A convergence study is presented here to explain the selection of mesh size based on optimum combination of accuracy and computational cost.

As stated before, shell elements used in analysis for this study are S4R (4-node doubly curved general-purpose shell, reduced integration with hourglass control, finite membrane strains) elements. The size of mesh to be used for the initial attempts of simulations executed for this analysis was based on experience and intuition. We modeled the given setup with four different

sizes of mesh and result of each run was compared on different parameters. The computational aspects of each mesh size and simulation are given in table 4.2. The numbers presented in this table are from the case of 0.006 radian roller misalignment case. This case was chosen at random. All other parameters are same as listed in table 4.1

Elements /inch (Size Shell)	Number of Elements	Number of Nodes	Total Time Required
2 (0.5" Shell)	2481	2700	1 Hr
3 (0.35" Shell)	5024	5337	2.5 Hrs
4 (0.25" Shell)	*9801*	*10234*	*46 Hrs*
10 (0.1" Shell)	61329	62412	152 Hrs

Table 4.2 Computational Details of 0.006 Rad Misaligned Roller Model

Figure 4.3 presents a study carried out to examine convergence of the model for lateral web behavior on misalignments of 0.004 and 0.006 Rad at 12.3 lbs web tension. It compares the lateral deformations (v_j) of web on the roller *R3*. On horizontal axis, the mesh density is shown in number of elements shown per unit inch length. Primary vertical axis represents the execution time for each run in hours. Secondary vertical axis gives normalized results of values given by different sizes of shell elements. The lateral deformation (v_j) is compared with expression *(4.6)* which is assumed as 100% accurate result. This chart, along with Table 4.2 confirms the use of 0.25" shell elements would be best in terms of both, the accuracy and computational cost.

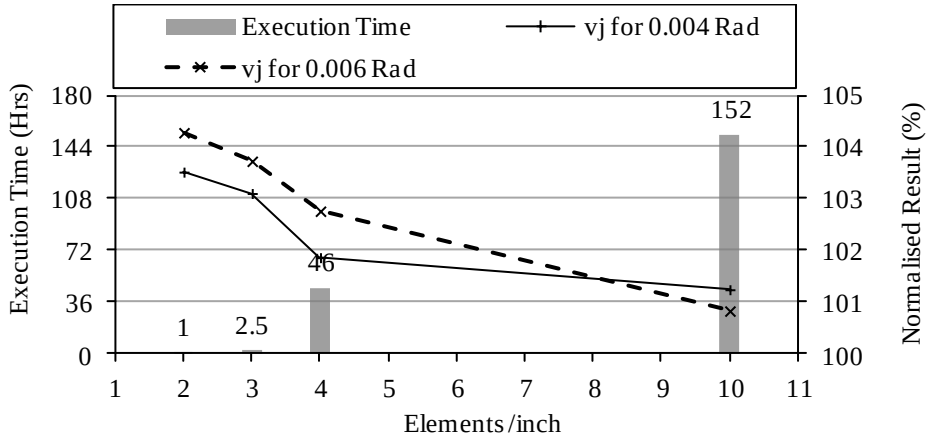

Figure 4.3 Convergence Studiy for Lateral Deformation (v_j) on Misaligned Roller

4.3 Results and Discussion

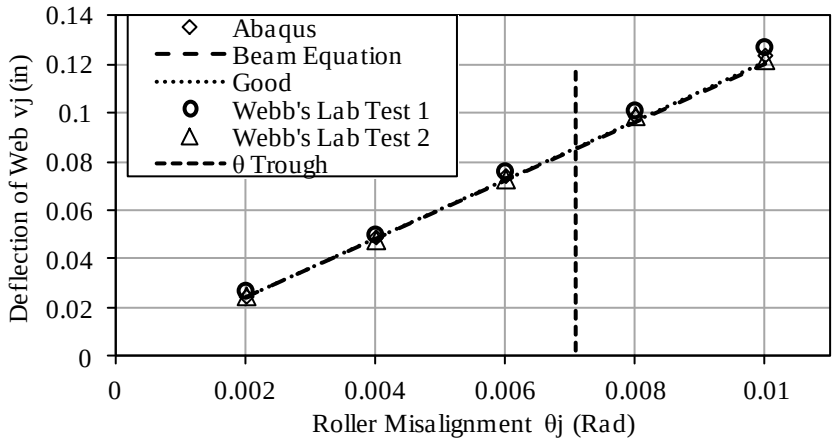

Figure 4.4 Comparison of Lateral Behavior of a Web on Misaligned Roller

Figure 4.4 shows comparison of deflection of web on misaligned roller *R3*. It compares results of deflection of web v_j as obtained in Webb's laboratory tests shown as 'Webb's Lab Test 1 and 2' with Beam equation given as

$$v_j = \left[\frac{2}{3}L\right] \times \theta_j \qquad (4.5)$$

It also shows results by Good's [12] equation obtained through matrix structural analysis where the value of v_j given by

$$v_j = \frac{4}{3}\frac{\left[30EIL + TL^3\right]}{60EI + TL^2} \times \theta_j \qquad (4.6)$$

Further, the values obtained by Abaqus simulations are also plotted. The web deflection value predicted by Good's equation is more precise since it considers all the parameters affecting deflection of web on roller. It looks like the simulations have predicted values correct up to considerable accuracy. The slight variation in the value of v_j after θ_{Trough} could be attributed to the out of plane variations produced in the web trying to affect lateral behavior on misaligned roller.

As discussed earlier, the web in the span behaves as end loaded cantilever beam. It is assumed that the friction between web and roller is sufficient to dictate the boundary conditions. As per normal entry rule, the web will enter the misaligned roller at an angle which is equal to the roller misalignment. This misalignment will generate a force *Fyj* in the web. It will cause a moment in web span. Web behavior similar to end loaded cantilever beam causes this moment increase linearly from zero at misaligned roller to maximum at upstream roller. According to Shelton, the σ_x distribution just upstream to the misaligned roller should be uniform. This results in having no moment at the point where the web enters misaligned roller *R3*. We tried to explore this if this behavior of web is reflected in our simulations the same manner. The MD stress distribution is seen to be almost uniform at the point of web entering the misaligned roller. The moment distribution at any point can be calculated with the following formula:

$$M_{bi(Abaqus)} = \int_{-W/2}^{W/2} (\sigma_{MD} yA) dy \qquad (4.7)$$

Where, *W* is the width of web, *y* is distance of the point from centroidal axis and A is the area of cross-section for each element. This moment is found to be almost equal to zero for all the cases of misalignment shown in Figure 4.4. The moment was found to be zero at the line of nodes just after the exact point of entry of web on roller. It looks like we have this zero moment condition on the roller surface. This confirms that the Abaqus model follows the moment boundary condition as denoted by equation *(4.7)*.

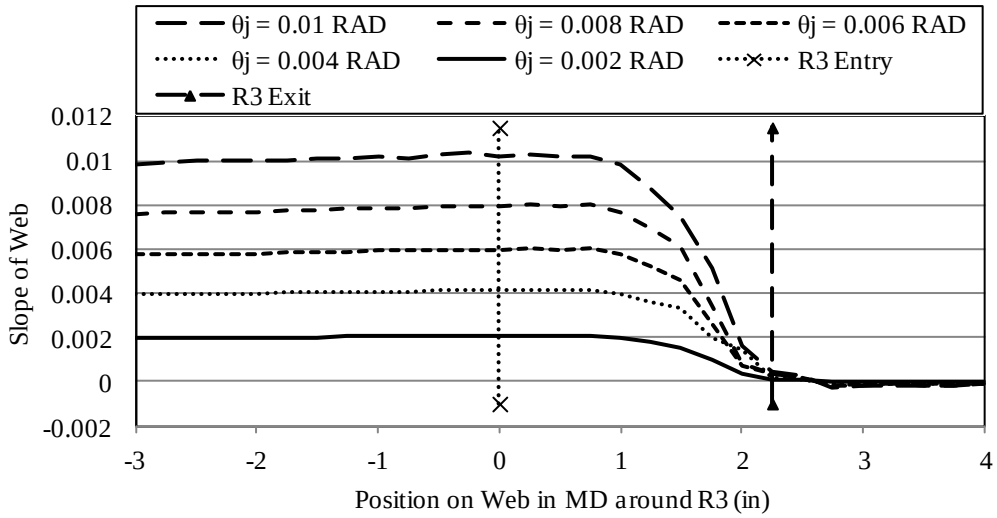

Figure 4.5 Slope of Web (θ_j) at Entry of Downstream Roller (R3)

Similarly, the angle of web entering misaligned roller can also be derived by enquiring the lateral movement of web on roller at various node points and then calculating the slope of this lateral deformation. The central difference method is used to calculate slope of web between two nodes. Figure 4.5 represents results of web slope calculated for various misalignments in radians from the simulations across the web coordinate in machine direction. It also shows the exact entry and exit locations of web on roller R3. It follows from this chart that the web enters the roller normally as per entry rule at an angle which is equal to angle of misalignment.

This reinforces that the model is following boundary conditions correctly. In every case of misalignment, the web is entering the roller exactly perpendicular to roller axis, and hence we can reinstate $\theta_j = \theta_{Misaligned\_roller}$. The web behavior on the roller surface could also be studied from figure 4.5. The slope of web remains constant even after it enters roller till half the wrap angle around roller. It looks like the slippage of web on roller starts after it has passed almost

half the roller surface in machine direction. This is an interesting observation and is studied with more details in [10].

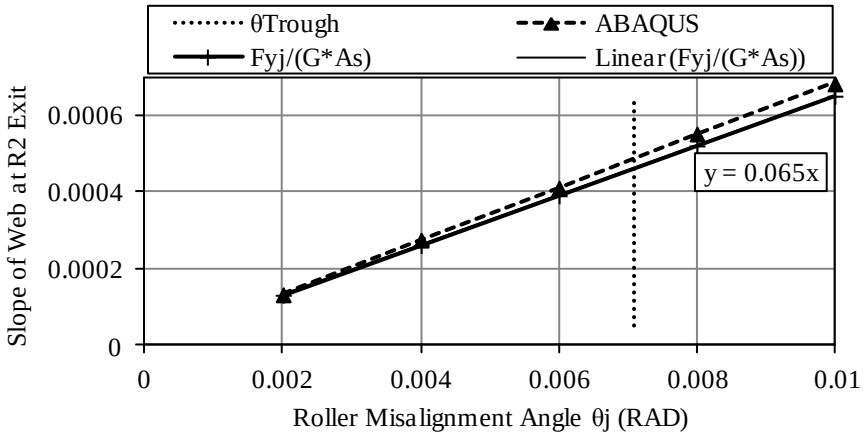

Figure 4.6 Slope of web (θ_i) at EXIT of Upstream Roller (R2)

Figure 4.6 displays comparison of slope of web θi at exit of upstream roller R2 by Abaqus and the closed form solution given by equation *(4.2)*. The slope of web while exiting upstream roller is affected by F_{yj}, the shear in the web span due to roller misalignment, Shear modulus G and the area reacting shear A_s. For the calculations of shear in the web, the equation given by Good and Beisel in [13] was referred. The disagreement in the values of θ_i for higher misalignment angles was expected since there is disagreement in lateral behavior of web on R3 for those θ_j values. Moreover, as stated before the out of plane disturbances produced in web for values higher than θ_{Trough} are also responsible for affecting the lateral behavior of web on both rollers. For the range of the values concerned, it looks like our codes have done a satisfactory job in achieving precise web behavior considering we did not assume any boundary conditions other than velocity and web tension in this study.

In conclusion of the study presented here in, it could be stated that the explicit method has been shown to produce results with reasonable accuracy and satisfaction for a web approaching a misaligned roller case. The explicit method will now be applied to more complex cases such as contoured roller in subsequent chapters.

CHAPTER V

FINITE ELEMENT MODELING OF WEBS ON CONCAVE ROLLERS

Increased demand of higher production in lesser time is one of the main reasons for a manufacturer to desire greater web speed and hence higher web tension or faster driven rollers in given web line. More web tension may result in problem such as width wise contraction. Other concerns that results from higher tension and speed are troughs, wrinkles and baggy lanes. Concave Rollers could be an effective solution to various problems such as stated above. Though these devices are employed in web handling industry with varying levels of success since many years, a very little is known about their mechanics. The interaction between the web and concave roller is not yet fully understood. This chapter presents a study of web on a concave roller using explicit FE techniques. As always in here too we assume only very basic boundary conditions, average web velocity and tension for example. Distribution of MD and CMD stresses, study of different webline geometries, several roller concavities, friction coefficients and materials are presented.

5.1 Spreading of Web by Concave Roller

The nominal geometry of a web moving over a concave roller is shown in Figure 5.1. The specifics indicated in the figure are the basis for calculating the nodal locations, directions and deformations required by the model. The origin of the coordinate system is located at the center of the roller where the center line of the web and roller intersect. Since the roller geometry is not a simple cylinder, the web material cannot conform to the surface of the roller without being strained and hence the web experiences a profile of MD strain with respect to the CMD similar in form to the roller radius profile. A variation in surface speed across the width of web results from the variation in radius.

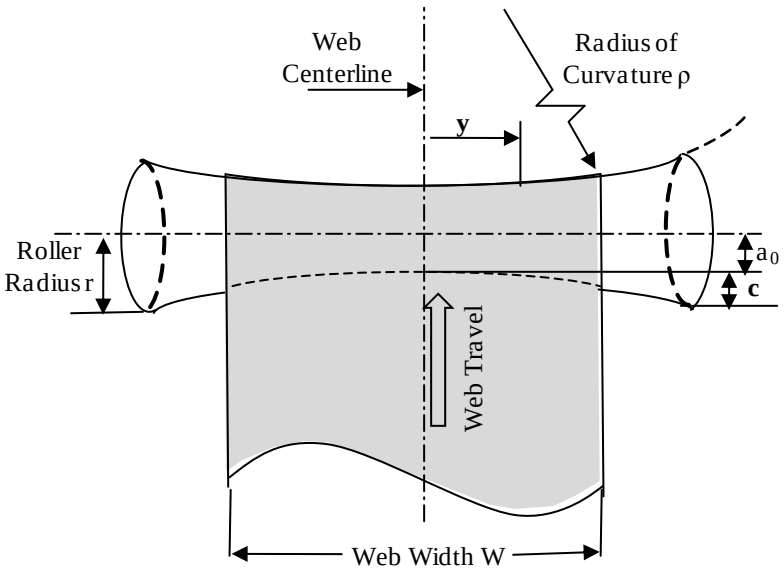

Figure 5.1- Nominal Geometry and Configuration of Concave roller

The variation in the MD length or change in diameter profile experienced by the web is seen in Figure 5.1 where we see the edges of web are curved showing wrap around concave roller. Because the diameter of the roller varies in CMD, the magnitude of the deformation also varies.

The change in profile of diameter causes variation in surface speed across the width of web. This results in more tension at edges than center, which is replaced by equivalent tensile force and moment at the centroid of Web. The only way to get the web back to *Normal Entry* is by superposition of an outward lateral force, causing the spreading of the web.

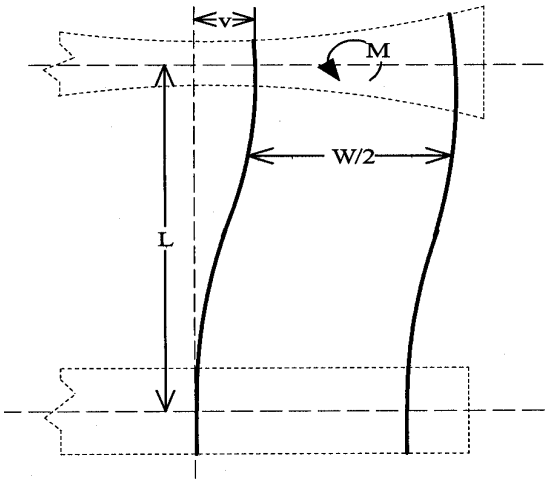

Figure 5.2 Spreading Mechanism of Web on Concave Roller: Classical Theories

The spreading mechanism of a concave roller using the classical theories is briefly explained here onward. Roisum[31], Swanson[40], and Markum *et al* [25,26] have given synopsis on different spreading devices and its modeling. For the analysis of concave roller, web is treated a beam and classical matrix structural analysis is used to describe its behavior. As shown in Figure 5.2, it is assumed that web can be analyzed as two separate beams of width *W/2* each, that will be steered outward by the roller. Given the properties of the web and roller profile, assuming normal entry of the web to the roller, considering only elastic stiffness, the lateral deflection (*v*) imparted to the web by spreading roller can be calculated. The derivation of the centroidal moment *(M)* involves calculations of strain (ε_{md}). This strain and subsequent stress is given by Markum and Good [25] as

$$\sigma_{md} = E\varepsilon_{md} \quad \text{Where} \quad \varepsilon_{md} = \frac{V_{(y)} - V_{avg}}{V_{avg}} \tag{5.1}$$

This stress and strain equation was derived in terms of web velocity assuming the web remains in traction with the roller and moves with the same velocity as the portion of the roller with which it contacts. The web velocity (V_y) is simply the roller surface velocity which is the roller radius (r) times the roller's angular velocity (ω).

Web line geometries and configurations have a wide variety as per their desired use and functionality. Effectiveness of a concave roller as a spreader is dictated by various factors such as entering and exiting span lengths, width of web on roller, geometries of roller profiles, friction and web material properties. It is always difficult to test all these parameters at once. The study presented here onward is divided in two sections depending upon the aspect ratio of web, which is defined as ratio of entering span (L) to web width (W). Configuration where aspect ratio is less than 1 ($L/W < 1$) is considered as wide web configuration. For all other cases, ($L/W \geq 1$) it assumed as a narrow web configuration in this study. Each of the case considered, the geometry and other related parameters are explained in tables given later in this chapter.

5.2 Finite Element Modeling and Simulation of Narrow Web

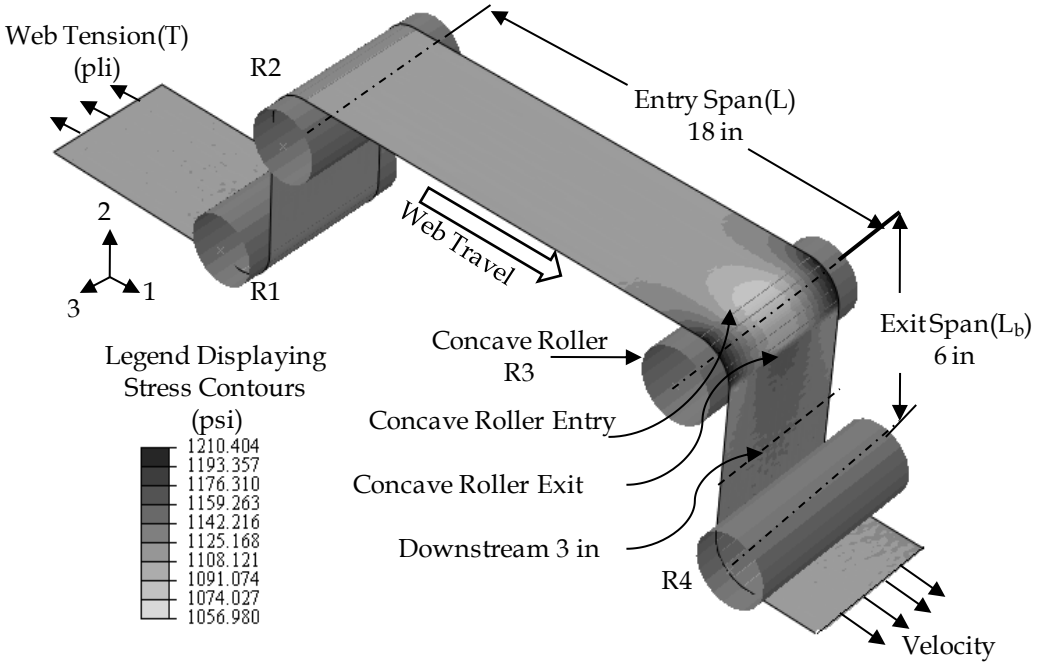

Figure 5.3 Narrow Web Model Setup and MD Stress Distribution in Web on Concave Roller

The concave roller is modeled in the third position (R3) of a four roller setup as shown in Figure 5.3. Rollers R1, R2, and R4 are cylindrical rollers with a nominal radius of 1.45 in. The concave roller was modeled with three different concavities given in Table 5.1. The concavity is described per the method of Markum and Good [25] where the roller radius is prescribed by the expression

$$r = a_0 + a_1 y^2 \qquad (5.2)$$

where *y* is a CMD coordinate measured from the center location of the roller as shown in Figure 5.1. All the four rollers are free to rotate around their longitudinal axis. The simulations are completed typically in twenty time steps. The first step consists of applying a known value of uniform tension load at the upstream end of the web while the downstream end is restrained at

zero velocity. In the second time step a prescribed value of MD velocity is set at the downstream end of the web for the remaining time steps. During the first time step as web tension develops, contact pressures also develop between the web and rollers. When the web begins moving in the second time step friction forces between the web and rollers begin to turn the rollers, much as any idler roller would be driven by a web.

Property	Values for Radius of Curvature ρ		
	ρ = 400 in	ρ = 600 in	ρ = 800 in
Parabolic roller profile coefficient a_0 *(in)*	1.43875	1.4425	1.4444
Parabolic roller profile coefficient a_1 *(1/in)*	0.00125	0.00083	0.00062
Depression at the center *c (in)*	0.02	0.0133	0.01
End Radius *(in)*	1.45875	1.4558	1.4544

Table 5.1: Geometrical Properties of Concave Rollers

Since we are applying velocity boundary conditions to the downstream end of web, it is going to experience acceleration in certain time span. For the simulation to execute accurately, this acceleration and sudden change in the physical state of web should be induced smoothly. Gradually increasing values of acceleration result in smooth velocity and hence gradual displacement of elements. This could be controlled by providing appropriate fractions for ramping the values of given parameter in Abaqus® by controlling the amplitude values. Figure 5.4 shows the velocity and tension boundary conditions and their amplitude ($A_{(t)}$) ramped gradually from the initial value $(A_{(s)})$ to the final value $(A_{(f)})$. These values are ramped till it matches the specified value of each boundary condition and keeps on the same value till the end of simulation. Representative results are shown till 10 sec. No kinematic boundary conditions between the web and rollers are enforced with the exception that the web is prevented from penetrating the rigid analytical roller surface by the contact algorithm. Only friction forces between the rollers and web dictate the lateral behavior of the web.

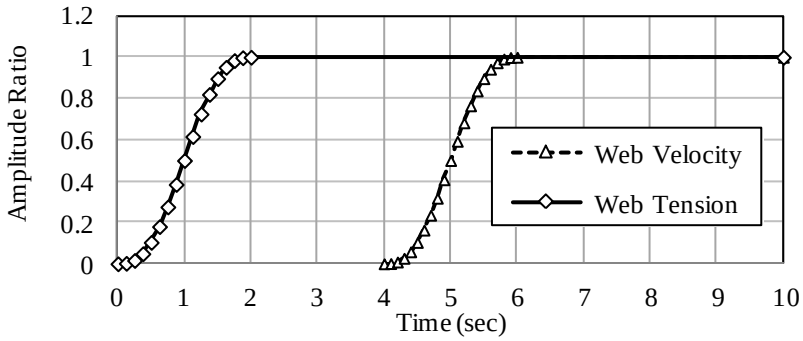

Figure 5.4 Amplitude Variations for Boundary Conditions of Narrow Web Model

The concave roller models consist of total with 60428 Elements and 61492 Nodes. An HP® Workstation with an Intel® Xeon® CPU processor with a speed of 3GHz and 3 GB of RAM were used for this simulations. The base parameters for study of concave rollers with explicit simulations are chosen such that it matches web materials and equipments used in web handling industry. Various parameters of the models are shown in Table 5.2. Solution times were nominally 64 hours. During these simulations about 127 cm (50 in) of web would pass over the four rollers.

Property	**Value**
Web Width *(W)*	6 inch
Web Thickness *(h)*	0.00092 inch
Young's Modulus *(E)*	20000 psi
Poisson's Ratio *(υ)*	0.3
Entering Span to concave roller *(L)*	18 inch
Pre-entering span *(L_a)*	6 inch
Web Tension *(T)*	1pli
Roller Radius *(r)*	1.45 inch
Wrap Angle *(β)*	90 degrees
Web Velocity *(v)*	0.5 inch/sec
Coefficient of Friction *(μ)*	0.5

Table 5.2: Parameter Values for Narrow Web Model for Concave Roller Analysis

5.2.1 Convergence Analysis

As stated in previous chapter, sufficiently small element size is needed to accurately realize the surface mechanics underlying the interacting surfaces. This is particularly important

for concave roller case since the web is bent in vertical plane at the same time wrapping around the cylindrical roller. The optimum mesh size involves correct dimensioning and types of elements, suitable computational cost analysis and material properties. A convergence study is presented here to explain the selection of mesh size based on optimum combination of accuracy and computational cost.

We have used shell elements in this analysis. The S4R (4-node doubly curved general-purpose shell, reduced integration with hourglass control, finite membrane strains) elements are employed. The size of mesh to be used for the initial attempts of simulations executed for this analysis was based on experience and intuition. We modeled the given setup with four different sizes of mesh and result of each run was compared on different parameters. The computational aspects of each mesh size and simulation are given in table 5.3. The numbers presented in this table are from the case of radius curvature 400" case. This case was chosen at random. All other parameters are same as listed in table 5.2.

Elements /inch (Size Shell)	Number of Nodes	Number of Elements	Total Time Required	Stable Time Increment
3 (0.35" Shell)	5514	5210	1.5 Hr	2.149×10^{-4}
4 (0.25" Shell)	10079	9656	9 Hrs	1.634×10^{-4}
10 (0.1" Shell)	*61492*	*60428*	*64 Hrs*	6.504×10^{-5}
12 (0.08" Shell)	96870	95540	288 Hrs	2.194×10^{-5}

Table 5.3 Computational Details for ρ = 800" Concave Roller Model

Figure 5.5 presents results of convergence analysis carried out for the model. It compares the MD stress σ_{MD} developed in web edge and center at the point where web touches the roller. On horizontal axis, the mesh density is shown in number of elements shown per unit inch length. Primary vertical axis represents the execution time for each run in hours. Secondary vertical axis

gives normalized results of values given by different sizes of shell elements. The MD stress *(σ_{MD})* is compared with expression *(5.3)* which is assumed as 100% accurate result. Abaqus has calculated excessive values for stress at center and lesser values at web edge than compared to the closed form solution. This chart, along with Table 5.3 confirms the use of 0.1" shell elements would be best in terms of both, the accuracy and computational cost of simulation.

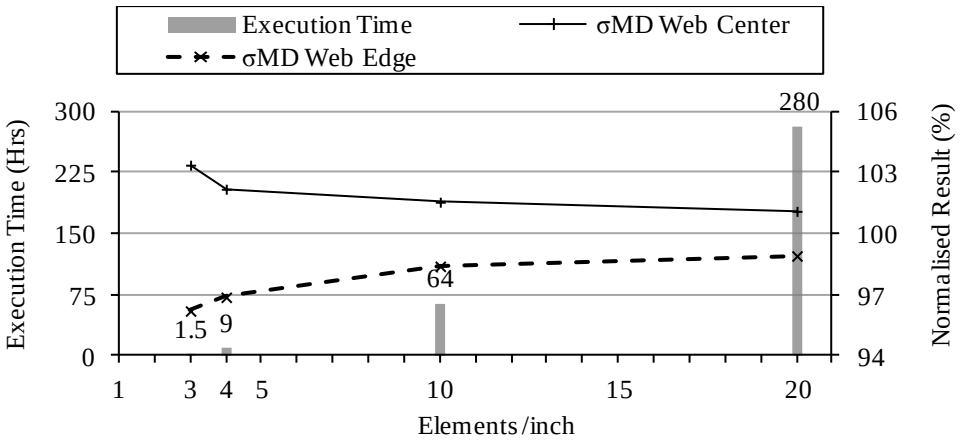

Figure 5.5 Convergence Study for MD Stress in Web on Concave Roller

5.2.2 Narrow Web Model Results and Discussion

As explained earlier in this chapter, the concave roller profile induces a higher surface velocity at the web edges than at the web center due to the larger radius at the web edges. If friction is sufficient the web attains the variation in surface velocity of the roller which will induce higher MD strains and stresses at the web edges with respect to the web center. Markum and Good [25] developed a closed form expression for calculating MD stress (σ_{md}) related to MD strain (ε_{md}) based on uniaxial Hooke's law. They chose to do this since they assumed they were spreading a web that had laterally collapsed back to a planar form. This expression relates the stress at any point where the web enters the concave roller with the CMD distance of that point from the centroidal axis of web. Since the CMD centers of the web and concave roller are

assumed to coincide, the stress distribution is symmetrical about the centroidal axis. This expression relates web and roller parameters with the MD stress across web width.

$$\sigma_{MD}(y) = E\frac{a_1(y^2 - W^2/12)}{a_0 + a_1 W^2/12)} + \frac{T}{h} \qquad (5.3)$$

Where, E is web modulus, y is the distance of given point from centroidal axis of web, W is web width, T being web tension, h is thickness of web and a_1 and a_0 as per table 5.1. The largest MD stress occurs at the web edge and is due both to the concave roller and the web tension T. This could be obtained by inputting $y = W/2$ in equation *(5.3)* as

$$\sigma_{MD}(W/2) = \frac{2Ea_1W^2}{12a_0 + a_1W^2} + \frac{T}{h} \qquad (5.4)$$

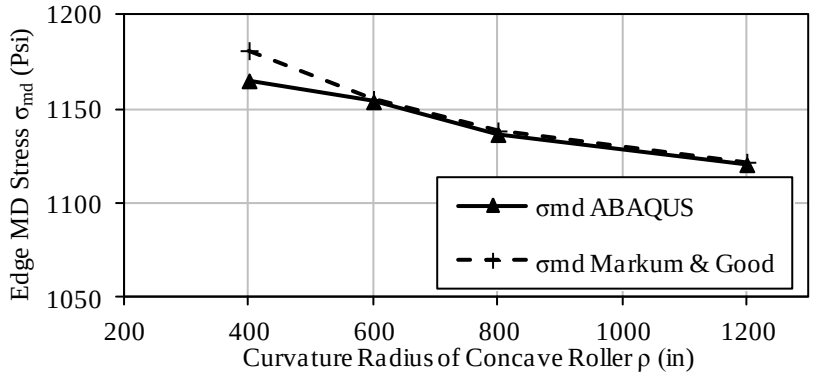

Figure 5.6 MD Stress Induced by Concave Roller (R3) of varying Curvature Radius

A comparison of stress values calculated by this relation with those results obtained from Abaqus model is shown in Figure 5.6. This comparison is for stresses at the edge of web at the entry point where the web first contacts the concave roller. The results shown in Figure 5.6 are in good agreement with value of MD stress for higher curvature radius of concavity and deviates away as the curvature radius shortens. It is seen from the figure that radii for which deviation does exist,

the Abaqus result is less than the result given by expression *(5.3)* which suggests some slip may exist between the web and roller surface. This disagreement could be reduced by using finer mesh that defines the web over concave roller. A fine mesh can form better curved surface for lower values of curvature radius. Expression *(5.3)* was derived assuming the web attained the velocity of the roller at the entry point. It is based on the assumption of *no slip*. The Abaqus simulations incorporate no such assumption.

5.2.3 MD and CMD Stresses in Narrow Web

Abaqus® provides values of selected parameter (this parameter must be the desired pre-selected from list available in field-output database) at given node/element location. The query tool helps in extracting these values from output file. Various quantities are preselected based on the parameters to study in the given analysis. The MD stress at entry and exit locations is shown as a function of CMD position in Figure 5.7. These stresses are compared with Markum and Good's model as explained earlier. As seen previously in Figure 5.6, the MD stress values shown by Abaqus at the edge are slightly less than that calculated by Markum and Good's expression. It is evident from the charts that the web undergoes a reversal of MD stresses as it travels from the roller to next free span. It also appears that the MD stress profile is not greatly affected by the radius of curvature of the roller.

The impact is larger than appears here since the mean level of web stress due to tension is large compared to the variation caused by the concavity. The location of point of stress reversal occurs very near to web exit on roller surface and must be accompanied by slippage. It looks like the amount of slippage of web on roller at the edge is more for concave roller with lower radius of curvature. Moreover, the point of stress reversal is also seen shifting its place towards edge of web as the roller radius of curvature is increased.

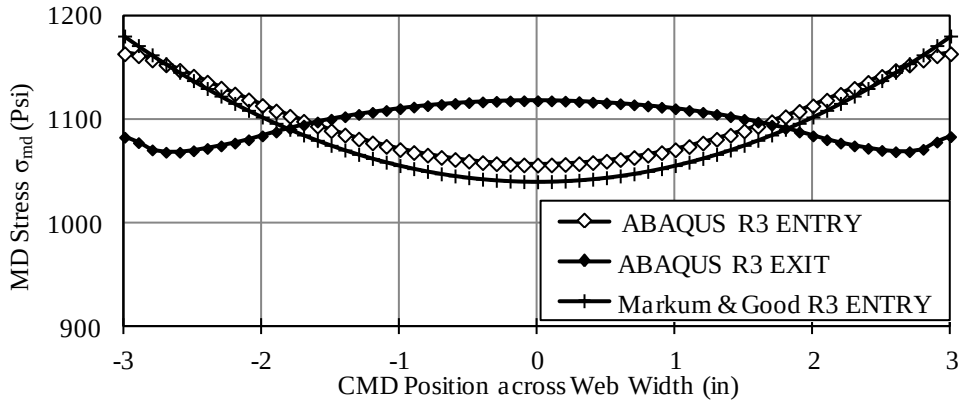

a) Roller Curvature Radius **ρ = 400 in**

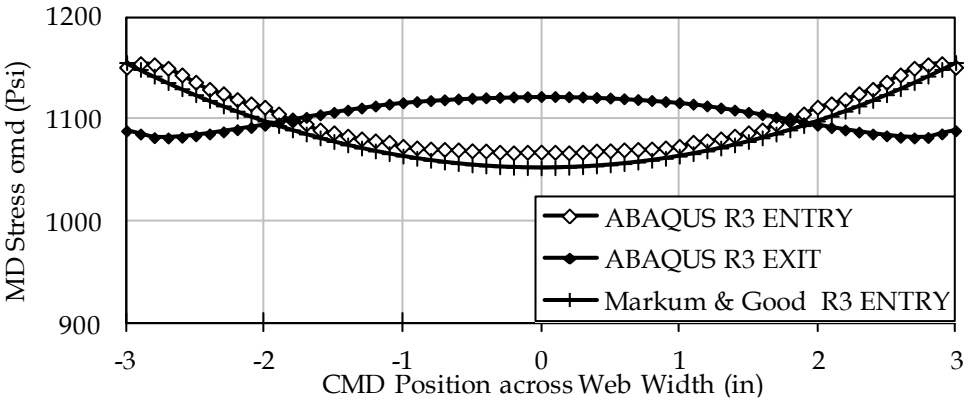

b) Roller Curvature Radius **ρ = 600 in**

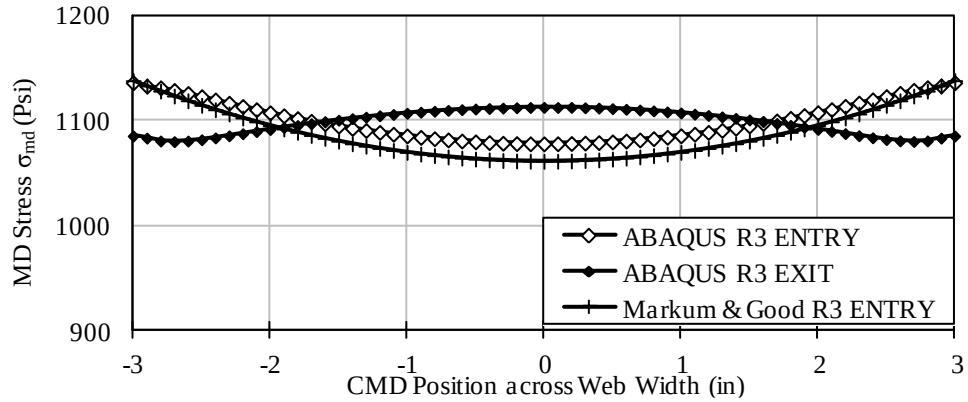

b) Roller Curvature Radius **ρ = 800 in**

Figure 5.7 MD Stress as a Function of Curvature Radius (ρ) at Entry and Exit

It is interesting to note about the stress distribution that the maximum MD stress value is seen to be induced somewhere on the roller and not at entry. This is more curious in the light of what we have previously thought it would be. The stress values obtained clearly shows that MD stress attains its maximum value at a location on the wrap on Concave Roller. Previous research

conducted by Delahoussaye *et al* [7] was based on an enforced boundary condition of no slip over entire web wrap on roller. With such an assumption the MD stress variation seen at the entry of the roller would have remained unchanged until the web exited the roller.

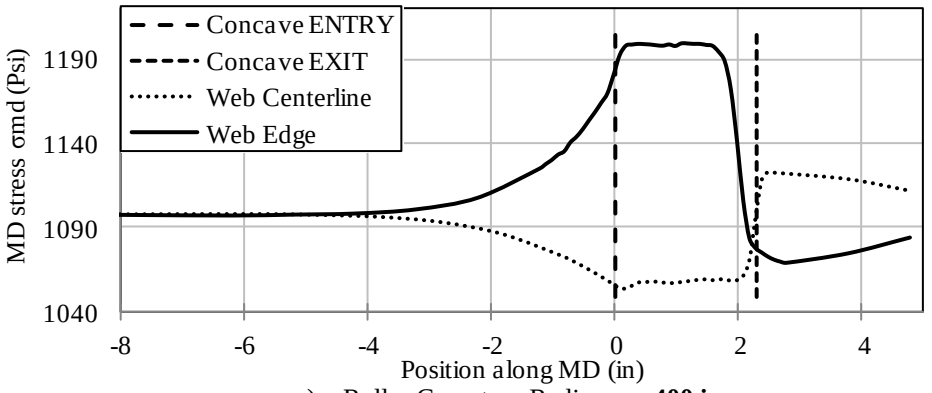

a) Roller Curvature Radius **ρ = 400 in**

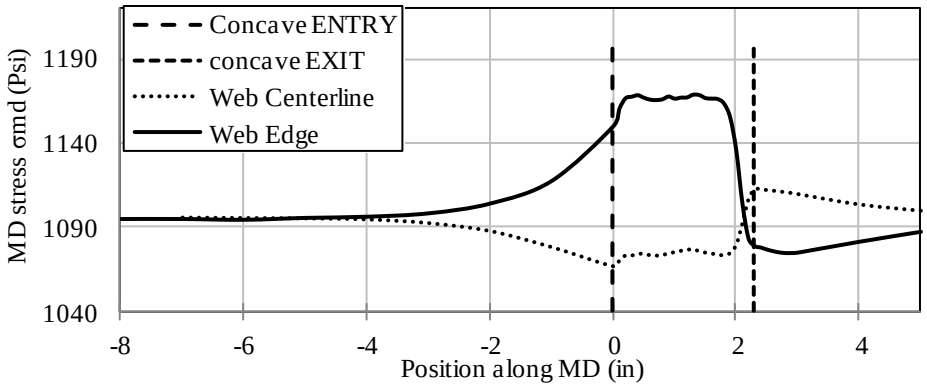

c) Roller Curvature Radius **ρ = 600 in**

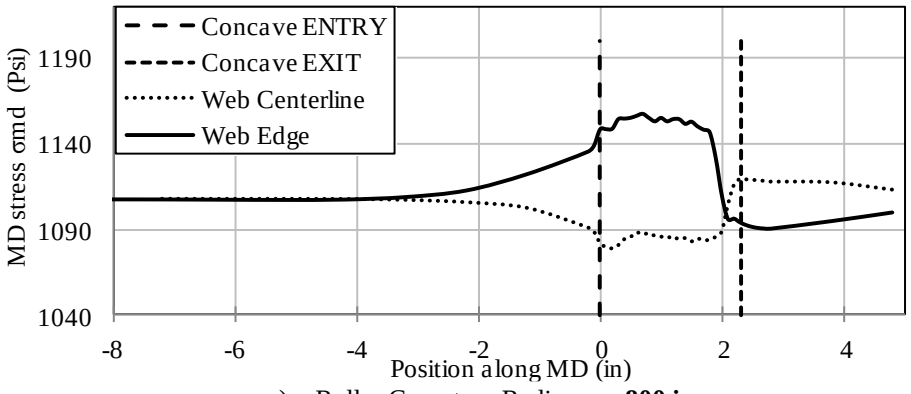

c) Roller Curvature Radius **ρ = 800 in**

Figure 5.8 MD Stresses on Edge and Center of Web Transiting a Concave Roller

The Abaqus simulations include no such assumption and it is obvious from Figure 5.7 that for the cases studied that a no slip assumption is valid for a partial wrap of web on roller. To further study the MD stress variation occurring in the web transiting the concave roller the plots of Figure 5.8 are prepared where the MD stress distribution along the centerline and the edge is shown. The line of observation starts approximately 8 in upstream, proceeds in the MD to the concave roller, transits the roller and finally ends 3 in downstream of the concave roller exit.

As expected the MD stress values should have lesser variation than normal web tension as the roller becomes flat i.e. the radius of curvature increases. The charts indicate that the MD stresses undergo change as the web passes over the roller and that an assumption of no slip is valid for partial wrap of web on the given roller. The MD stresses are seen suddenly dropping near exit of roller. This is yet another indication of slip but is additional evidence that assumptions used in earlier analyses [7, 8] are not always valid. The locations shown as Entry and Exit of concave rollers are marked at exact horizontal distance on abscissa. This location might not provide the exact estimate of stress on edge or centerline since the resolution of mesh was 0.1 inch. If the exact point of entry/exit of web on roller is between two consecutive nodes 0.1 inch apart, the stresses shown at that location are average of the previous and next node stress value.

Similar charts of the CMD stresses are shown in Figure 5.9. The largest CMD spreading stresses are witnessed on the centerline of the web. These stresses decrease towards the web edges where they become zero as required by surface equilibrium. The charts in Figure 5.9 show the CMD spreading stresses, on the web centerline, rise as the web approaches the entry to the concave roller. They then remain constant or decrease slightly and then rise to a peak as the web exits the roller. These peaks at the exit are the result of the rising MD stresses that were seen on the web centerline in Figure 5.7. The rising MD stress will result in a contracting strain in the CMD direction due to the Poisson effect. The contraction of the web is restricted by CMD friction forces near the exit resulting in an increase in the CMD stress. After exiting the roller the

tensile spreading stress decreases and then becomes negative. Webs can react very little compressive CMD stress without buckling and forming web troughs. The appearance of compressive stresses in the exit section on the web center line was reported by previous researchers [6, 7] too.

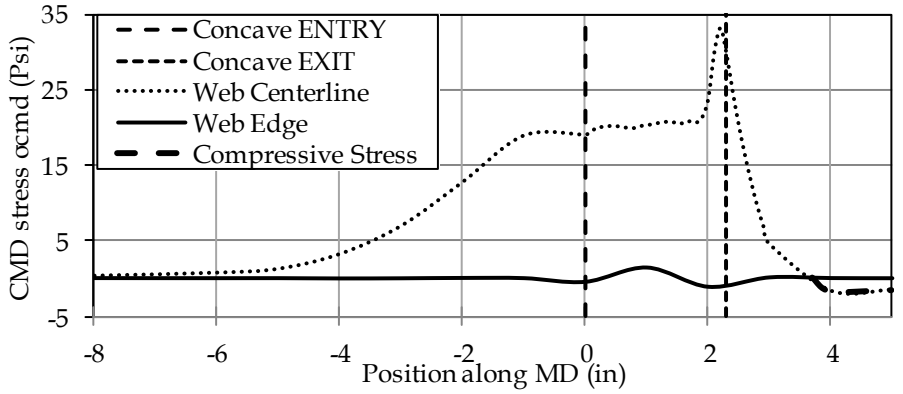

a) Roller Curvature Radius **ρ = 400 in**

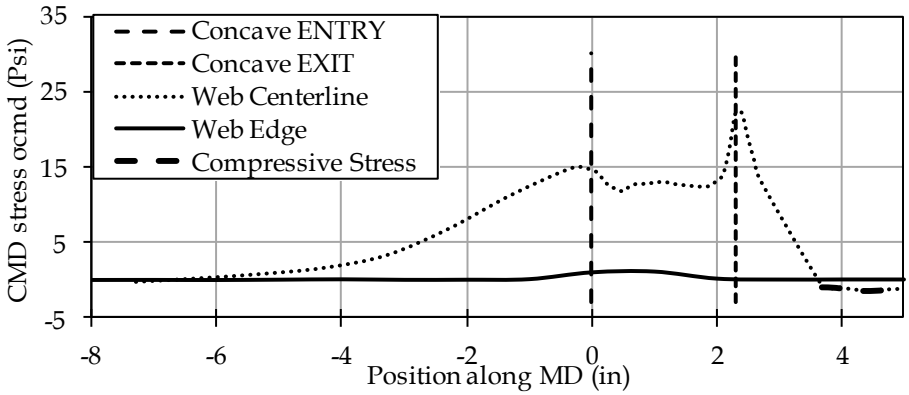

b) Roller Curvature Radius **ρ = 600 in**

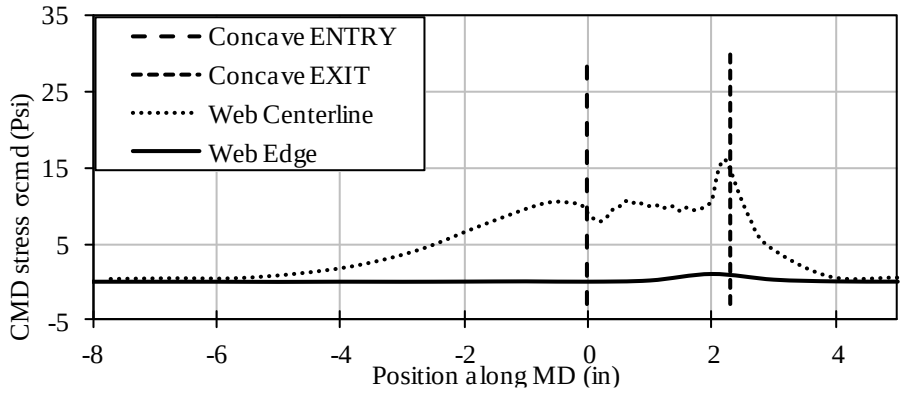

c) Roller Curvature Radius **ρ = 800 in**

Figure 5.9 CMD Stresses on Edge and Center of Web Transiting Concave Roller

Thus a device that is employed to spread webs can also be responsible for buckling the web in the exit span. It looks like these compressive stresses are function of material properties and the roller geometry since such stresses are not seen in immediate exit span of 800 in roller for the given combination of materials and roller concavity.

5.2.4 Study of Negative CMD Stresses and Troughs in Exit Span

The development of negative CMD stresses in the exit span of the concave roller was explored further. The CMD stress output was used to produce charts of CMD stress versus CMD location at the entry and exit of the concave roller and then at a downstream location in Figure 5.10. Again the CMD spreading stresses in the web are shown to increase between the entry and exit of the concave roller. Note the CMD stresses in the web at the exit of the roller are tensile at the centerline but become negative (compressive) as the web edges are approached where they finally decline to zero. But also note that midway through the exit span (3 in downstream of the concave roller exit) the CMD stresses are negative and small. Also note that these stresses undulate slightly near the web centerline. This is prominently seen in the case of roller with smallest curvature radius ($\rho = 400$”). For this reasons, the same roller profile was chosen to study behavior of web in exit span especially in the light of trough formation.

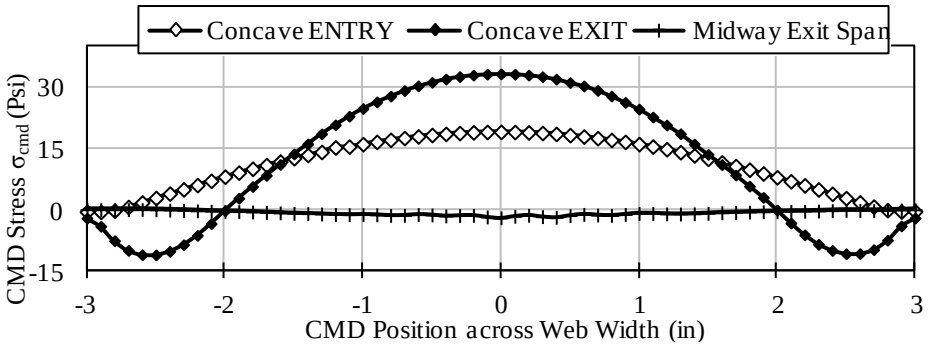

a) Roller Curvature Radius **ρ = 400 in**

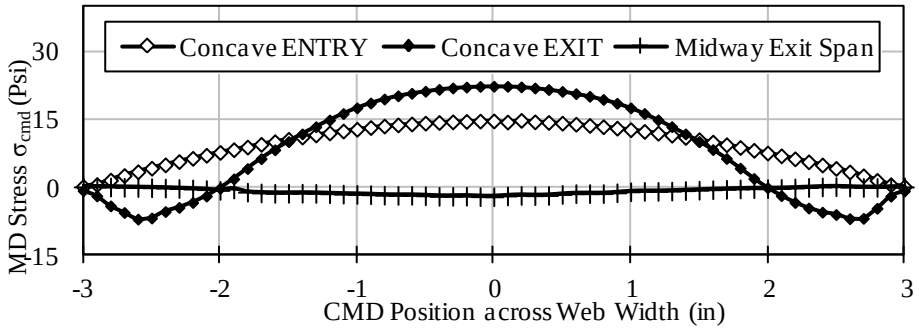

b) Roller Curvature Radius **ρ = 600 in**

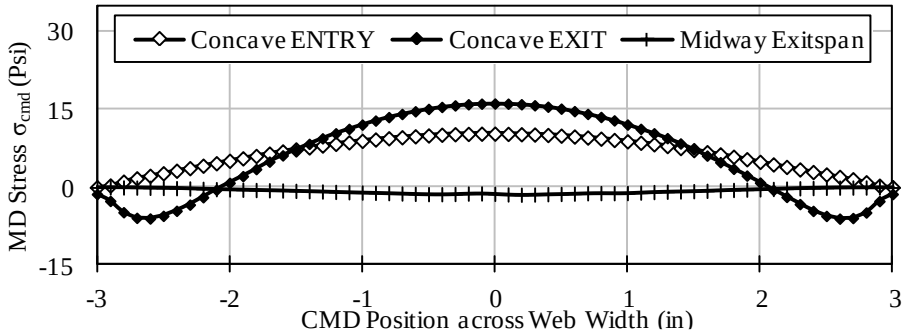

c) Roller Curvature Radius **ρ = 800 in**

Figure 5.10 CMD Stresses across the Width of Concave Roller. Compressive CMD Stresses developed at Midway Exit Span.

Web troughs occur due to instabilities in the web plates between rollers. Troughs results due to the presence of compressive stresses in CMD. Beisel [2] developed an expression for the value of critical negative CMD stresses which will induce troughs in an isotropic web. If the stresses attain a value more negative than this critical value, troughs are formed. The expression for the critical stress is given as

$$\sigma_{ycr} = -\frac{\pi h}{\sqrt{3}L}\sqrt{\frac{\sigma_{MD}E}{\left(1-\nu^2\right)}} \qquad (5.5)$$

where *h* is the web thickness and *L* is the span length. For the web properties given in Table 5.2 and an exit span length of 6 in a critical buckling stress of -1.359 psi is produced using expression *(5.5)*. Note the minimum CMD stresses seen in the exit span in Figure 8 are never less than –1.45 psi. This is indicative that buckling has occurred. When webs buckle into a troughed shape the wavelength λ or the distance between the trough crests can also be predicted. Again from Beisel *et al* [2]

$$\lambda = \frac{2L}{\sqrt[4]{1+\frac{\sigma_x}{\sigma_e}}} \quad \text{Where} \quad \sigma_e = \frac{\pi^2 D}{L^2 h} \quad \text{and} \quad D = \frac{Eh^3}{12(1-\nu^2)} \qquad (5.6)$$

For an exit span length (L_b) of 6 in and for the web properties from Table 5.2 a wavelength of 0.30 in is calculated. In Figure 5.11, traces of the CMD surface stress on the bottom web surface and the out-of-plane deformation across the web width are shown for the case of curvature radius (ρ) 400 in. These traces are shown since they exhibit evidence of the troughs and their wavelengths. While the wavelength calculated does not exactly match the wavelength shown in Figure 5.11, it does fall within the realm of modeling error since the element size is 0.1 in.

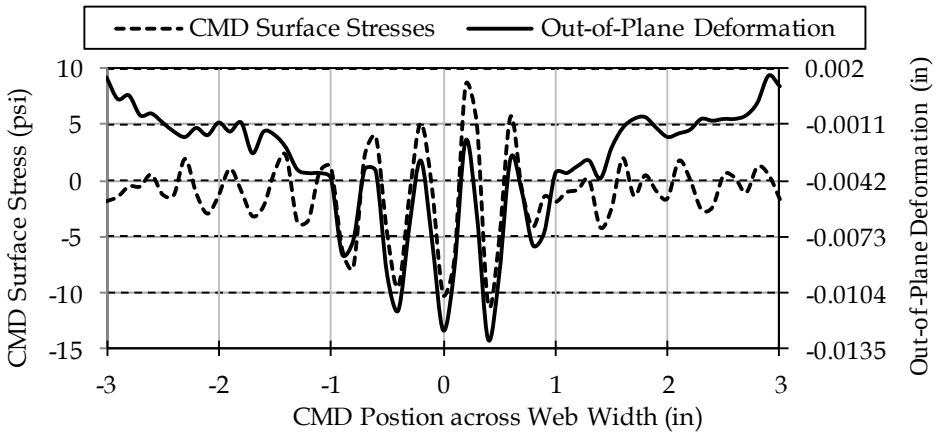

Figure 5.11 Trough Formations due to CMD Surface Stresses with Out-of-Plane Deformation of Concave Roller ρ = 400 in.

5.2.5 Friction and Slippage on Roller Surface

Web tension is responsible for the development of normal pressure between the web and roller surfaces. The web, while in contact with the roller can transmit shear as well as normal forces across the contact interface. The relationship between these forces is a cause of the stresses at the interface dictated by friction. The friction in the present modeling is governed by Coulomb friction model. According to this model, two contacting surfaces can carry shear stresses up to a certain magnitude across their interface before they start sliding relative to one another. This stress is defined as critical shear stress, τ_{crit}, at which sliding of the surfaces starts. It is given as

$$\tau_{crit} = \pm \mu p \qquad (5.7)$$

Where μ is the friction coefficient between web and roller surface and p is contact pressure. A plot of the equivalent shear $\bar{\tau}$ contact $\bar{\tau} = \sqrt{\tau_1^2 + \tau_2^2}$ stress (obtained as) against the fraction of contact pressure is shown in figure 5.12. Where τ_1 and τ_2 are two components of shear stress defined in Abaqus as Cshear1 and CShear2.

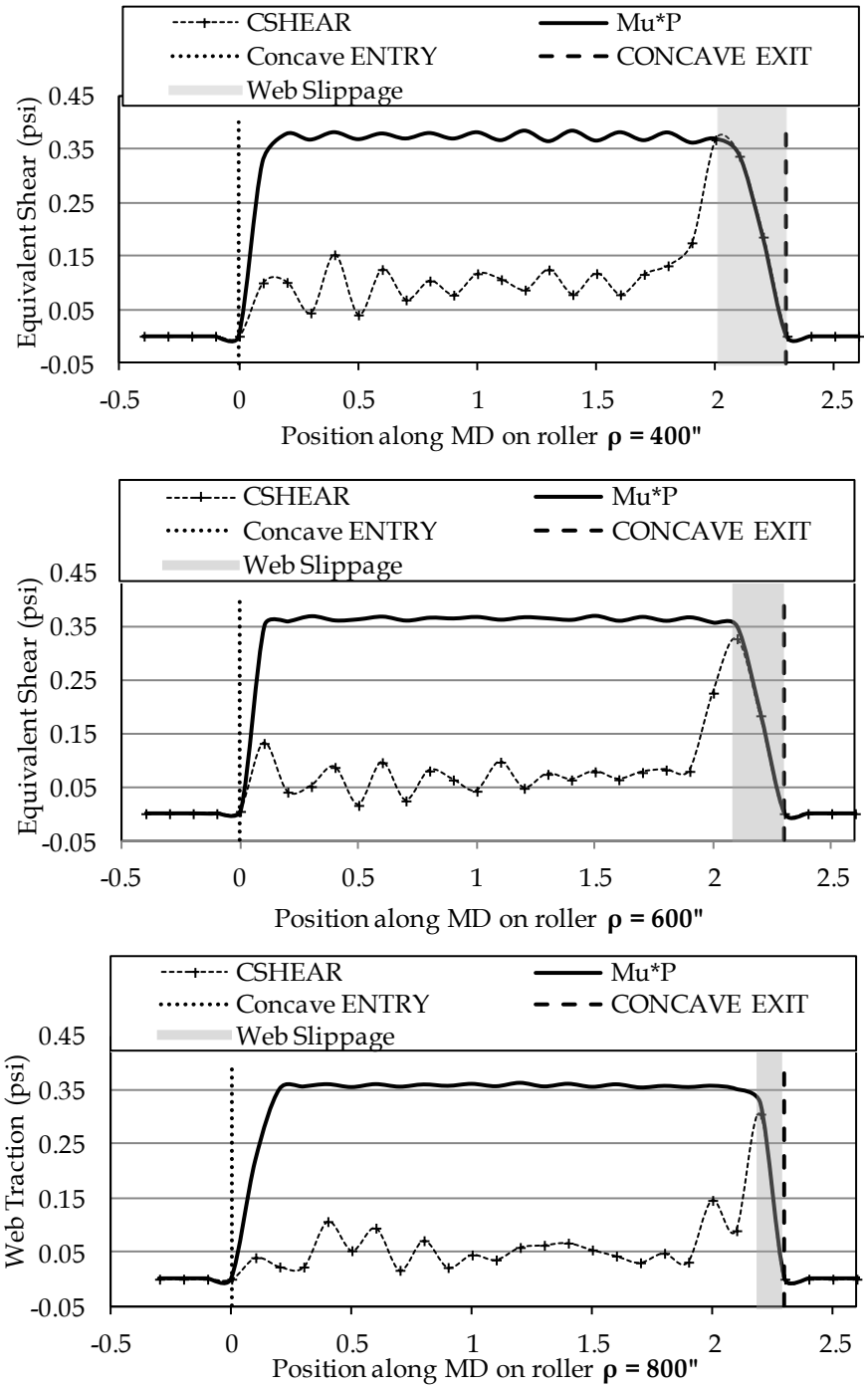

Figure 5.12 Slippage of Web Edge on Concave Roller

The values of contact shear stress are extracted from the edge nodes where the line starts 0.5in before roller entry, continues on roller wrap and extended almost 0.5in beyond exit. The behavior

of the contact shear stress can be linked to the MD and CMD stress profiles across the web width shown in Figures 5.8 and 5.9, respectively. As stated earlier the web exits roller with rising MD stresses at the center than that of the edges of web. It causes a contraction due to Poisson's effect in CMD. This contraction is limited by the shear contact stresses in the CMD which are shown in the figure.

In all these plots, the shaded area near concave Exit, is the part of web wrap on the roller surface that has occurred to have equivalent shear stress($\bar{\tau}$) matching the envelop value of critical shear (μp). Since the maximum amount of shear stress that the given coefficient of friction can withstand at given conditions is reached, the web is under slipping conditions. Some fluctuations in the values of critical shear stress are also seen for the case of least radius of concavity since the web elements being curved due to the roller surface experience slight changes in friction behavior. The width of this web slippage area increases as we reduce the radii of curvature of rollers. This is expected since the aggressive concavity causes more MD and CMD stresses generated in web causing higher values of shear stress.

5.3 Finite Element Modeling and Simulation of Wide Web

As stated before, during various operations in web handling industry webs of larger width than that considered in previous sections are transported through process machines. A model is constructed and analyzed here to investigate effect of changed roller geometry and aspect ratio of span (L) to web width (W). For this study, a web with aspect ratio less than one (L/W < 1) is considered a wide web. The model is developed here for a case that was originally presented by Brown [5]. In this case, the aspect ratio is 0.4, much smaller than previous case of L/W = 3.

5.3.1 Wide Web Model

The model used for studying wide web is very similar to the model described earlier except the geometries, web properties and application of load. The concave roller is placed at the R3 location. There is a different way we start this simulation compared to the previous effort about narrow webs. Amplitudes of load application, velocity and roller movement is different. The web is laid flat in the beginning of the simulation with R1 and R4 at its final position. R2 and R3 are vertically below the web but at their final locations in the X direction. This allows the model of the web to be defined with uniform web length prior to the beginning of the simulation. The first step consists of applying a known value of uniform tension load at the upstream end of the web while the downstream end is restrained at zero velocity. Rollers R2 and R3 are then moved into their final vertical positions in the second step. The web velocity is enforced at the downstream end of the web after a lapse of nearly 5 seconds. This time was given to allow the web out-of-plane dynamic motion to cease which was due to moving rollers R2 and R3 into position. These amplitudes are shown in figure 5.13.

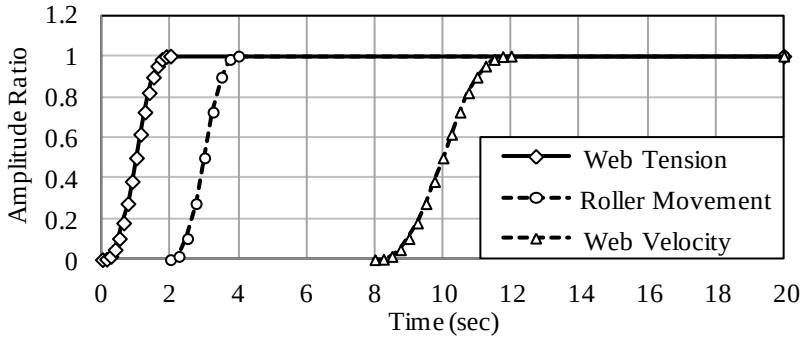

Figure 5.13 Amplitude Variations for Boundary Conditions of Wide Web Model

When the web movement begins, the friction forces between the web and rollers begin to turn the rollers, much as any idler roller would be driven by a web. For these simulations again no kinematic boundary conditions between the web and rollers were enforced. Only friction forces between the rollers and web dictate the lateral behavior of the web. The base parameters for study of concave rollers with explicit simulations are chosen such that it matches web materials and equipments used in Brown's study. Various parameters of the models are shown in Table 5.4. The concave roller achieved concavity with a depression of 0.005 in at its center. A web length of 54 in passed over the four rollers during the simulation.

Property	**Value**
Web Width *(W)*	60 in
Web Thickness *(h)*	0.0005 in
Young's Modulus *(E)*	600,000 psi
Poisson's Ratio *(υ)*	0.35
Entering Span to concave roller *(L)*	24 in
Exiting span *(L_b)*	24 in
Web Tension *(T)*	0.5pli
Roller Radius *(r)*	3 in
Wrap Angle *(β)*	90 degrees
Web Velocity *(v)*	0.5in/second
Coefficient of Friction *(μ)*	0.5

Table 5.4: Concave Roller Model Parameters Values for Wide Web Study

Figure 5.14 shows the convergence of the MD stresses at the centerline and the edge of the web and also the CMD stresses at centerline of web during the simulation. Each simulation runs for 100 seconds of total time. The processes of web tension building occur in the first 2 seconds. Rollers are moved into position from 2 to 4 seconds. Next 4 seconds are given for stresses to stabilize in web and then bringing the web to its final velocity value is achieved as shown in the figure 5.13. The remainder of the simulation time is spent bringing the MD and CMD stresses to converged values. The MD stresses stabilize sooner than the CMD stresses in this case.

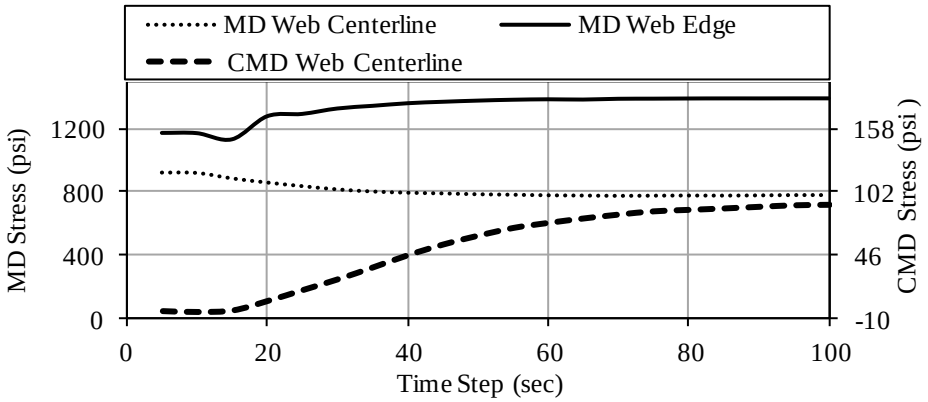

Figure 5.14 Convergence of MD and CMD Stresses at the Entry of Concave Roller in Wide Web over the Total Simulation Time

5.3.2 Wide Web Model Results and Discussion

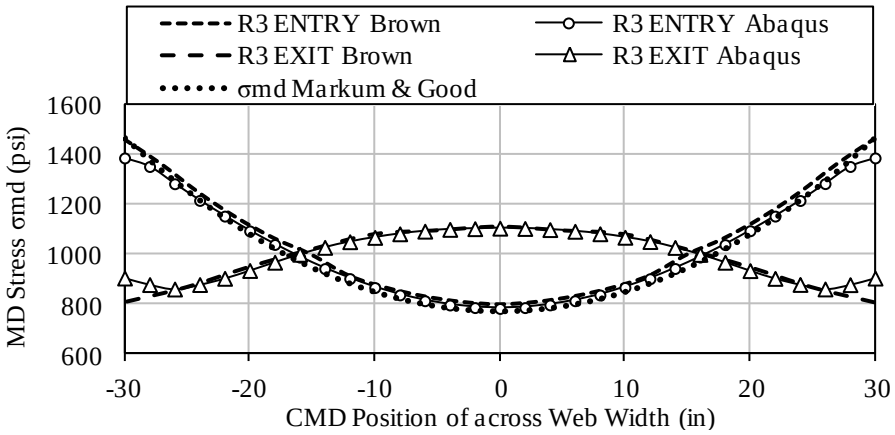

a) MD Stress Distribution for Wide Web at Entry and Exit of Concave Roller

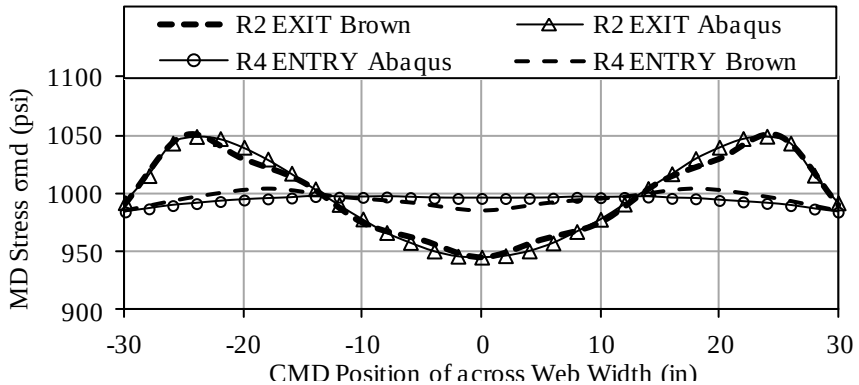

b) MD Stress Distribution for Wide Web at Far Ends of Entry and Exit Spans

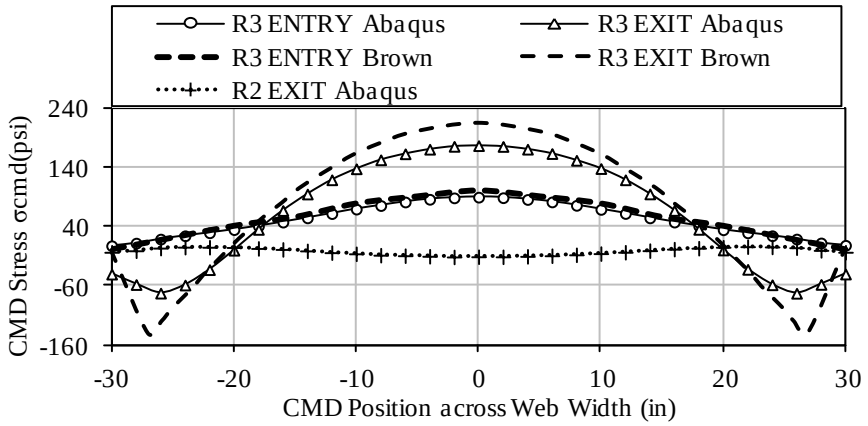

c) CMD Stress Distribution for Wide Web at Entry and Exit of Concave Roller

Figure 5.15 Stresses in Wide Web at Entry and Exit of Concave Roller (c = 0.005in) and Entry-Exit Spans

The results of the Abaqus simulations were compared with stress values communicated by Brown [5]. The modeling parameters were input to the closed form solution *(5.4)* given by Markum and Good in their paper [25]. The distributions for the MD and CMD stresses are shown across the web width in Figure 5.15. The values match very well from these two independent sources and show very similar trends. As expected the web is undergoing an MD stress reversal as it exits the wide concave roller. Though there is a change in the geometry and proportions of rollers used in each study, the pattern of stresses and Entry and Exit of roller is very similar for both web cases. The CMD stresses calculated by Browns code are slightly higher values than Abaqus presumably since he assumes no slip on the roller.

Also note the MD and CMD stresses have been shown at the exit of roller R2 which is also the beginning of the entry span of the concave roller. Often the ability of a spreader roller to spread the web is limited by the length of the entry span. The MD stress variation induced by the concave roller R3 is sufficient in this case to cause MD and CMD stress variation at the exit of roller R2. This is an example where there could have been benefit in making the entry span longer. This would have allowed uniform MD stress and zero CMD stresses at the exit to R2 and there would thus be no slippage at the exit of roller R2. Herein the focus has been to study how a concave roller affects a planar web. These devices are often used to spread webs that have laterally collapsed or compacted. Markum and Good [25] showed the spreading ability for such webs was proportional to the square of the entry span length.

5.3.3 Study of Boundary Conditions

In the development of the models for both the narrow and wide webs it has been emphasized that no kinematic boundary conditions have been enforced that would affect the lateral deformation of the web. Now the lateral deformations will be examined to determine if

some kinematic boundary conditions may be applicable. Both, the Narrow and the Wide web model results are used in this study.

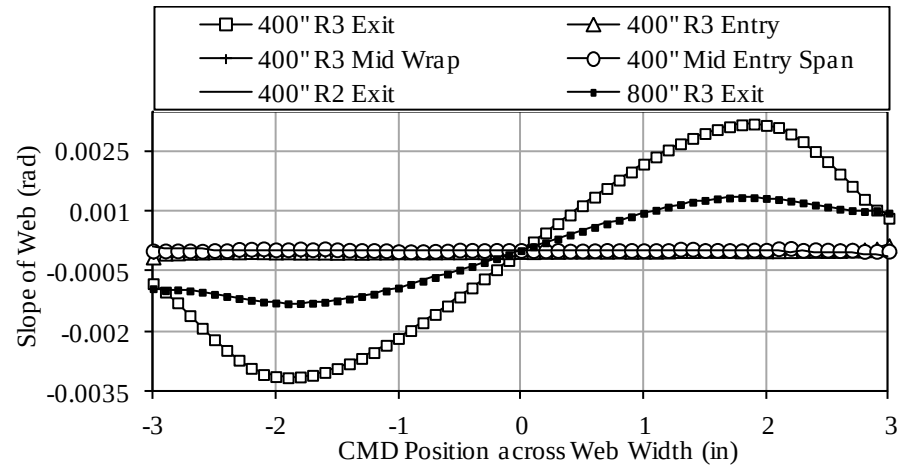

a) Slope of Lateral Deformation of NARROW Web

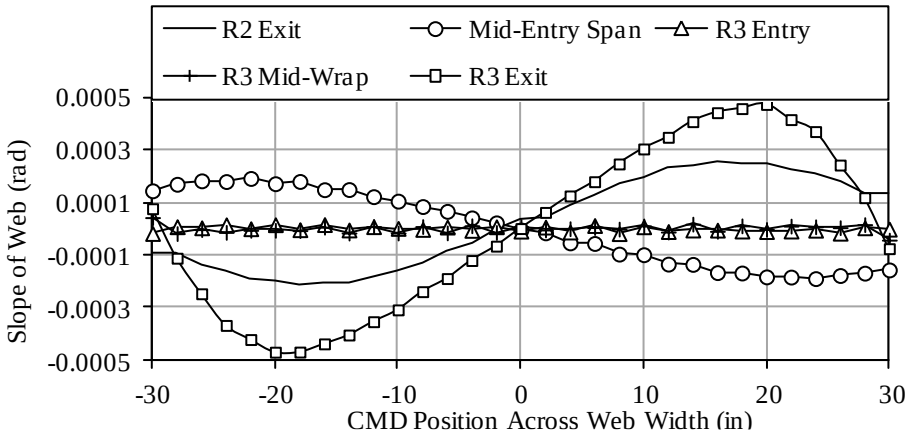

b) Slope of Lateral Deformation of WIDE Web

Figure 5.16 Comparison of Slope of Lateral Deformation of Wide Webs

For both the cases of Webs, the lateral deformations were harvested from several MD locations and the slope or derivative of those deformations were taken with respect to the MD coordinate. One focus was on the entry span to the concave roller. The slopes were evaluated across the web width as the web exited roller R2, mid span, and finally at the exit of the span where the web enters roller R3. A second focus was the web in contact with the concave roller

R3. The slope was evaluated across the web width as the web entered R3, half way through the angle of wrap and finally as the web exited R3. The results are shown in Figure 5.16.

The nature of boundary conditions of web on concave roller varies with the change in aspect ratio of web. Figure 5.16a slope of lateral deformation of narrow web is presented for the cases of concave roller studied earlier. We clearly see slope of Narrow web being zero at the exit of upstream roller R2, mid-entry span and at the entry of concave roller R3. Web enters the concave roller with zero slope and maintain the same on mid-wrap on roller. The slope of web is non zero as it is exiting roller. This slope at R3 exit is shown for two concavities of rollers namely 400 and 800 in. Again the effect of roller concavity is seen on the web slope at the exit. So for this case of combination of web properties and roller concavity, there is no slippage occurring at exit of upstream roller R2, but it is present at the exit of concave roller R3.

Figure 5.16b shows the slope of Wide web encountering a concave roller. It enters the entering span non-zero slopes, and continues with being non-zero in the mid-entering span too. The fact that these slopes are non-zero at the exit of roller R2 indicates that slippage is occurring for Wide web, probably the result of the short entry span length compared to the web width. It does appear for this case also, that Swift's normal entry boundary condition may apply at the entry of the concave roller R3 at the end of the entering span. In the same figure, the results for the Wide web on the concave roller R3 are also shown. It is clear that the slopes are near zero at the entry to R3 and mid-way through the wrap of R3. It is concluded that Swift's normal entry boundary condition [41] would be applicable for both of these particular webs, concave rollers and machine operating conditions. Note the slopes calculated as the web exits R3 are the highest seen in the simulation and indicative of the slippage occurring between the web and roller at that location.

5.4 Development of Static Model for Web on Concave Roller

The preceding sections of this chapter employed the Explicit Finite Element for studying the details of web behavior in contact with concave rollers. Through the efforts presented before, we know that the web always follow normal entry to concave roller and it sticks to roller surface till very close to its exit from roller. Though the analysis presented has proved very useful in knowing the exact boundary conditions for this type of webline behavior, it utilizes considerable computational resources in order to produce good results. The explicit analysis poses challenges in terms of requirement of high computational capability and time. The analyses presented here before were accomplished in the given time through extensive use of computational facilities available in WHRC labs. Such computational capabilities might not be possible or available for every researcher. A need has been felt to develop easy and computationally economical static codes that could be executed with the use of simple computational facilities.

5.4.1 Web Coupon with Parabolic End-Loading due to Concave Roller

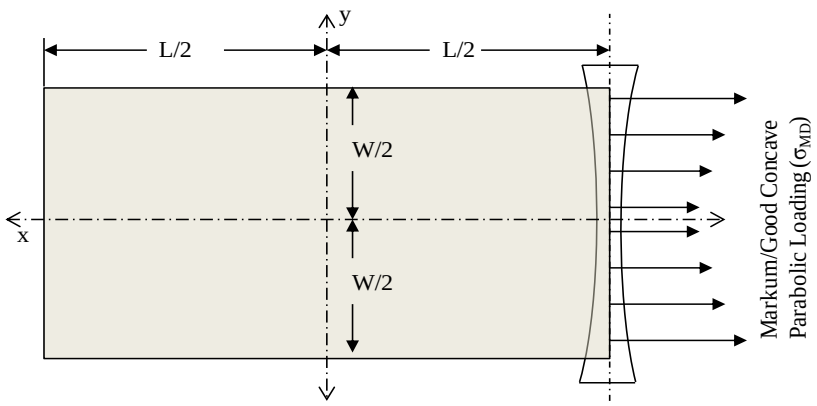

Figure 5.17 Web Approaching a Concave Roller: Static Analysis

Fig 5.17 shows a web coupon approaching a concave roller. The length and width for this coupon are nothing but the web span length (L) and the web width (W). This coupon is subjected to a parabolic loading profile due to a concave roller. This loading is a function of web line parameters and concave roller geometry. The loading expression is given by Markum and Good (Eq 5.3) for MD stress (σ_{md}) resulting due to roller concavity. This expression relates the stress at any point where the web enters the concave roller with the CMD distance (y) from the centroidal axis of web. Abaqus/Standard was utilized for studying the response of web coupon to the loading described above. The coupon is made of material properties similar to that of the web described in table 5.1.

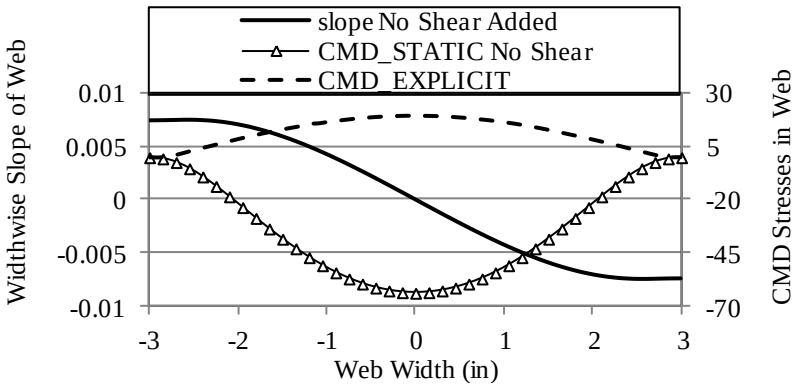

a) CMD Stresses and Slope of Web for L 18″ T 6 lb case

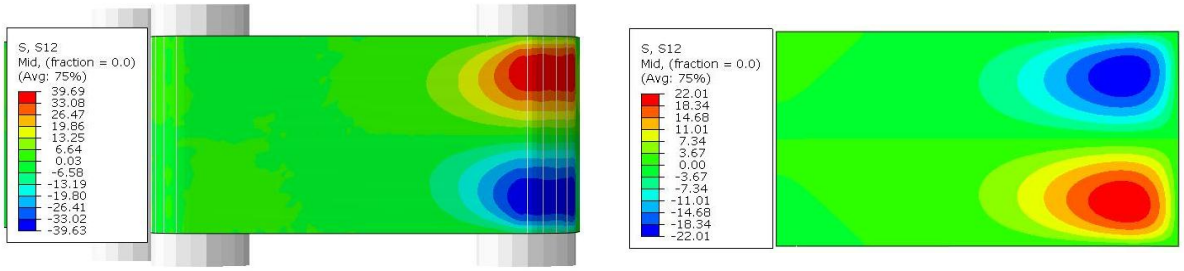

b) Comparison of Shear Stress (τ_{xy}) by Abaqus solution and the Web Coupon analysis

Fig 5.18 Discrepancies in the Results of Web Coupon Study of Concave Roller Analysis for ρ = 400” Roller, L = 18 in, T = 1pli.

Fig 5.18 shows the discrepancy in the analysis results when the coupon is subjected to a parabolic loading as described before. The result of Shear stress (τ_{xy}) in CMD directions are compared with that of successful results from Abaqus/Explicit. The shear stress shows a different distribution than that of observed in Abaqus study. One of the reason for this difference in the shear stress the normal entry boundary condition. This is evident from the calculation of slope of web elements at the point where the coupon touches roller. The slope is not seen uniform all along the entry of Coupon to concave roller. It leads to the conclusion that for the Web Coupon analysis, the normal entry boundary condition is not followed. The web is not enforced to enter the roller normally. This could be achieved by introduction of a shear force in CMD. We have the profile and distribution of shear stress available from the Explicit output. We plot this across the web width as shown in Fig 5.19. The shear stress when multiplied by web thickness (*h*) would give the shear force distribution across the web width.

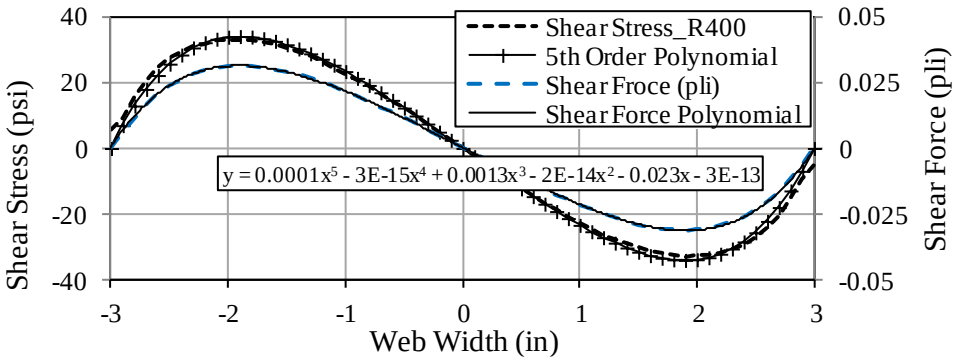

Fig 5.19 Actual and proposed closed form Shear force and Shear stress distribution in Web Entering a Concave Roller

The shear stress and hence the shear force inscribes the distribution in the form of a sine wave which is very much expected since we saw the same pattern in the Abaqus/Explicit output. The discrepancy in the nature and magnitude of slopes as well as the CMD stresses generated by the coupon was further studied. It was recognized that the differences in slope and stresses shown in Fig 5.18 could be reduced by applying an edge surface traction in a form similar to that shown

in Fig 5.19. It was found that a 5th order polynomial relating the web width (W), the distance of a particular location from web centroidal axis (y) could be established that will trace the distribution of wave form very precisely.

$$\tau_{xy} = C_1\left(y - \frac{8}{W^4}y^5 - \frac{2}{W^2}y^3\right) \qquad (5.8)$$

This 5th order polynomial is multiplied by a random constant 'C_1' which matches the waveform of the shear stress equation. The constant C_1 depends upon web parameters, roller geometry and webline conditions and is unique for every case. The shear force (F_y) can be then deduced from this shear stress format and then applied at the location where the coupon touches concave roller. When the shear force given in the eq 5.8 is applied at the end of the coupon, it enforces the normal entry of web to roller and further matches with the CMD stress distribution shown by Abaqus/Explicit study. To make this match possible, we have to reiterate the constant C1 until we achieve the normal entry of web to concave roller. The process is briefly shown here in the flowchart:

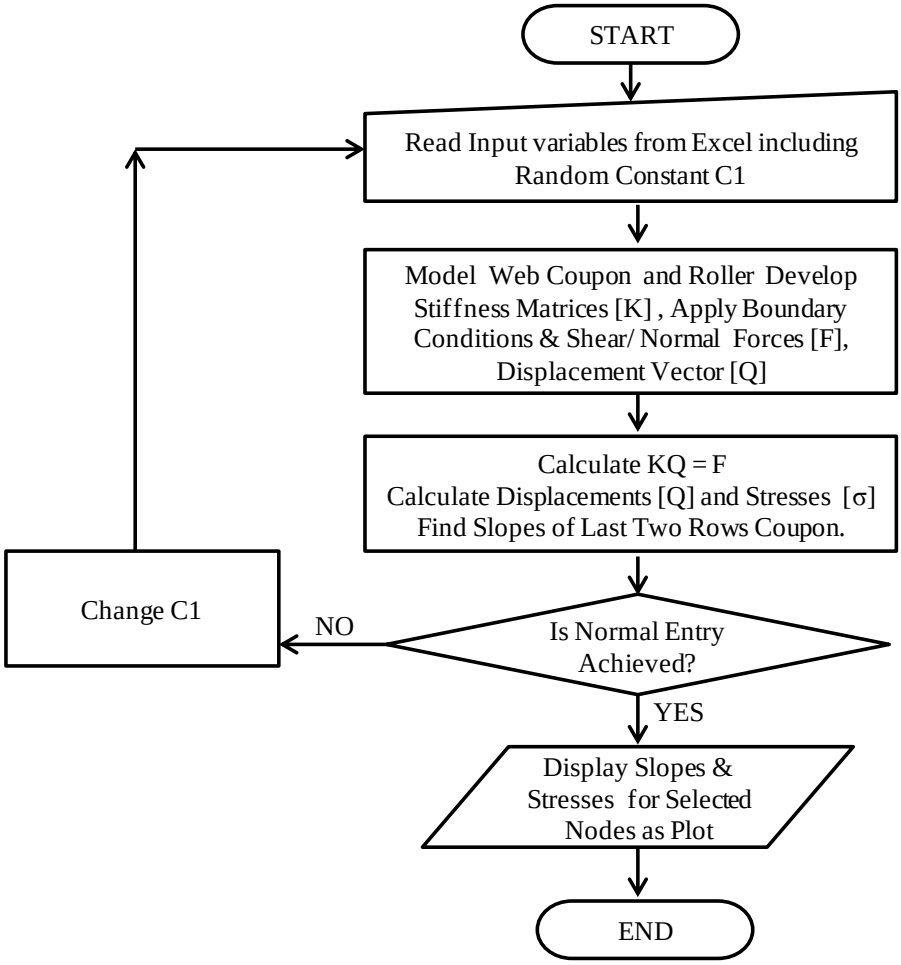

Figure 5.20 Flowchart for Static Code of Web on a Concave Roller

5.4.2 Results of Static Analysis of Web Entering Concave Roller

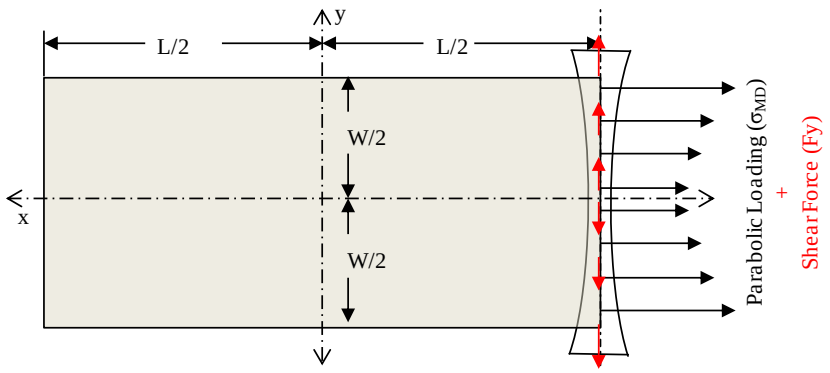

Figure 5.21 Web Approaching a Concave Roller: Enforcing Normal Entry

When the shear force is applied to the end of the coupon, the web achieves normal entry to roller. It is evident form the output of slope calculated at the last row of elements touching the roller. Moreover, the shear stress distribution and hence the CMD stress distribution in the coupon looks very much similar to that of the Abaqus/Explicit study. Fig 5.22 represents the comparison of CMD stresses induced in the web coupon as that of the Abaqus/Explicit study described in the earlier sections of this chapter. It also represents the slope calculations for the last row of elements of the coupon where the web is entering the concave roller. Fig 5.22(a) shows satisfactory agreement between the CMD stresses produced by the static code and explicit analysis, though time and resources required by the earlier techniques are least compared to the later one. Fig 5.22(b) is a plot of CMD slope of web entering the concave roller.

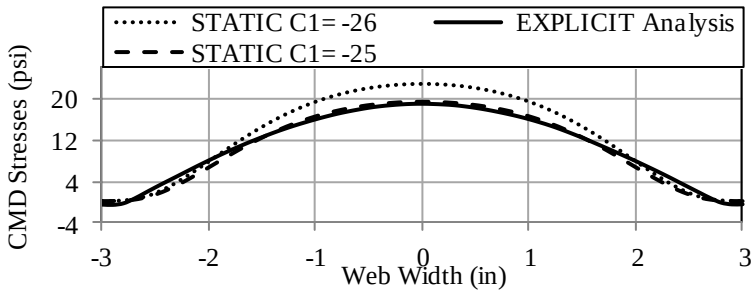

a) Comparison of CMD Stresses in Web for L 18″ T 6 lb case

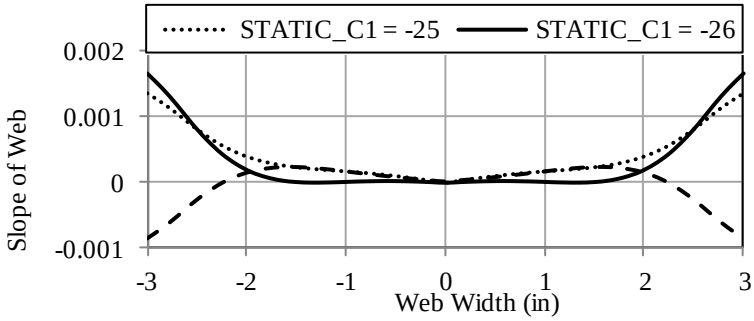

b) Comparison of Slope of Web at roller entry for L 18″ T 6 lb

Fig 5.22 Static Analysis results for L 18" T 6 lb case

This slope appears to be non-zero within approximately one inch of area of web width near its edge. This non-zero slope is practically insignificant since the main concern here being the prediction of the CMD stresses. These CMD stresses are generated in the central part of web

width where we see a satisfactory behavior of web following the normal entry boundary condition. The shear stress addition to parabolic end loading to the coupon has successfully enforced a normal entry of web to the roller. This kind of analysis is computationally very cheap compared to that of explicit analysis presented in the preceding sections which takes a lot of time and computational power to yield results. Nonetheless, the Abaqus simulations are valuable here in exploring the boundary conditions that should be applied to the static coupon for correct execution and analysis.

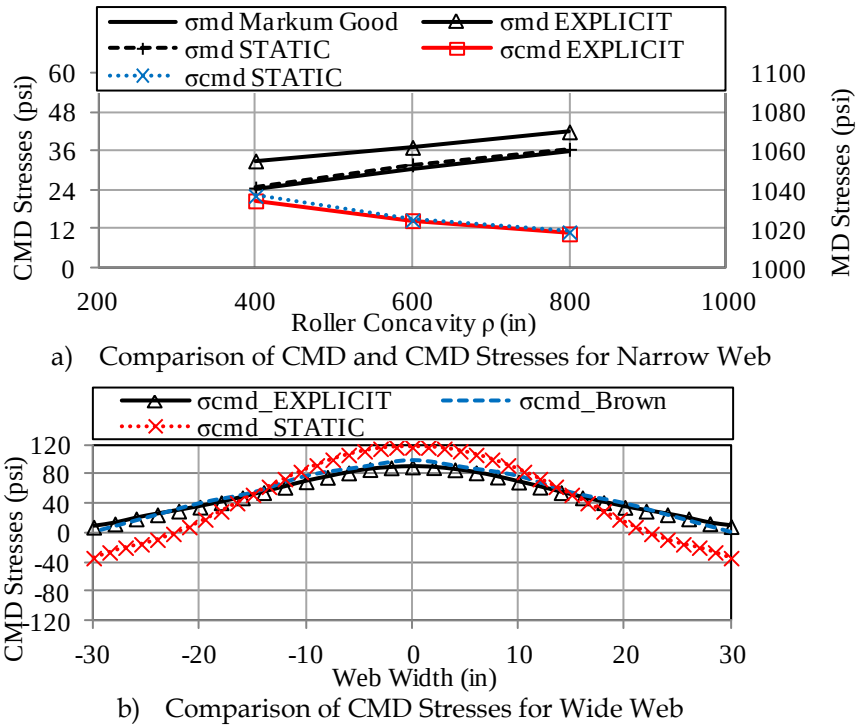

Fig 5.23 Comparative Study of MD and CMD Stresses

Fig 5.23 presents a comparative study of MD and CMD stresses developed by all three techniques for narrow web case. We see satisfactory agreement between the values of stresses in comparison. We see some disagreement in the values at the edges but this is not major concern since the tensile stresses are developed in the central part of web and we see satisfactory performance of static code in this area.

CHAPTER VI

FINITE ELEMENT ANALYSIS OF WEBS ON CROWNED ROLLERS

Crowned rollers have exactly opposite geometry as that of a Concave roller. It has higher diameter at the center compared to both ends of the roller. This gives a parabolic profile to roller surface. It could be flat at center and parabolic/tapered towards edges or any combination. First known use of such device was Belt-Pulley system. The earliest references (as old as the beginning of 20^{th} century) are found in literature from the time of industrial revolution for power transmission by belts where crowned pulleys were used to stabilize the belt running over it. One of the important work is by Swift [41, 42] where he explained very basic mechanism of Belt over a pulley. While stating his normal entry rule, he explained the reason a belt climbs over pulley-crown. Based on experiments, he developed guidelines and templates for the amount of crown or taper required on the pulleys (*rollers*), to control the wear and tear of belt (*web*). Unlike belts, webs are much thinner and have very less buckling resistance to compressive CMD stresses. Whenever a web is made to run over crowned roller, the crowned profile generates compressive stresses in web. If these compressive stresses pass beyond critical values CMD stress σ_{ycr}, instabilities in the form of troughs and wrinkles are generated in web. Extensive experimental work and initial finite element modeling was carried out by Beisel [1] where he performed trough tests with a variable crown roller that he designed and built at WHRC labs. He carried out wrinkle tests with a set of crowned rollers designed to generate a wrinkle for given webline properties. He

then presented FEM analysis of web approaching a Crowned Roller. We still do not have a robust closed form expression that links the roller crown and web properties with generated compressive CMD stresses.

6.1 Web Behavior on Crowned Roller

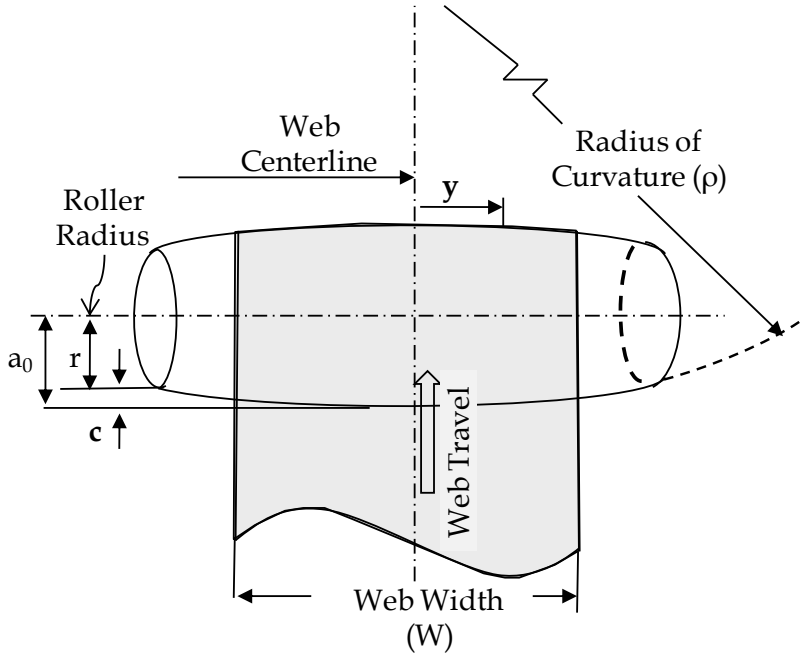

Figure 6.1- Nominal Geometry and Configuration of Crowned roller

The geometry of a web moving over a crowned roller is shown in Figure 6.1. The origin of coordinate system is located at center of roller where the center line of web and roller intersect. A variation in surface speed across the width of web results from the change in radius of roller. We assume the web material to confirm roller surface, which is *no slip* condition between the web and roller. The change in diameter across width of roller causes variation in surface speed across the Web width (W). This results in more tension at the center than edges of web, which is replaced by equivalent tensile force and moment at the centroid of Web. The only way to get the web back to *normal entry* is by superposition of an inward lateral force, causing the gathering of web. Hence a crowned roller is known as a web-gathering device.

6.1.1 Strain Energy Method for Analysis of Webs on Crowned Roller

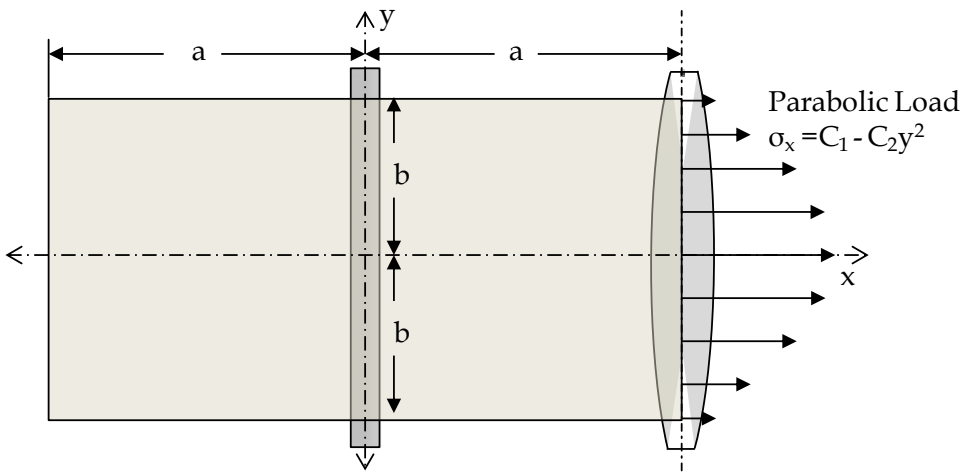

Figure 6.2 Rectangular Plate Subjected to Parabolic Edge Loading

The problem of a rectangular plate submitted to parabolic edge loading is being analyzed by Timoshenko and Goodier [44]. They solved this problem using Principle of Least Work and Airy's Stress Function. The rectangular plate of dimensions *2a X 2b* and unit thickness was subjected to a parabolic edge load in the form $\sigma_x = C_1 - C_2 y^2$ Where C_1 and C_2 are due to web tension and roller crown, *y* is the distance of given point from centroid of web. $\tau_{xy} = \sigma_y = 0$ was assumed at top and bottom edge. Further $\tau_{xy} = 0$ for the left and right end of plate. The strain energy was calculated as

$$V = \frac{1}{2E}\int_{-b}^{b}\int_{-a}^{a}\left[\sigma_x{}^2 + \sigma_y{}^2 - 2\upsilon\sigma_x\sigma_y + 2(1+\upsilon)\tau_{xy}{}^2\right]dxdy \qquad (6.1)$$

It was further assumed for the given boundary conditions that υ = 0, to simplify the problem. A stress function that satisfies these conditions is then found in the form

$$\phi = \frac{1}{2}C_1y^2 - \frac{1}{12}C_2y^4 + \left(x^2 - a^2\right)^2\left(y^2 - b^2\right)^2\left(\alpha + \beta\cdot x^2 + \gamma\cdot y^2 + \delta x^4 + \varepsilon y^4 + \xi x^2y^2\right) \qquad (6.2)$$

The constants *α, β, γ, δ, ε, and ζ* could be determined by minimizing the energy. The stresses are then obtained as

$$\sigma_{xx} = \frac{\partial^2 \phi}{\partial y^2}, \quad \sigma_{yy} = \frac{\partial^2 \phi}{\partial x^2} \quad \text{and } \tau_{xy} = \frac{\partial^2 \phi}{\partial x \partial y} \tag{6.3}$$

With given boundary conditions explained before, we get tensile CMD stresses on roller and zero shear stresses where the web enters the crowned roller. This kind of behavior of web on crowned roller is not what was seen by Beisel in experiments and contradicts with reality. It points out a flow in assumed boundary conditions, especially for shear stress at edges on roller needed to be altered for this approach to fit the case of web on a crowned roller. Further, a suitable stress function is needed to dictate stresses combined due to the effect of MD tension and roller crown profile together.

6.1.2 Matrix Structural Analysis of Webs on Crowned Roller

Another effort so as to explain the gathering of web could be with the help of matrix structural analysis. As shown in Figure 6.3, it is assumed that web can be analyzed as two separate beams of width *W/2* each, that will be steered inward by crowned roller. Given the properties of the web and roller profile, assuming normal entry of the web to the roller, considering only elastic stiffness, the machine direction stress σ_{md} can be related to the strain in the web by using Hooke's law as:

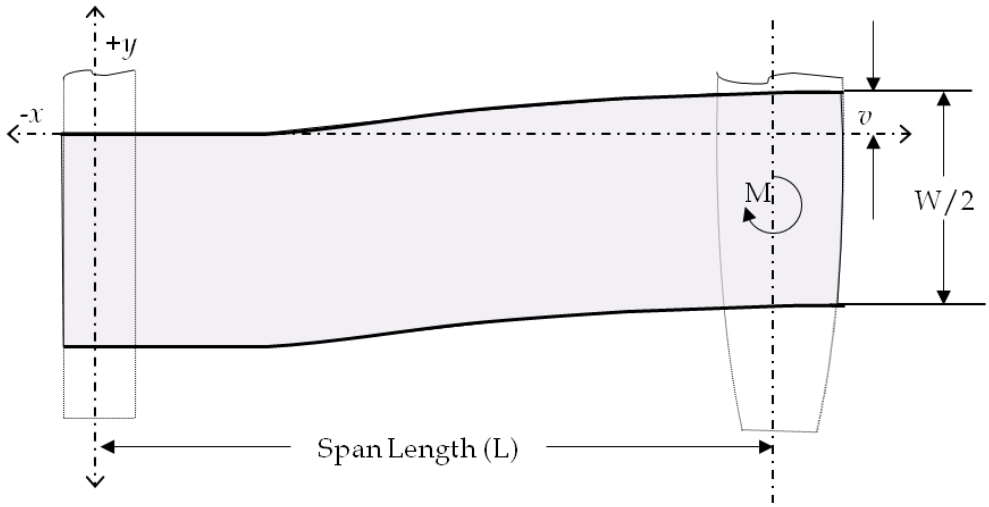

Figure 6.3 Crowned Roller as a Web-Gathering Device

$$\sigma_{md} = E\varepsilon_{md}(y) \tag{6.4}$$

Where, *E* is Young's modulus and *y* is the distance of given point from the centroidal axis of web. Assuming that the web remains in contact with roller and moves with the same velocity as roller with which it contacts, the web velocity $(V_{(y)})$ is simply the roller surface velocity which is the roller radius *(r)* time rollers angular velocity (ω). Hence the strain imparted to the web is solely related to the profile of roller as

$$\varepsilon_{md}(y) = \frac{V_{(y)} - V_{avg}}{V_{avg}} \tag{6.5}$$

Now, the velocity could be derived in terms of roller profile coefficients as:

$$r = a_0 - a_1 y^2 \tag{6.6}$$

So, the velocity is

$$V(y) = (a_0 - a_1 y^2)\omega \tag{6.7}$$

Where, a_0 is crown roller radius at intersection of web-roller centerline as shown in Figure 6.1 and a_1 is parabolic roller profile coefficient. The average velocity of web in contact with roller could be obtained by integrating the velocity given in equation *(6.7)* across half the web width

$$V_{avg} = \frac{1}{W}\int_{-W/2}^{W/2}(a_0 - a_1 y^2)\omega dy = \omega\left(a_0 - \frac{a_1 W^2}{12}\right) \qquad (6.8)$$

Substituting equations (6.8) and (6.7) into (6.5) yields,

$$\varepsilon_{md}(y) = \frac{a_1 W^2 - 12 a_1 y^2}{12 a_0 - a_1 W^2} \qquad (6.9)$$

Using above equation in equation (6.1) adding the stress due to MD tension *(T)* gives the total MD stress across the web width due to roller crown as

$$\sigma_{md} = E\frac{a_1 W^2 - 12 a_1 y^2}{12 a_0 - a_1 W^2} + \frac{T}{h} \qquad (6.10)$$

Where *h* is the web thickness. To find the moment generated in half the web width, this stress distribution is integrated over *W/2* with the *y* coordinate transformed to the half width coordinate y_c

$$y = y_c + \frac{W}{4} \qquad (6.11)$$

$$M_{centroid} = \int_{-W/4}^{W/4}\sigma_{md}\, y_c\, h dy = \frac{-Ea_1 t W^4}{16(12a_0 - a_1 W^2)} \qquad (6.12)$$

Narrow webs are analyzed as a classical beam to incorporate the tension stiffening effect on lateral behavior of webs on roller. The tension and web properties add more rigidity to web reducing the amount of lateral deflection (v_j) of web on roller. This could be studied with the

help of matrix structural analysis of stiffened beams. The stiffness matrix given by Przemieniecki [28] is referred to get the following condition:

$$v_j = \frac{M_{centroid}}{-\left(\frac{6EI}{L^2} + \frac{T}{10}\right)} \tag{6.13}$$

Substituting value of $M_{centroid}$ in above equation and assuming half web width would carry half the web tension, we get expression for deflection of half web span on a crowned roller as

$$v_j = \frac{5Ea_1tW^4L^2}{(12a_0 - a_1W^2)(5EtW^3 + 4TL^2)} \tag{6.14}$$

Again from the matrix given for tensioned beam, we have

$$F_{yj} = \left(\frac{12EI}{L^3} + \frac{6T}{5L}\right)\left(v_j\right) \tag{6.15}$$

Using T/2 for half web span,

$$F_{yj} = \frac{(5EtW^3 + 24TL^2)}{8L}\left(\frac{Ea_1tW^4}{(12a_0 - a_1W^2)(4TL^2 + 5EtW^3)}\right) \tag{6.16}$$

This is the amount of shear force imparted by roller crown and web tension on half the web span when the given web encounters a crown roller. It will generate compressive stresses in web that will induce buckling in the form of troughs or further, wrinkles depending upon the magnitude of developed compressive stresses. Timoshenko [43] developed a buckling criterion for shell that was later proven useful in predicting when a wrinkle will form of a roller by Good *et al* as

$$\sigma_{ycr} \approx -\frac{\pi h}{L}\sqrt{\frac{\sigma_x E}{3(1-\nu^2)}} \tag{6.17}$$

Where σ_x is the MD stress in web due to web tension. If the compressive CMD stresses in web get more negative than this value, troughs are expected in web span. There are no direct means of measurement yet known to measure these negative CMD stresses in webs interacting with a crowned roller.

We have trough and wrinkle data available from Beisel's experiments that is documented in his PhD Thesis [1]. He designed and created an adjustable crowned roller so as to examine web behavior for various levels of roller crown. The roller inner diameter had a stepped profile from inside that was thicker at the roller edge and thin at the center. It could be pressurized with a grease gun to vary its crown at the center. Grease was used to pressurize the roller shell due to its non-compressibility. In combination of the variable crown roller, Beisel used different tension levels and span lengths for his experiments. He observed a small dependence on span length and a greater dependence on web line tension for his trough data. This is due to the nature of plate buckling criteria as shown in equation *(6.17)*.

6.2 Modeling of Adjustable Crown Roller

The adjustable crown roller gains the parabolic profile from pressure of grease inside it. Beisel attributed various pressure levels with the generated crown profiles on the adjustable crown roller in his thesis. It was necessary to have exactly the same profile modeled in Abaqus to generate similar web behavior in the given web line conditions. We extracted the data of profiles for different pressure levels from Beisel's thesis and converted it in mathematical format so that we can get similar points to recreate the same profile in Abaqus. Figure 6.4 displays the resulting relative profiles and the mathematical curve-fit profile for representative pressure levels. These representative pressure levels were selected from the experiments Beisel conducted to study effect of roller crown on troughs and wrinkles formed in given web line conditions.

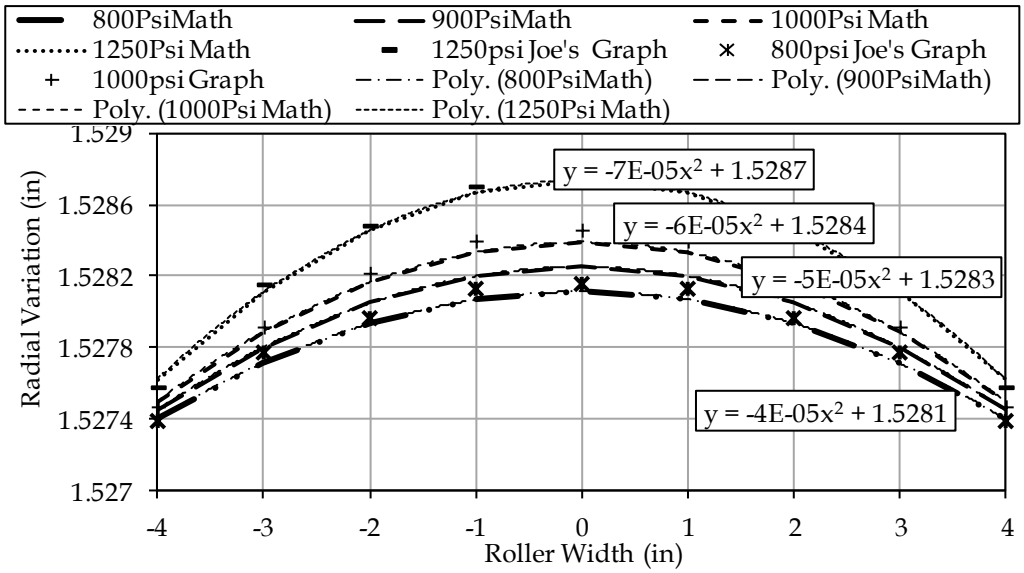

Figure 6.4 Mathematical Conversions of Adjustable Crowned Roller Profiles

Experimental results obtained through the use of adjustable crown roller by Beisel are classified as Trough formation and Wrinkle formation results. We aim to model both these cases so as to understand the web behavior on crown roller and formation of machine direction troughs and wrinkles due to roller crown.

6.2.1 Trough Formation due to Roller Crown

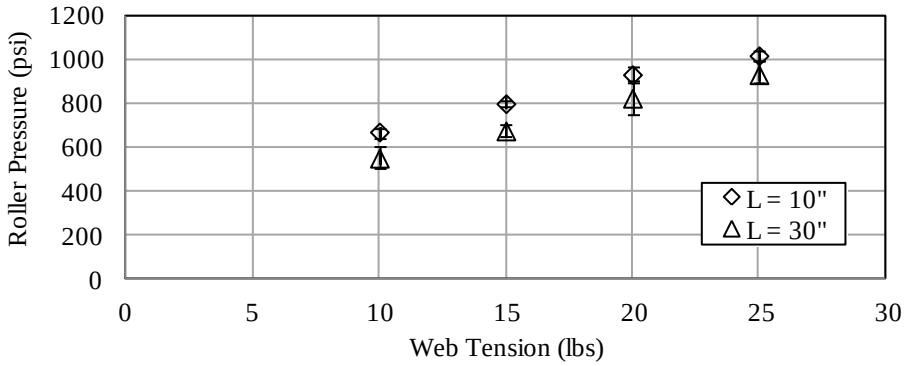

Figure 6.5 Beisel's Crowned Roller Data for Troughs Generated due to Roller Crown

Figure 6.5 represents Beisel's experimental data where he studied effect of roller crown on trough formation in given webline condition. His experiments consisted of bringing the pre decided web line tension followed by slowly increasing the internal roller pressure of variable crowned roller. The increase in internal pressure changed the convexity of roller profile causing roller to form a crown. This crown imparted instability at the end of webline causing troughs in web. Web line condition and internal roller pressure were recorded as soon as a trough was seen in the web span.

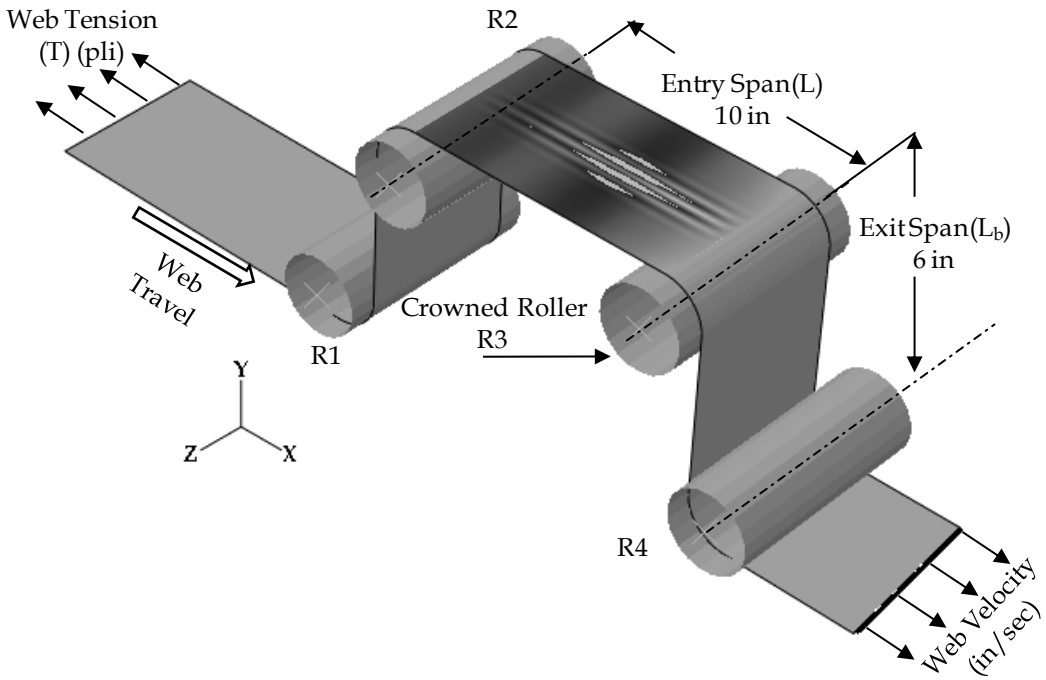

Figure 6.6 Crown Roller Model Setup and Trough Formation in Entering Span

Every Abaqus model constructed here have fixed values of parameters such as roller crown, webline tension and webspan. It is not possible to change the roller crown as it was done in the experiments considering the computational limitations of simulation. As explained in the earlier chapter, it was realized that web length equal to three times that of the web span is required to travel through the considered web line setup so as to achieve steady state and hence better converged results. Since definite point of trough formation is not known in terms of amount of web travel and time, separate model is constructed for each tension level studied by Beisel. It was further realized from the documentation that for the given tension value, there is not much difference in the amount of crown required to generate trough for both (i.e. 10" and 30") span-length *(L)* conditions considered in Beisel's experiment. Other webline conditions and modeling parameters are given in table 6.1

Property	Value
Web Width *(W)*	6 inch
Web Thickness *(h)*	0.00092 inch
Young's Modulus *(E)*	712000 psi
Poisson's Ratio *(υ)*	0.3
Entering Span to concave roller *(L)*	10 inch
Pre-entering span *(L_a)*	6 inch
Roller Radius *(r)*	1.45 inch
Wrap Angle *(β)*	90 degrees
Web Velocity *(v)*	0.5 inch/sec
Coefficient of Friction *(μ)*	1

Table 6.1: Parameter Values of Trough Formation Model for Adjustable Crown Roller

The crowned roller is modeled in the third position (R3) of the typical four roller setup shown in Figure 6.6. Rollers R1, R2, and R4 are cylindrical rollers with a nominal radius of 1.45 in. The radius of crowned roller is described per the method explained in earlier section of this chapter where the roller radius is prescribed by ($r = a_0 - a_1 y^2$) where, a_0 is crown roller radius at intersection of web-roller centerline as shown in Figure 6.1, a_1 is parabolic roller profile coefficient and *y* is CMD coordinate measured from the center location of the roller. The results presented here are from a model of crowned roller resulted by the profile of 800psi pressure, 10in of span length and several webline tension levels.

6.2.2 Mesh Convergence Study

The computational time and resources needed for executing every successful simulation greatly depends on mesh refinement. Reduction in the size of smallest element increases number of elements to be handled during given analysis causing additional time for job execution. Sufficiently small element size is needed to accurately define contact mechanics underlying the interacting surfaces. This is particularly important when cylindrical objects such as rollers or shells such as web on roller are being modeled. Finalizing optimum mesh size involves correct dimensioning and types of elements, suitable computational cost analysis and material properties.

A convergence study is presented here to explain the selection of mesh size based on optimum combination of accuracy and computational cost.

The initial modeling efforts involved modeling of web as membrane with element size of 1/4 inch. General purpose membrane elements were used since the deformation of the web on crowned roller can evolve in three dimensions. We used M3D4R (4-noded quadrilateral, with reduced integration and hourglass control) element for this study. For the convergence analysis, different sizes of mesh were considered and its effect on the quality of results is verified. Figure 6.7 displays a chart of MD stresses induced at the entry of crowned roller using different size membrane element for model. These stresses are generated by a crowned roller that has similar profile of Beisel's adjustable crown roller at 800psi pressure level. A 10" entering span with web tension of 15 lbs is used for all cases considered during this particular study. These MD stresses are compared with the model proposed earlier in equation *(6.10)*. In the same chart also shown on secondary axis, is the out of plane *(U2)* deformation of web in entering span.

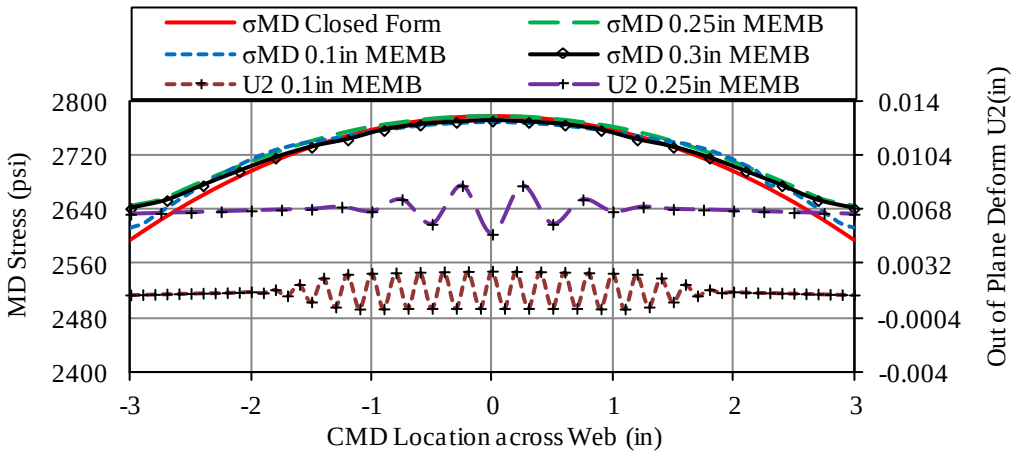

Figure 6.7 MD Stress and Out of Plane Deformation of Web for 800psi Crowned Roller in 10 in Webspan and 15Lb Web Tension with Different *Membrane* Mesh Sizes.

As expected, we have reached a better agreement with the closed form solution by using finer mesh. Though all sizes of mesh yield similar result for MD stresses at roller center, the difference

is at the edge where actual strains are supposed to be realized. The MD stresses exhibited by 0.1 in mesh are quite satisfactory, when stress distribution is concerned.

During his experiments, Beisel used visual appearance of trough in web span as a mean to deduce the formation of troughs for the given combination of web properties and webline parameters. We use the out of plane deformation *(U2)* of web across the web width as a measure to see if a trough is formed in the given span or not. The wavelength *(λ)* of the trough formed as a result of shear force at the end of web span can be predicted using the equation given by Beisel *et al* [2]

$$\lambda = \frac{2L}{\sqrt[4]{1+\frac{\sigma_x}{\sigma_e}}} \quad \text{Where} \quad \sigma_e = \frac{\pi^2 D}{L^2 h} \quad \text{and} \quad D = \frac{Eh^3}{12(1-\nu^2)} \qquad (6.18)$$

For the given web line parameters *(E=712Ksi, L=10", T=15 lbs)* and crown roller properties, above expression yields a wavelength value of 0.75". The wavelength that is plotted by membrane elements in figure 6.7 looks different. The reason for this is the nature and behavior of membrane elements in Abaqus. These elements are surface elements that transmit only in-plane forces and hence, no moments. As a result of this behavior they do not have bending stiffness, and so is evident from the wavelength shown by both, 0.1" and 0.25" size mesh. For this reason we use shell elements for further study and the convergence of using shell elements to model webs will be studied further.

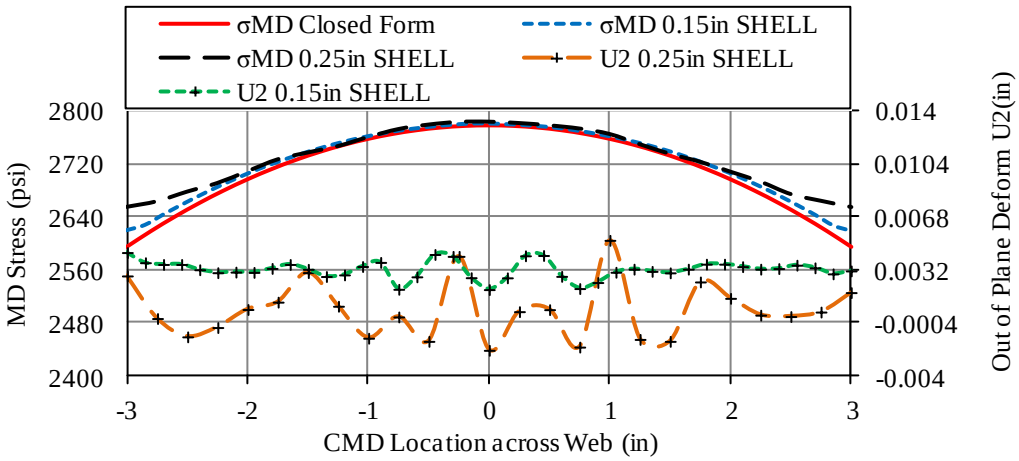

Figure 6.8 MD Stress and Out of Plane Deformation of Web for 800psi Crowned Roller for 10 in Webspan and 15Lb Web Tension with Different *Shell* Mesh Sizes.

The shell elements used in analysis for this study are S4R (4-node doubly curved general-purpose shell, reduced integration with hourglass control, finite membrane strains) elements. The least size of shell elements used in Figure 6.8 is 0.15". Unlike the 0.1" membrane case, simulations of shell elements of same size required quite a bit longer time for execution of the same job. The feasible option is to increase the elements size. It looks like we can achieve acceptable agreement for the wavelength *(λ)* by using 0.15" shell elements. Hence further studies of trough analysis will have a shell element size of 0.15 inches. Table 6.2 presents the computational aspect of simulations ran with various sizes of shell elements for the case of 800psi crowned roller with 10" web span and 15 lbs of web tension.

Elements /inch (Size Shell)	**Number of Nodes**	**Number of Elements**	**Total Time Required**	**Stable Time Increment**
3 (0.3" Shell)	4540	4308	3 Hrs	3.253×10^{-5}
4 (0.25" Shell)	7454	7136	8 Hrs	2.678×10^{-5}
6 (0.15" Shell)	*23169*	*22568*	*48 Hrs*	1.628×10^{-5}
10 (0.1" Shell)	51671	50768	194 Hrs	1.085×10^{-5}

Table 6.2 Computational Details of Different Sizes of Shell Elements

Figure 6.9 presents a study carried out to examine convergence of the models for web behavior on 800psi crowned roller with 10" web span and 15 lbs web tension. It compares MD stress induced and CMD deflection of web on crowned roller. On horizontal axis, the mesh density is shown in number of elements shown per unit inch length. Primary vertical axis represents the execution time for each run in hours. Secondary vertical axis gives normalized results of values given by different sizes of shell elements. Though it looks like we achieve good accuracy for calculating the listed parameters using all sizes of mesh, the fineness of the mesh is real concerned when inscribing the wavelength is considered. The mesh is required to be fine enough so that it can mark the wavelength at least using 4-5 elements. The MD stress at the edge of web at roller entry is again compared with expression *(6.10)* which is assumed as cent percent accurate result. For all the other parameters, values given by 0.1" mesh are considered enough accurate to be assumed as 100%. The deformation of web-edge on crowned roller is converged quickly as compared to stresses. This chart confirms the use of 0.15" shell elements would be best in terms of both, the accuracy and computational cost of simulation.

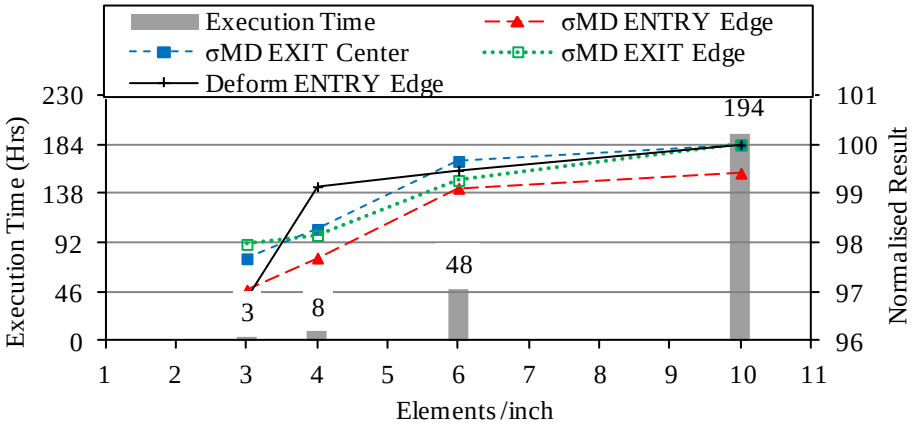

Figure 6.9 Convergence of results for MD Stress and CMD Deformation on Crowned Roller

The MD stress at entry and exit locations is shown as a function of CMD position in Figure 6.10. These stresses are compared with the model proposed earlier in equation *(6.10)*. The kind of behavior shown in

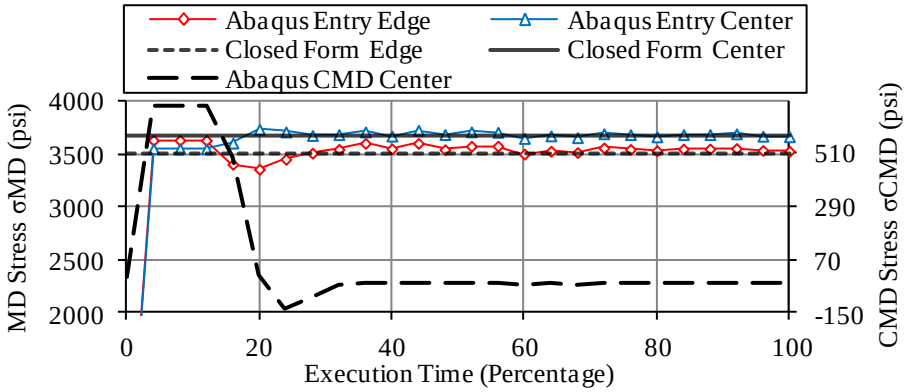

Figure 6.10 MD and CMD Stress Convergence through Execution Time for L=10", T=20 lbs Webline Condition and 800psi Crown Roller Model

charts here was very much expected from the previous experience of web encountering a concave roller. The web undergoes a reversal of MD stresses as it travels from the roller to next free span. As expected, the location of point of stress reversal occurs somewhere on the roller surface and must be accompanied by slippage. Equation *(6.10)* predicts the stresses at the entry of crowned roller very well except at the edges, which is seen with a slight disagreement which could be due to slippage. Since the model proposed is based on the no slip assumption and there is no such assumption in Abaqus analysis. Figure 6.10 shows the convergence of MD and CMD stresses along the entire execution time (expressed in percentage). The MD stresses converge faster than that of CMD stresses. The MD stresses at the center of web achieve convergence earlier than edge. Conversely, CMD stresses take longer time to converge. The Amplitude variation is exactly similar to what explained in earlier chapter through Figure 5.4. The web behavior at entry, on the wrap and after the web exits a concave roller is explained in details in previous chapter and it was seen from the Abaqus simulations that it is exactly opposite here for the case of a crowned roller.

For this fact being considered, we will not explore web behavior through the same type of charts but will continue on trough analysis in the direction Beisel has explored in his experiments.

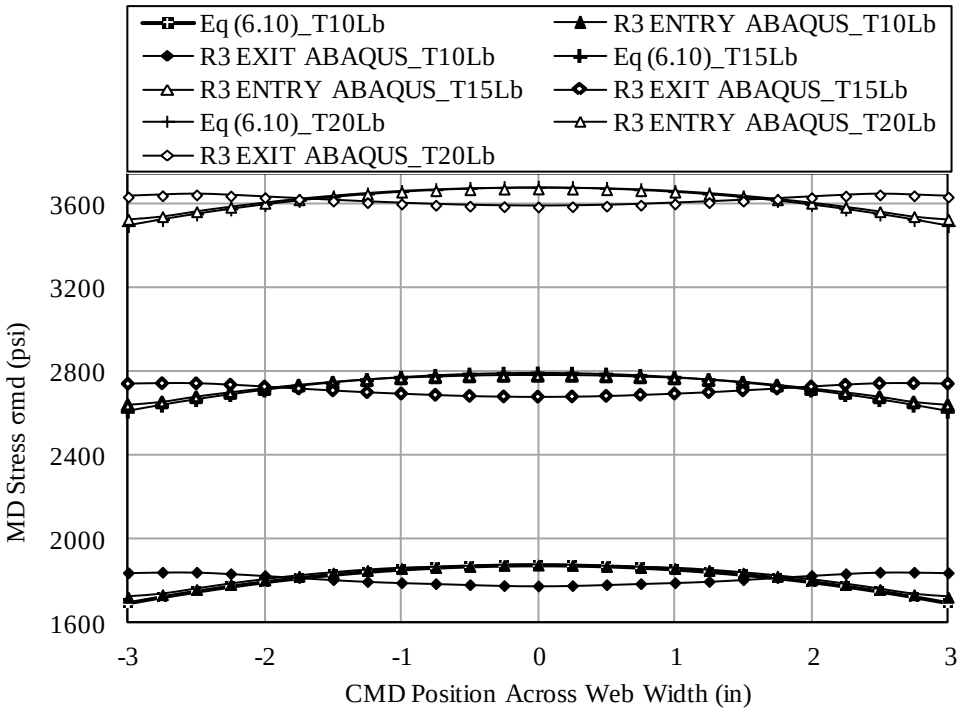

Figure 6.11 Comparison of MD Stress at Entry and Exit of Crowned Roller for Different Web Tension Values

As stated before, a crown roller imparts a shear force on the web due to a combined effect of web tension and the crown profile. Though traditionally crowned roller served as a stabilizing device for stiff belts, it might not work so with very thin webs because a very less lateral force is sufficient for a web to buckle. The compressive stresses induced due to roller crown might give rise to troughs and hence wrinkles in thin webs, depending upon the amount of roller crown and webline properties. If the compressive CMD stresses in web get more negative than the value given by buckling criteria stated in equation *(6.17)*, troughs are expected in web span. Further, the out of plane deformation of web in entering span could be studied across the web width that could be compared with the buckling equation to explore trough wavelength.

6.3 Trough Model Results and Discussion

Several Abaqus simulations were created and ran for the study of trough formation due to various levels of roller crown at different web tensions. The geometry and web line configurations of these simulations were based on Beisel's study of trough generated by crowned roller displayed in Figure 6.5. Results of all these simulations would be presented here. During this study, it was not possible to recreate exact experimental procedure as documented by Beisel, since it would be computationally very expensive to model a continuously varying crown roller profile. Instead, we have simulated each pressure level profile with difference of 100psi internal pressure in variable crown, used for every web tension case of given web line setup. All simulations have entering web span L=10".

From the data presented in Figure 6.5, it looks like Beisel saw troughs formed for 10Lb and initiated for 15 lbs due to variable roller crown at an internal pressure level of 800psi. Further it appears that no troughs were seen either initiated or formed for the same roller crown at 20 lbs and 25 lbs case. The same profile was created in Abaqus and various web tension levels were simulated for given web line conditions as shown in Figure 6.12.

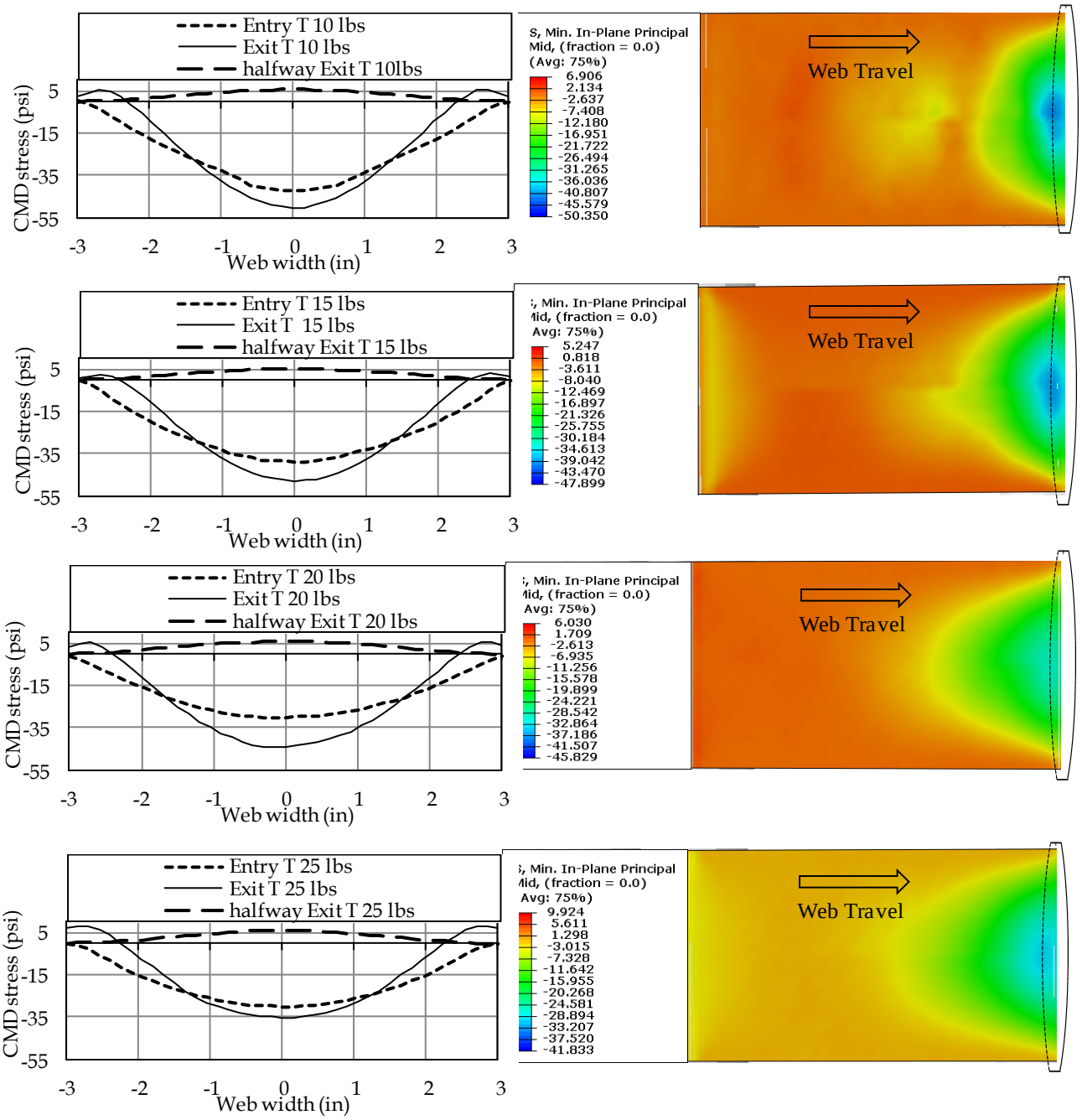

Figure 6.12 CMD Stress behavior of Web on 800psi Crowned Roller at various Tension Levels

CMD stress behavior of web due to roller crown significantly changes with change in web tension. The CMD stresses at the entry of crowned roller are most negative at the center of web. Moreover, it reduces and become less negative as the web tension is increased. Similarly the

negative CMD stress at the exit of crowned roller also reduces with increase in tension. Note the CMD stresses in the web at the exit of the roller are compressive at the centerline but become positive (tensile) as the web edges are approached where they finally decline to zero. Also, we see positive CMD stresses generated at halfway exit span (around 3" downstream) in web. Both these observations are consistent with our finding of web behavior at the exit for concave roller. The positive stress generated at the exit of crowned roller does not seem to have any effect of change in web tension.

Figure 6.12 also shows the CMD stress contour of the entering span at each tension level. In all the cases we see a 'stress pocket' developed at the end of entering span where web meets the crowned roller. This kind of behavior is congruous during all the simulations for cases considered at various pressure levels for variable crown roller. The negative stress developed at this pocket is much more negative than expected or than the buckling criteria discussed before. Beisel also found this kind of occurrence of concentration of compressive stress near the entry of crowned roller. He reconciled his experiments with FE analysis through the help of a terminology called 'effective' plate length. According to this assumption, the region of the web experiencing substantial compressive stress may be used to determine an effective plate length, which when used with the buckling criteria (equation *6.17*) for trough formation, would give close stress levels as seen during Beisel's FE analysis and our Abaqus observations. If we input the value of entering span equal to what it seem from the stress contour (around 4"), we get quite close CMD stress values by equation *(6.17)* to that of our Abaqus output.

$$\sigma_{ycr} \approx -\frac{\pi h}{L_{eff}}\sqrt{\frac{\sigma_x E}{3(1-\nu^2)}} \qquad (6.17a)$$

We further explore the out of plane behavior of web for all the above tension levels, so to see if we form troughs and the if this is coherent with Beisel's findings. Though the exact point of initiation and formation of web trough is very difficult to record, Beisel rested his conclusion of trough formation on visual observations.

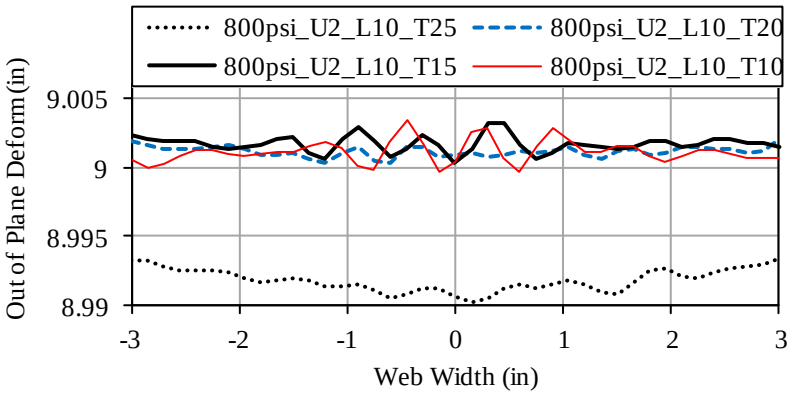

Figure 6.13 Out of Plane Deformation of Web for Various Tension Levels on 800psi Crown Roller Profile and Entering Span L=10"

Figure 6.13 shows the out of plane deformation of web just upstream to crowned roller across the web width. It appears that troughs are distinctively formed for the tension levels of 10 lbs and 15 lbs. The out of plane deformation for 20 lbs web tension appears almost flat. Though there are undulations seen for 25 lbs case, they are not definite as trough.

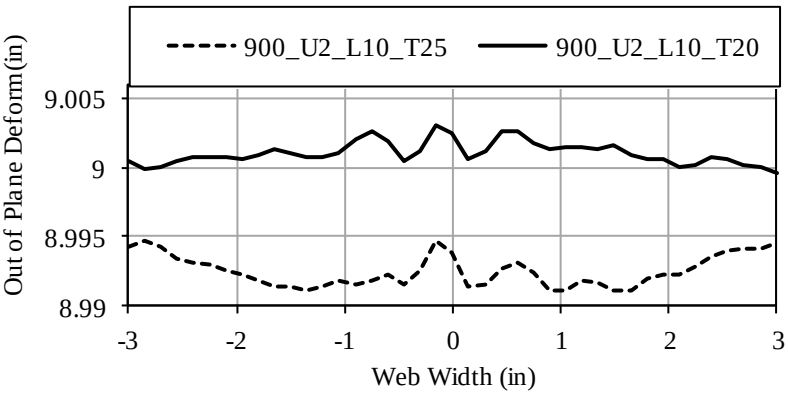

Figure 6.14 Out of Plane Deformation of Web for Various Tension Levels on 900psi Crown Roller Profile and Entering Span L=10"

Figure 6.14 and 6.15 shows the out of plane deformation of web across the web width for 600, 900 and 1000psi pressure levels for adjustable crowned roller. It appears that troughs are distinctively formed for both the tension levels of 20 lbs and 25 lbs for 900psi. Further troughs are also seen appeared for 1000psi crown roller at 25 lbs. This means for this particular case troughs are *formed* for lesser roller crown than 1000psi. Hence we conclude that troughs are *initiated* at 900psi for 25 lbs web tension value.

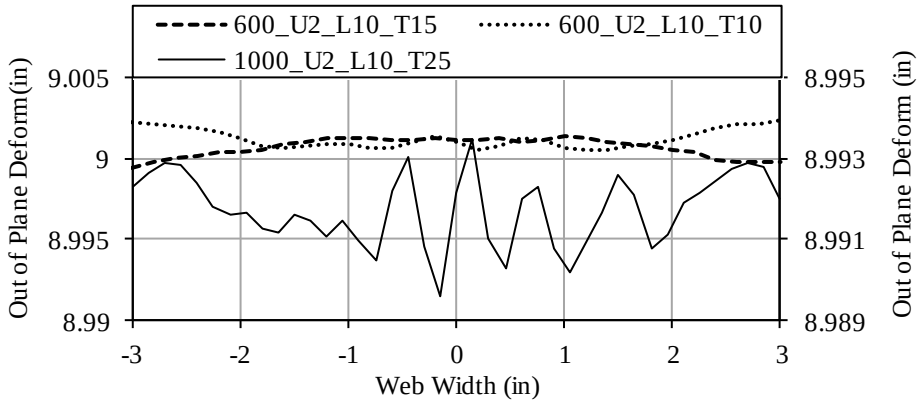

Figure 6.15 Out of Plane Deformation of Web for Various Tension and Internal Pressure Levels for Variable Crown Roller, Entering Span L=10"

Similarly, from Figure 6.13 and 6.14 considering 800 and 900 psi internal pressure cases at 20 lbs and examining it's out of plane deformations, we can say troughs are *initiated* at 800 psi pressure for web tension of 20 lbs. Concluding analogously, such pressure levels for all other cases considered by Beisel, we plot Abaqus data showing troughs generated due to various roller crowns and different web tensions. This plot is shown in Figure 6.16.

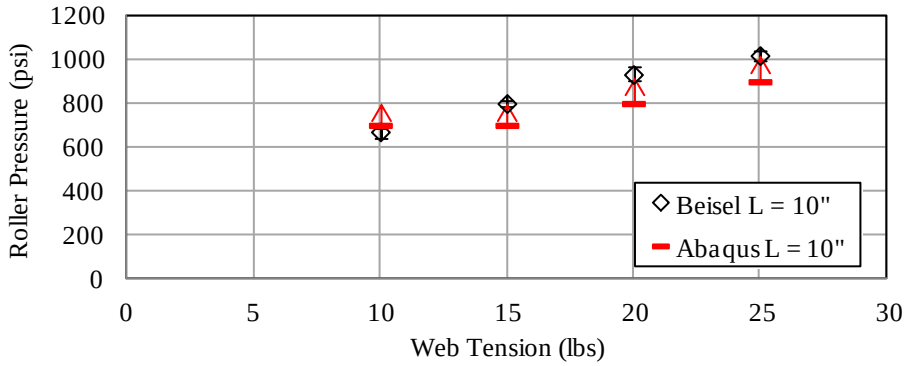

Figure 6.16 Troughs Generated at various Roller Crowns and Webline Tensions

A satisfactory agreement was observed with experimental study of formation of trough on crowned roller. For Beisel's study, the realization of the trough is *initiated* at given particular tension level was based on visual appearance. Unlike the experiments, exact out of plane deformation could be plotted from Abaqus simulations. Hence except for the case of 10 lbs web tension, the initiation point is seen at lower roller crown than compared to Beisel's value.

From the above discussion presented so far, it looks like the initiation and formation of trough in webspan due to crown roller has shown greater dependence on web tension than span length given other web properties are constant. The CMD stress behavior of web around and on the crowned roller was observed exactly opposite to our concave roller conclusions, which was very much expected. Very much like the negative (compressive) CMD stresses in the exit span of a concave roller, we saw positive (tensile) CMD stresses in exit span of crown roller. It was seen that much more negative (compressive) stresses were developed at the entry of a crowned roller than the buckling criteria of trough formation equation *6.17*(Approximately -9 psi) would have predicted for the given webline conditions.

6.4 Wrinkles Due to Roller Crown

When the convexity of a crowned roller is more aggressive, higher amount of shear force is imparted on the web running over it. This higher shear force then generates more negative stresses in web. This gives rise to the next level of instability in web-lines: *Wrinkles*. Much larger compressive stresses are required to buckle web (in the form of a shell) on roller compared to web (as a flat plate) in open spans. There is interaction between the degree of crown and trough amplitude. At a given web line conditions and friction as the roller crown is increased from zero beyond a critical value, we have the onset of toughs in a pocket in entry span. Now, we must keep increasing the crown to cause a wrinkle. While doing so, the trough length and amplitude keeps on growing. Finally the trough amplitude grows to a level that a wrinkle forms on the crown roller. Shell requires higher stresses to buckle than a plate. The web on a roller acts similar the sector of cylinder that is internally pressurized. The internal pressure is due to web tension. Timoshenko [43], developed the failure algorithm for a shell and is given by

$$\sigma_{ycr} = -\frac{Et}{R\sqrt{3(1-\nu^2)}} \qquad (6.19)$$

The same criteria can be used to calculate stresses required to wrinkle web on the roller for given webline conditions.

Experimental data of a wrinkle generated due to a roller crown for different webline conditions is available from Beisel's experiments and is documented in his thesis [1]. He calculated that the 0.006in diametric crown for 8in wide roller would definitely produce a wrinkle for a 92 ga polyester film that he used. It was further known that this wrinkle generated would be removed by increasing the tension in webline. He used the same crowned roller for different webspan values. His wrinkling tests began at high tension (which decreases trough amplitude) so as to stabilize web on roller and machine line then decreasing tension until wrinkles were seen

traversing the crown roller. This experiment was repeated several time and tension values were noted as shown in figure 6.8. It could be inferred from his chart that higher web tension is needed for generating a wrinkle in shorter web span.

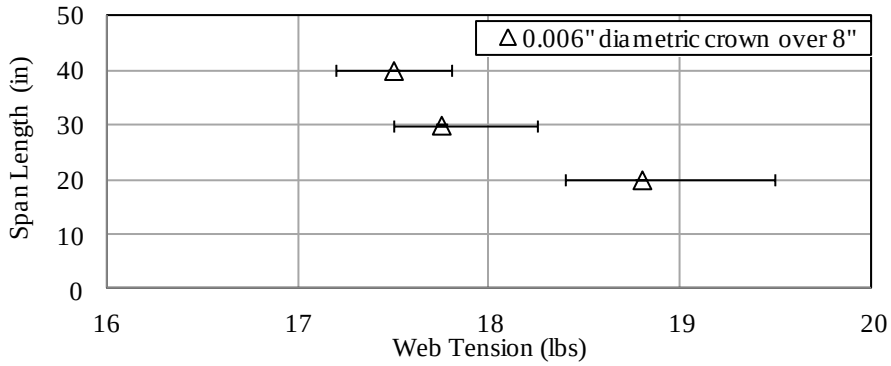

Figure 6.17 Beisel's Crowned Roller Data Showing Wrinkles Generated due to Roller Crown (R_0 = 1.5")

6.4.1 Modeling Wrinkle on Crowned Roller

The model setup for studying wrinkling due to roller crown is essentially the same as described in previous section and shown in figure 6.11. The crowned roller is modeled in the third position (R3) of the typical four rollers with a nominal radius of 1.5 in. The roller used has a diametrical variation of 0.006" implying crown roller radius at intersection of web-roller centerline (a_0) is 1.503". Other webline parameters are the same as shown in table 6.1. The mesh density for studying wrinkle behavior is a concern in presented study since it greatly affects the computational cost. Due to very high computational time, it is almost impossible to model adequately fine mesh so as to capture the buckling and folding of webs into a wrinkle. It further creates complex situations to handle for the contact algorithm that requires high computational power. It is realized that it would not be beneficial to have mesh density being determined by the wavelength of a wrinkle. The attempt of refining mesh size so as to inscribe a wrinkle formed in web requires very fine mesh. Analysis with this mesh size will take enormous amount of time to

yield results with the available resources of computations. Refining the mesh until we get convergence of the CMD stresses upstream of a roller is sufficient for this kind of study. The formation of wrinkle at given point is said to be occurred whenever the compressive stresses at that particular point equal or less negative than Timoshenko's buckling criteria given by equation *6.19* (-265psi for webline conditions considered here).

The modeling effort was started with the case of 20"web span. This being the shortest web span amongst all cases experimented, was the fastest run possible through time since the length of web needed for modeling is less, implying less number of nodes and elements. According to Beisel's documentation for given webline properties, a wrinkle should not be generated at 20lb of web tension. Further on reduction of which, a wrinkle is generated starting at 19.5lb. The least value of web tension recorded to generate a wrinkle was 18.4lb. Since there is no possibility of recreating the similar conditions of dynamic load reduction in the model, we started with 20lb web tension case. Figure 6.12 represents the CMD stresses across the web width at entry and exit of the crowned roller. It also shows the CMD stresses induced in web at mid-exit span. It is understood here that whenever stresses in web attain more negative value than the Timoshenko's buckling stresses, a wrinkle is induced. Since the wrinkle is formed at the entrance of roller, stresses at the entry of roller are of greater concern here. It looks like web leaves the crowned roller with much more negative stresses compared to the stresses at its entry to the roller.

Figure 6.18 (a) displays the CMD stresses at roller entry for the case of 20 lb web tension. It could be seen here that we do not induce enough stresses (-265psi) and hence there is no wrinkle formed which is in consistency with Beisel's experiments. Now 6.18(b) is CMD stresses for reduced tension value of 18 lb. We induce far more stresses than -265 psi for this particular tension value. These two cases give us a window of tension value and stresses induced in web at

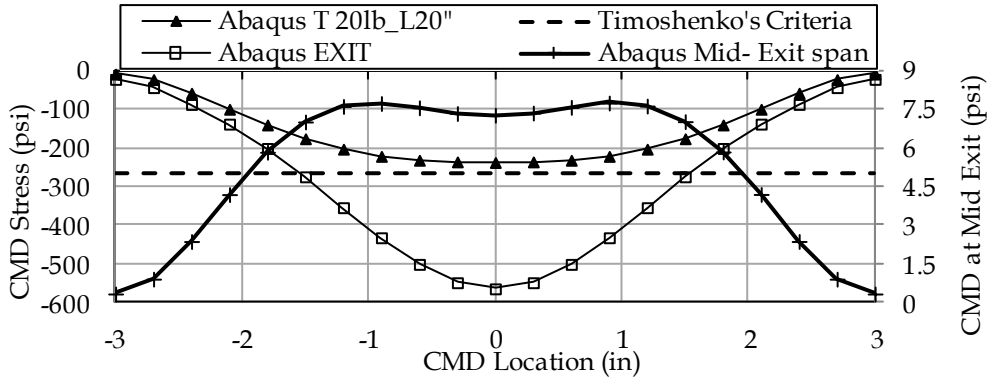

b) CMD Stresses for 18lb Web Tension

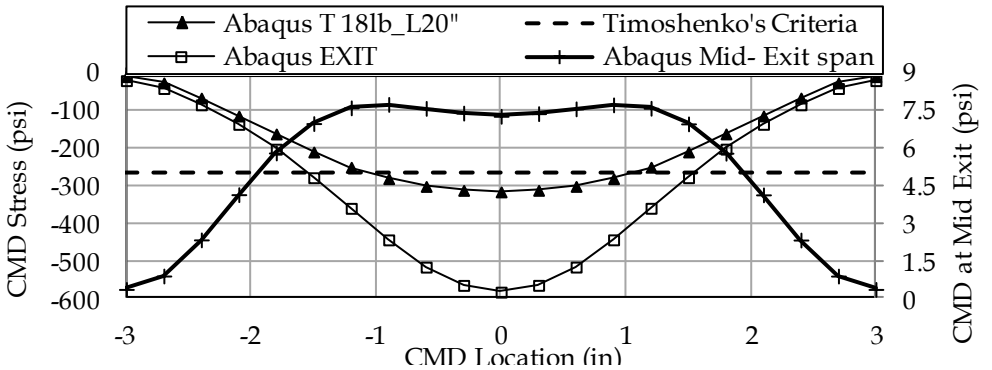

a) CMD Stresses for 20lb Web Tension

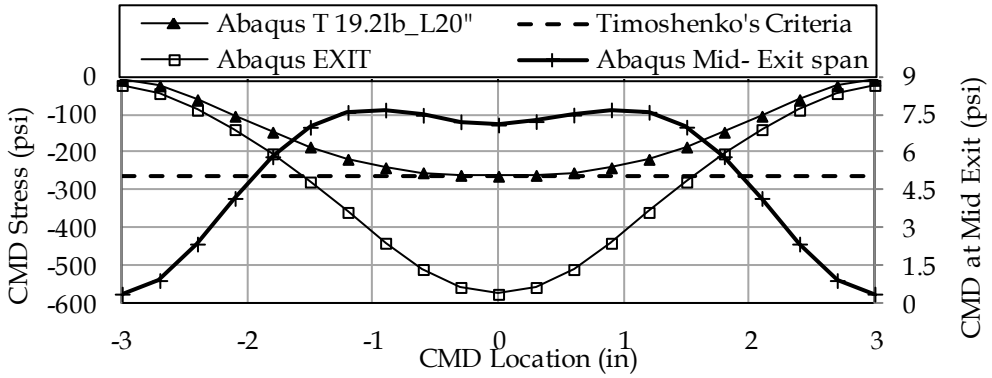

c) CMD Stresses for 19.2lb Web

Figure 6.18 Negative CMD Stresses on Crowned Roller for different Web Tension Values for 20in Entering Span (L=20")

the entry of 0.006" crown roller. We manipulated that a web tension value of 19.2 lb would just start to induce a wrinkle at the entry of roller, which is evident by stress distribution shown by figure 6.18 (c). In all the cases considered above, we have observed positive CMD stresses half way down the exit span. This is consistent with our observation of negative CMD stresses at the mid-exit span of concave roller. Not unlike negative stresses at the exit of roller, these positive CMD stresses developed in exit span does not seem to have effect of changed tension values in line.

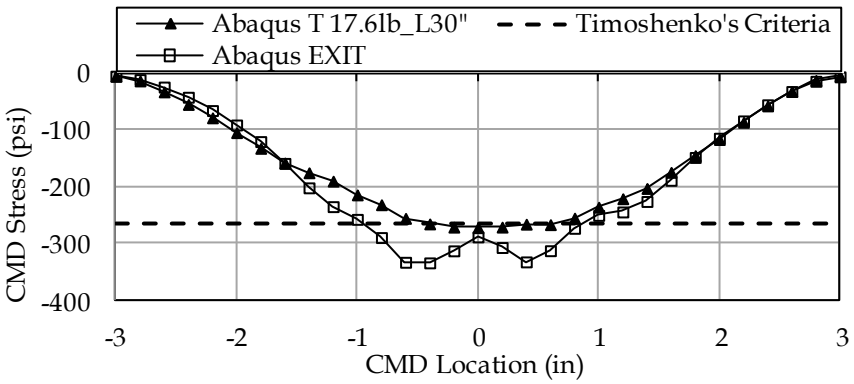

a) CMD Stresses for 17.6 lbs Web Tension, 30" Web Span

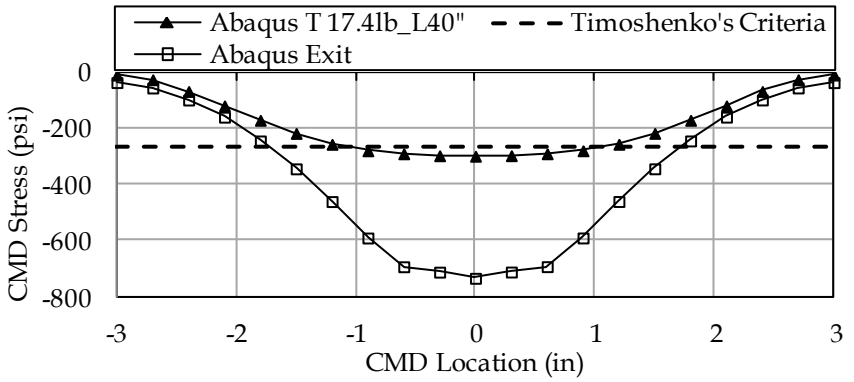

b) CMD Stresses for 17.4 lbs Web Tension, 40" Web Span

Figure 6.19 Prediction of Timoshenko's Critical Stress Value to form a Wrinkle on Crowned Roller

In the further attempts to simulate a wrinkle formed due to roller crown and given web line conditions, we modeled a case of 40" span length and T=17.4lb tension. For these parameters, a wrinkle was observed experimentally by Beisel. Figure 6.19 (b) represents the Entry and Exit CMD stresses for the exact webline conditions. The stresses are induced in simulations appear more negative than the buckling criteria. This means for the given web line conditions, according to our simulations web should buckle at stresses very near to Timoshenko's critical stress for slightly higher tension than 17.4lb. The plots presented in Figure 6.19 shows the prediction of webline parameters so as to expect wrinkle at prescribed web tension. Similar abaqus simulations were made for other webline parameters used by Beisel and the result is shown in Figure 6.19.

Unlike troughs, the wrinkles forming on crown roller show greater dependence on span length as well as tension. Abaqus simulations enable us to gather much more information about stresses and strains responsible for wrinkles. This should be helpful in deciding guidelines as when a wrinkle would be formed due to roller crown for the given webline conditions. With these datasets in hand, we overlay our simulation results on Beisel's experimental data so as to get an idea of what abaqus tells us about expecting wrinkles in given webline conditions and specified roller crown.

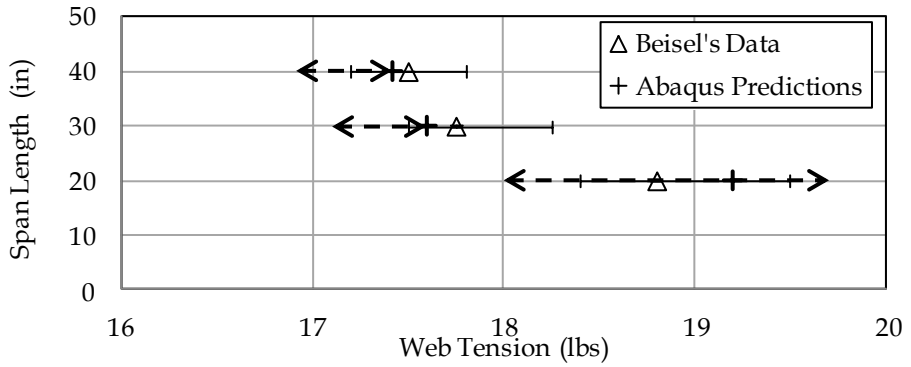

Figure 6.20 Prediction of Wrinkle for Webline Conditions and Roller Crown

6.5 Static Analysis of Web Instabilities due to Roller Crown

The static analysis of a coupon explained for concave roller is extended for crowned roller here. The procedure and analysis steps are very similar to that explained in the concave roller analysis. First a coupon is created resembling the web properties explained in Table 6.1 and the webline conditions such as web span (L) and the web width (W). Boundary conditions and parabolic loading is applied to this coupon those arise from the roller geometry and web tension (T). The static analysis is then carried out which yields results which are discussed here.

6.5.1 Parabolic Loading for a Static Coupon

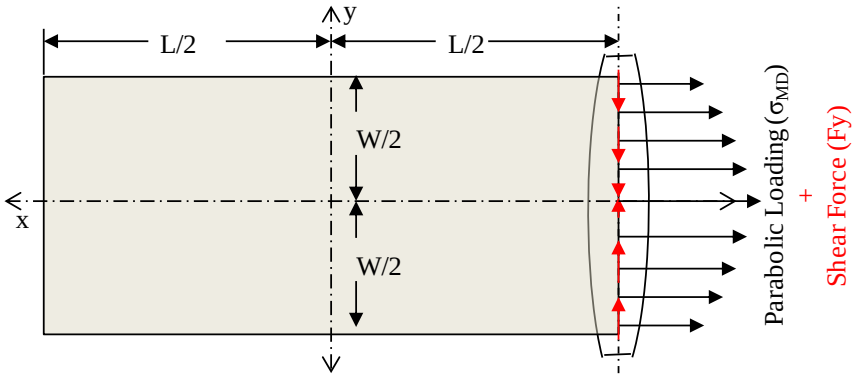

Figure 6.21 Web Approaching a Crowned Roller: Static Analysis

The rectangular coupon is loaded with the Parabolic loading (σ_{MD}) at the end where it is supposed to touch the crowned roller. The last row of elements is also loaded with the Shear force (F_y). The parabolic loading is a result of webline parameters and the roller geometry as explained before and is given by

$$\sigma_{md} = E\frac{a_1W^2 - 12a_1y^2}{12a_0 - a_1W^2} + \frac{T}{h}$$

This closed form expression relates the MD stress at any point where the web enters crowned roller with the CMD distance (y) from the centroidal axis. The shear force is also applied in the form of 5th order polynomial found from the studies of Explicit analysis output as explained earlier. The shear stress is given by

$$\tau_{xy} = C_1\left(y - \frac{8}{W^4}y^5 - \frac{2}{W^2}y^3\right) \qquad (6.20)$$

The constant C_1 depends upon web parameters, roller geometry and webline conditions and is unique for every case. The shear force (F_y) can be then deduced from this shear stress format and then applied at the location where the coupon touches crowned roller. When the lateral shear force given in the equation 6.20 is applied at the end of the coupon, it enforces the normal entry of web to roller and further matches with the CMD stress distribution shown by Abaqus/Explicit study. To make this match possible, we have to reiterate the constant C1 until we achieve the best normal entry possible for maximum width of web entering a crowned roller. Fig 6.22 shows the comparison of study for the case of webspan L = 10in and web tension T = 20lb case. The crowned roller profile as generated by 800psi pressure for Beisel's variable crown roller is used for these calculations. Fig 6.22(a) represents the CMD stress output from explicit study compared with Static coupon code output using different values of arbitrary constant C_1. Fig 6.22(b) compares the slopes of web a the location where it touches the crowned roller so as to show the enforcement of normal entry of web to crowned roller.

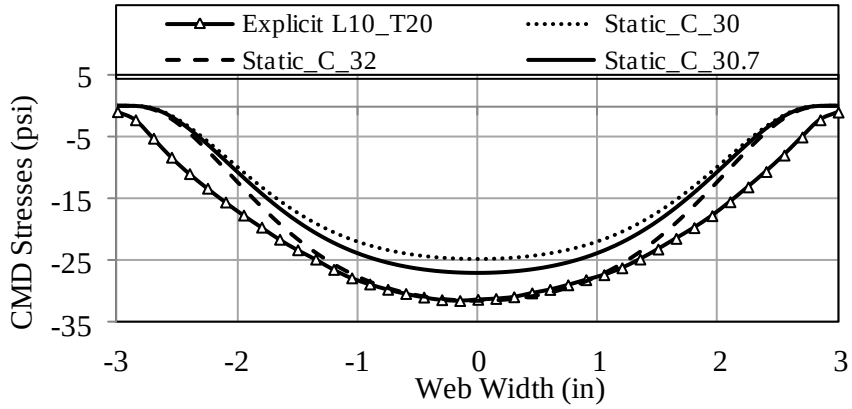

a) CMD Stresses in Web for on 800psi Roller Crown; L 20″ T 20 lb case.

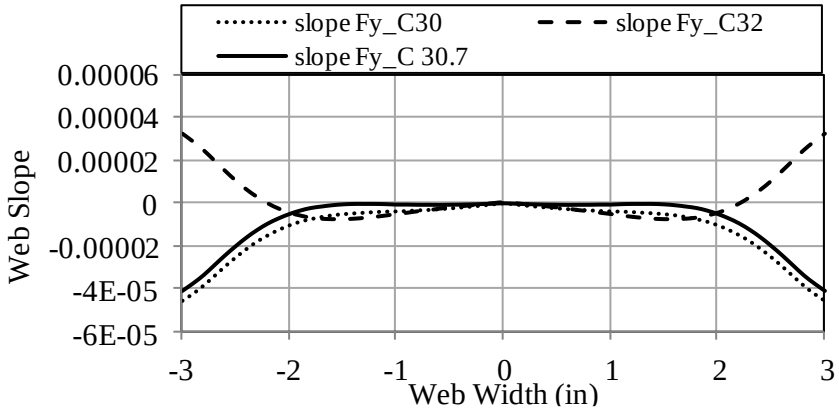

b) Slop of Web for on 800psi Roller Crown; L 20″ T 20 lb case.

Figure 6.22 Static Analysis results of web on Crowned Roller; L 20" T 20 lb case

From both chart shown above, it appears that the static analysis of web has predicted the CMD stresses quite satisfactorily when we force the normal entry of web to roller. The Static analysis CMD stress values are very close those of explicit analysis. The web slopes at the location of roller entry are also shown. It seems the effect of change in C_1 on the values of slope of web across the width is not as prominent as it was seen for the case of Concave roller. All the values of slopes are very close to normal entry for the range of C_1 considered.

6.5.2 Prediction of Troughs using Static Crowned Roller Model

The buckling criterion of a trough formed in a webspan is already explained before. Whenever the CMD compressive stresses go more negative than the value σ_{ycr} given by equation *6.17* (Approximately -9 psi for given conditions), a web span is buckled in the form of trough. The end loading values to the coupon is varied according to webline parameters and the roller geometry. This loading induces negative compressive stress in the panel.

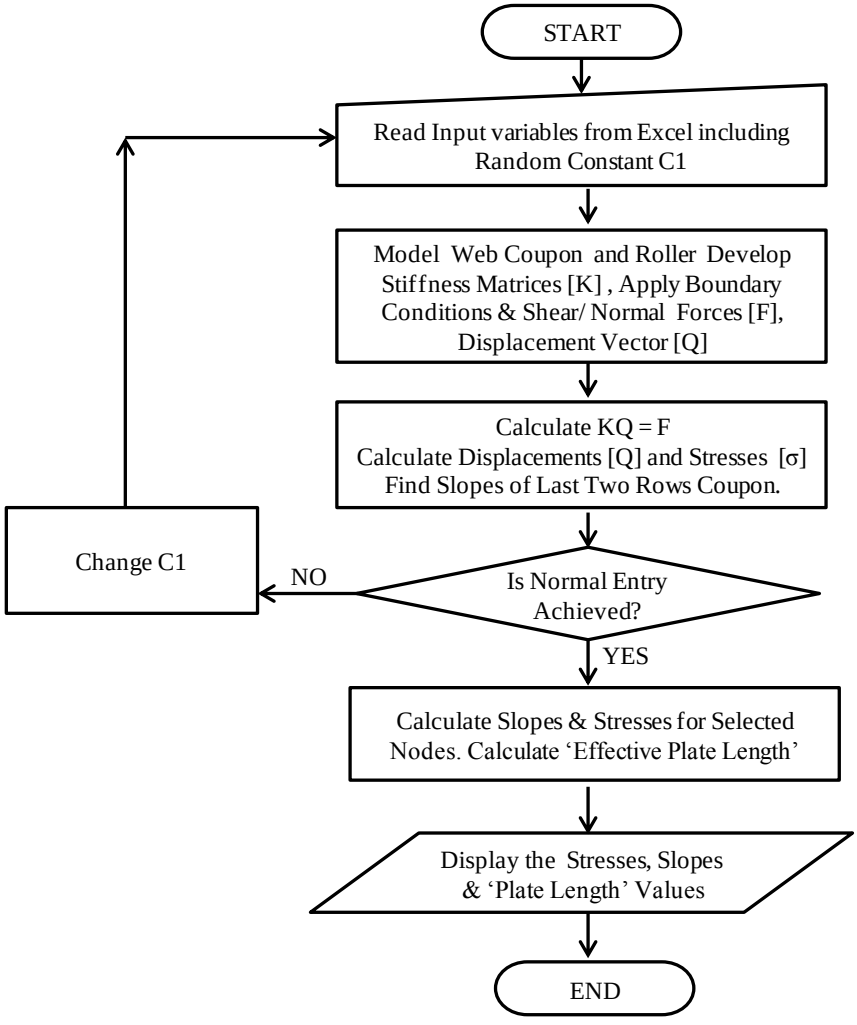

Figure 6.23 Flowchart of Static Analysis of web on Crowned Roller

In all the static coupon cases studied, very much like it was seen in explicit analysis we see a 'stress pocket' developed at the end of entering span where web meets the crowned roller. This kind of behavior is congruous with all the simulations for cases considered at various levels for roller crown. The negative stress developed at this pocket is much more negative than expected or than the buckling criteria (equation *6.17*) discussed before. Beisel also found this kind of occurrence of concentration of compressive stress near the entry of crowned roller. As discussed before, we assume this area where the stress pocket is developed as the 'effective plate length'. The region of the web experiencing substantial compressive stress may be used to determine an effective plate length, which when used with the buckling criteria for trough formation, would give close stress levels as seen during static FE analysis and explicit analysis observations. If we input the value of entering span equal to what it seem from the stress contour (Assumed as L_{eff}), we get quite close CMD stress values by equation *(6.17)* to that of static analysis output.

The availability of correct boundary conditions and the knowledge of the shear forces to be applied to the web coupon from our research has made it possible to formulate an easy, fast and economical excel® code that will give the correct effective plate length value based on the webline parameters and roller geometry. This excel code is formulated such that it will try to get correct value of C_1 bringing the web to the normal entry and further it will calculate correct plate length value that when input to the buckling criteria would yield the correct CMD stresses developed for the given webline conditions. It was observed through the comparative study of Static FEA code results with test data and abaqus simulations that the Static code is predicting trough formation very close to that documented by Beisel and our explicit simulations discussed earlier.

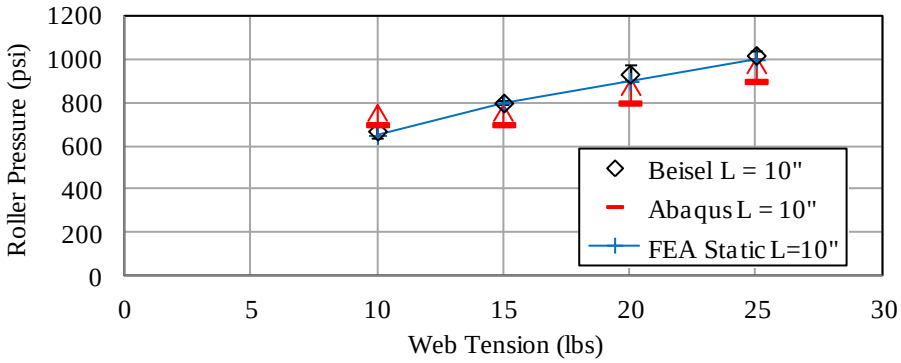

Figure 6.24 Troughs generated on Crowned Roller

6.5.3 Prediction of Wrinkles using a Static Crowned Roller Model

The Static Code developed for studying Troughs due to roller crown cannot be used for studying wrinkling since the elements used is this code are quadrilateral thin shell elements. These elements are not suitable for studying wrinkling. The commercial code COSMOS® is used here since the Wrinkling Membrane elements (Shell4) can successfully model a wrinkle developed in webspan. This code was used by Beisel [1] successfully to study wrinkling as result of misaligned, tapered and crowned roller before. He demonstrated the capability of the wrinkling membrane elements of COSMOS® in his PhD Dissertation.

The Static model constructed for studying wrinkling due to roller crown is shown in Fig 6.25. It contains five panels of elements depicting the roller and webspan arrangement alternatively. All rollers and the exiting webspan are modeled using the ordinary shell elements and for the entering span Wrinkling Membrane elements are used. The model is constrained in y direction at both ends and center line. The webline tension (T) is applied as pressure at the end of the model.

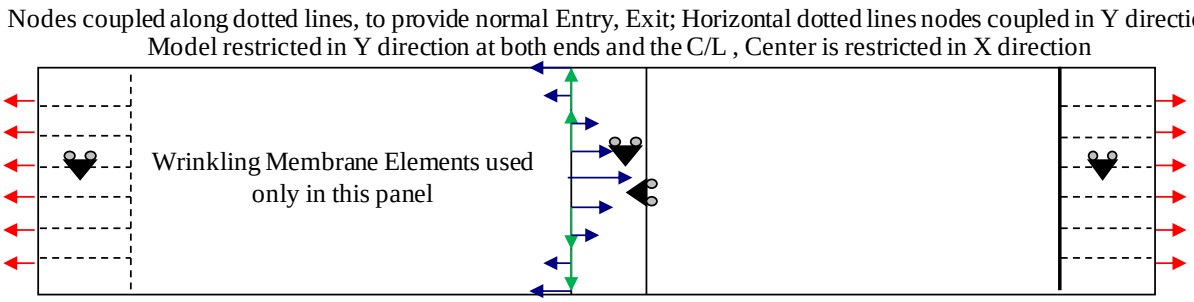

Figure 6.25Boundary Conditions and Loading for Wrinkling due to Roller Crown

The values are selected from the range of webline tensions documented by Beisel that was required to develop wrinkles in given span and webline parameters. The parabolic loading (in x direction) resulting from the roller geometry and web properties calculated using the equation 6.10 is applied to the middle panel. These MD forces should not be applied to first row of nodes of middle panel (crowned roller). The MD forces applied to the web should create same MD stress profile given by equation 6.10. It requires changing the magnitude of applied forces near the edge of the web until the desired MD stress profile is achieved. As the parabolic profile dictates, some forces are in positive x direction while others (mainly at the edges) are in negative x direction. The model is then executed and checked for normal entry boundary condition with respect to last two rows of entering span. Now the Shear forces calculated by the 5^{th} order polynomial is introduced and the value of C1 is changed until we see the normal entry occurring for the last two rows as explained before. Once the normal entry is satisfied, we check for CMD stresses in the entering span and see how they compare with the Timoshenko buckling criteria for the given webline condition. We try to choose C1 such that the CMD stresses are close to σ_{ycr} value for Wrinkles (-265psi approximately).

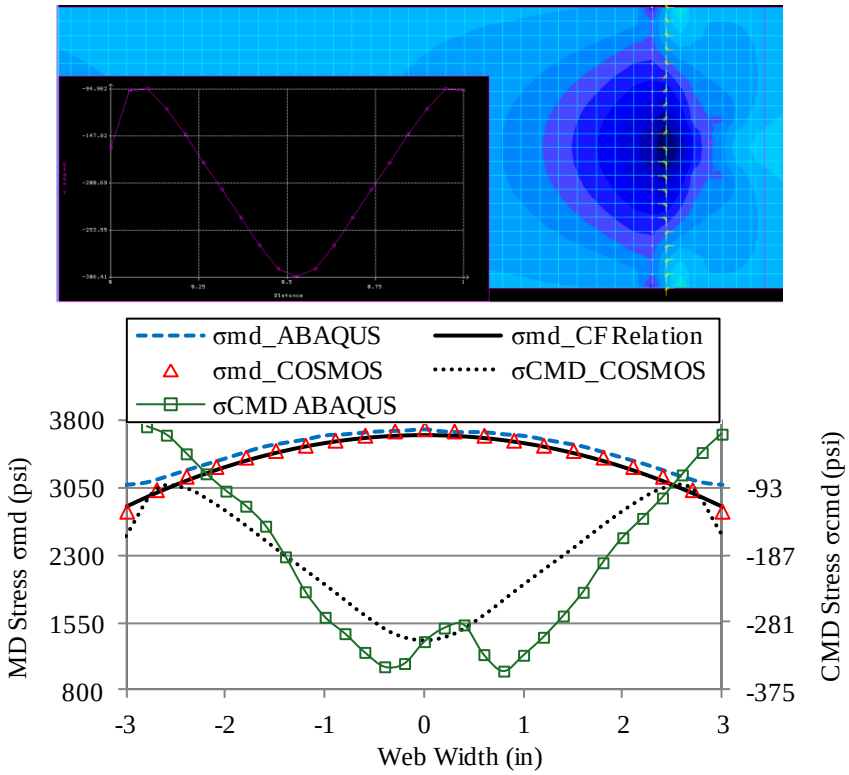

Figure 6.26 Critical CMD Stresses in Wrinkling Model of Roller Crown

With this Static analysis technique, we have a tool that yields results for Wrinkles due to Crowned Roller in very economical and faster way compared to Abaqus/Explicit analysis. We now overlay the results obtained from this model over Beisel's test results and our Abaqus/Explicit results discussed before.

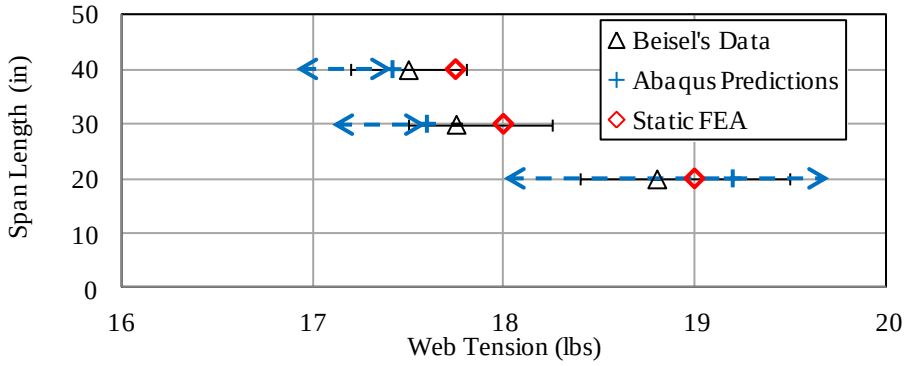

Figure 6.27 Wrinkles generated by Roller Crown

CHAPTER VII

ANALYSIS OF WEBS ON TAPERED ROLLERS

The occurrence of a linearly varying radius across the width of a roller is called a Tapered roller. These rollers are a common encounter in web handling industry. Mostly a tapered roller is outcome of inaccurate machining. The linearly varying radius results in varying tangential velocity across the width of roller. Assuming the *no slip* condition, the difference in velocity across the tapered roller creates the same effect in the web running on it. This velocity variation causes one edge of web travel faster than the other, giving rise to MD stain in the web. A strain results in stress which in turn generates moment in the web. This moment is the effect of taper in the roller. Whenever there is enough moment generated in any webspan, it will induce shear force on the web causing lateral deflection creating instabilities.

If we could relate the amount of taper, web properties and instabilities such as troughs and wrinkles generated due to taper, manufacturing guidelines and tolerances might be developed for rollers as well as webline parameters.

7.1 Theory and Experimentation of Webs on Tapered Rollers

Extensive theoretical and experimental work is already been done by Good *et al* [15] where they developed closed form expressions and verified in the lab that predict when instabilities such as troughs will results from roller taper. It is also shown that high compressive stresses needed to buckle web into wrinkles could be sourced due to roller taper. Beisel [1], treats the web on a tapered roller as a beam. As web contacts roller, it is assumed that it sticks to the surface of roller and travel with the same speed as the roller while in contact with the roller. The radius r*(y)* of the roller at any point across the width is given by

$$r(y) = my + Ro \qquad (7.1)$$

Where, *m* is the slope of the roller surface in terms of reduction in radial inch/in width of roller.

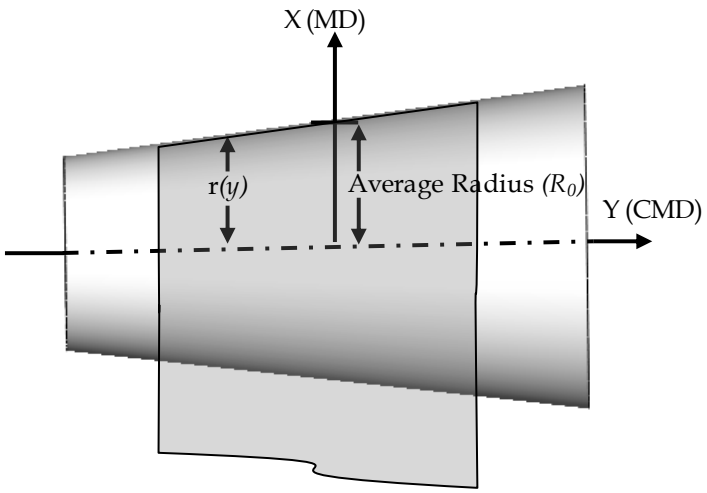

Figure 7.1 Tapered Roller Profile and Coordinates

The boundary conditions were developed assuming web as beam on support at upstream and downstream (tapered) roller. It was assumed that the web guide keeps web entry constant prior to upstream roller giving $v_i=0$. Further, Beisel attempts to account for shear deformation in addition to bending deformations in web. So the total deformation becomes $v = v_b + v_s$ and the

slope has two components as $\frac{dv}{dx} = \frac{dv_b}{dx} + \frac{dv_s}{dx}$. This gives the next boundary conditions as

$\theta_i = \left.\frac{dv}{dx}\right|_{x=i} = \left.\frac{dv_b}{dx}\right|_{x=i} + \left.\frac{dv_s}{dx}\right|_{x=i}$. It was assumed that the friction between the web and roller is

sufficient to prevent any bending deformation of the web and thus, $\left.\frac{dv_b}{dx}\right|_{x=i} = 0$. However the

slope $\left.\frac{dv_s}{dx}\right|_{x=i}$ which is the shear strain becomes non-zero immediately as the web enters the span.

This is due to the shear induced by the tapered roller, which is equal to f_{yj}, the member end force.

Thus we can write:

$$\theta_i = \underbrace{\left.\frac{dv_b}{dx}\right|_{x=i}}_{0} + \left.\frac{dv_s}{dx}\right|_{x=i} = \frac{f_{yj}}{GAs} = \gamma$$

Where *G* is Shear Modulus and A_s is the area reacting shear, i.e. $A_s = (5A/6) = (5\ tW/6)$. At the downstream roller *j,*

$$\theta_j = \left.\frac{dv}{dx}\right|_{x=j} = \left.\frac{dv_b}{dx}\right|_{x=j} + \left.\frac{dv_s}{dx}\right|_{x=j} = 0$$

This is due to Swift's law of normal entry [41]. The deformations and slopes defined as degrees of freedom have both bending and shear contribution. The fourth boundary condition is derived assuming that the web achieves a matching velocity to that of the tapered roller at the tangent entry point. Since the tapered roller has a linear variation in tangential velocity over its width we assume the web now has that same velocity variation. This results in a linear variation in strain and MD stress across the web width and results in a moment boundary condition for the web as

$$M_j = \frac{-mE_{MD}tW^3}{12R_o} \qquad (7.2)$$

Where, *m* is the slope that defines the taper of the roller and R_o is the nominal roller radius at the CMD center of the roller. After determining such boundary conditions, the elementary beam theory can be applied to web span. Uniaxial Hook's law was used to relate stress across web on roller with the strain at that point due to velocity variation as

$$\sigma(y) = E.\varepsilon(y) = \frac{E_{MD} m y}{R_o} \tag{7.3}$$

This stress was then multiplied by the incremental area of web and its *y* position across width and integrated as

$$M = \int_{-W/2}^{W/2} \sigma(y).t.y.dy = \frac{m E_{MD} t W^3}{12 R_0} \tag{7.4}$$

Equation *7.4* relates the total moment developed in the web at the tapered roller with the roller taper *(m)*, average roller radius *(R_0)*, web modulus *(E)*, web thickness *(t)* and web width *(W)*. Beisel used matrix structural analysis from Przemieniecki [28] to give his closed form models for web on tapered roller as expression for the lateral steering of a web due to a downstream tapered roller given as follows:

$$v_j = \frac{m E_{MD} t W^3}{6 R_o} \cdot \frac{-60EI + L^2(5GA_s - T)\cdot(1+\phi)}{\left[60EI + TL^2\cdot(1+\phi)\right]\cdot(T + GA_s)} \tag{7.5}$$

The shear force that is exerted on web due to downstream tapered roller is

$$f_{yj} = \frac{m E_{MD} t W^3}{L R_o} \cdot \frac{GA_s[10EI + TL^2\cdot(1+\phi)]}{\left[60EI + TL^2\cdot(1+\phi)\right](T + GA_s)} \tag{7.6}$$

These equations are valid for a web span up to the point of development of a slack edge. A slack edge is a condition where one edge of the web reaches zero tension and thus becomes

slack. When the MD stress due to moment becomes greater and opposite to the MD stress due to web line tension, zero web line tension will develop at that location in the web line. The onset of a slack edge for the tapered roller can be found from:

$$T_{slack} = \frac{E_{MD} mtW}{288 R_o} \qquad (7.7)$$

The experimental work done by Beisel about tapered roller could be divided into three parts. In his initial attempts he measured the deflection of web due to tapered roller. For this purpose he used four different rollers (0.00028”/in, 0.00056”/in, 0.00066”/in and 0.00075”/in) involving increasing slope levels, designated as ‘Low Taper Rollers’. These slope levels are the slope of roller surface per inch roller width as explained in Figure 7.1. He used three different web span lengths and five different web line tension levels for this study. Web tension was monitored by use of load cells located just prior to entry to the test span and controlled by use of a magnetic break. Each data point in his study was obtained by first running the web over a cylindrical roller to determine the normal position of the web in the machine. Then a tapered roller was used as replacement of cylindrical roller at same position. Steady state position of web was then recorded.

The trough measurement was done in the same experimental setup, tension being the variable conditions for the tests. Tests started at a relatively high web line tension and then slowly reduced until instability occurred in web. The onset of a trough was determined visually. The visibility of this occurrence was supported by the use of a line of laser light across the web. Whenever there is a trough formed in the webspan, the laser light incident with the web shows a wavy sinusoidal line instead of a straight line. He plotted his results of experiments against the analytical expression he developed as a guide for how much radial taper a roller can have before it causes buckling problems in a webline. The procedure of deriving this model is discussed in Beisel’s PhD thesis. The error bars in his plots of trough due to taper represent a maximum and minimum value measured where the onset of trough was noticed.

In the third part, Beisel recorded wrinkling in web lines due to roller taper. For this purpose he created additional rollers with aggressive taper value (0.001”/in, 0.00113”/in, 0.00136”/in and 0.00146”/in). He tested these rollers inducing wrinkle on three different span lengths and several tension values.

7.2 Modeling of Tapered Rollers

The tapered roller is modeled in the third position (R3) of the typical four roller setup shown in Figure 6.6. Rollers R1, R2, and R4 are cylindrical rollers with a nominal radius of 1.45 in. The radius of crowned roller is described per the method explained in earlier section of this chapter where the roller radius is prescribed by ($r(y) = my + R_o$) where, R_o is average radius of tapered roller, *m* is the slope of roller surface and *y* is CMD coordinate measured from the center location of the roller. Important webline conditions and modeling parameters are given in table 7.1

Property	Value
Web Width *(W)*	6 inch
Web Thickness *(h)*	0.00092 inch
Young's Modulus *(E)*	712000 psi
Poisson's Ratio *(υ)*	0.3
Entering Span to concave roller *(L)*	10, 20 inch
Pre-entering span *(L_a)*	6 inch
Roller Radius *(r)*	1.48 inch
Wrap Angle *(β)*	90 degrees
Web Velocity *(v)*	1 inch/sec
Coefficient of Friction *(μ)*	1

Table 7.1: Parameter Values of Tapered Roller Model

All the four rollers are free to rotate around their longitudinal axis. The simulations are completed typically in twenty five time steps. The first step consists of applying a known value of uniform tension load at the upstream end of the web while the downstream end is restrained at zero velocity. In the second time step a prescribed value of MD velocity is set at the downstream end of the web for the remaining time steps. When the web begins moving in the second time step friction forces between the web and rollers begin to turn the rollers, much as any idler roller would be driven by a web. No kinematic boundary conditions between the web and rollers are enforced with the exception that the web is prevented from penetrating the rigid analytical roller

surface by the contact algorithm. Only friction forces between the rollers and web dictate the lateral behavior of the web. For smoother simulation and accurate execution, the velocity and tensions are gradually increased to its final value by using Amplitudes as explained in previous chapters.

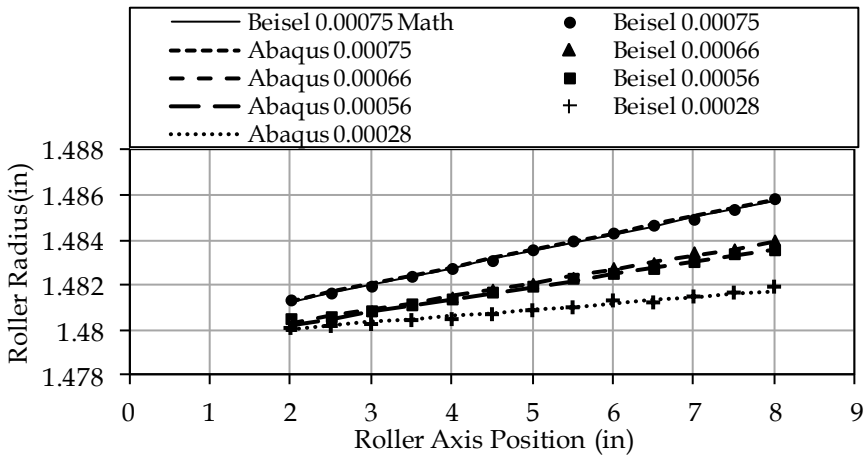

Figure 7.2 Low Taper Roller Profiles from Beisel Plots and Abaqus

Figure 7.2 displays the actual roller profile and its simulation version for four *low taper* rollers that were used in this study. The mathematical expression ($y = 0.0015x - 0.0005$) was documented by Beisel for 0.00075”/in roller and is plotted along with abaqus and actual roller profile for that particular series. The original plot from Beisel’s work involved relative diameters which are converted into radii and plotted so as to realize exact points of roller geometries.

7.3 Lateral Behavior of Web on Tapered Rollers

We will compare our results from Abaqus simulations with that of Beisel & Good's closed form solutions and experimental work. Figure 7.3 plots the deflection of web due to downstream tapered roller at R3 position. It compares the deflection calculated by Good & Beisel's closed form solution (equation *7.5*), Beisel's experiments and Abaqus simulations (R3 Entry). As far Beisel's data is considered, the filled triangles represent a planar web, while the open triangles indicate the presence of troughs in the test span.

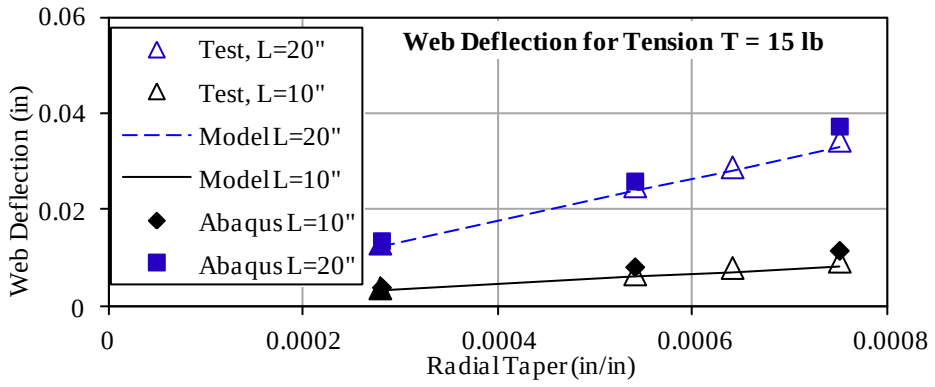

a) Deflection due to Taper, Web Tension T = 15 lb

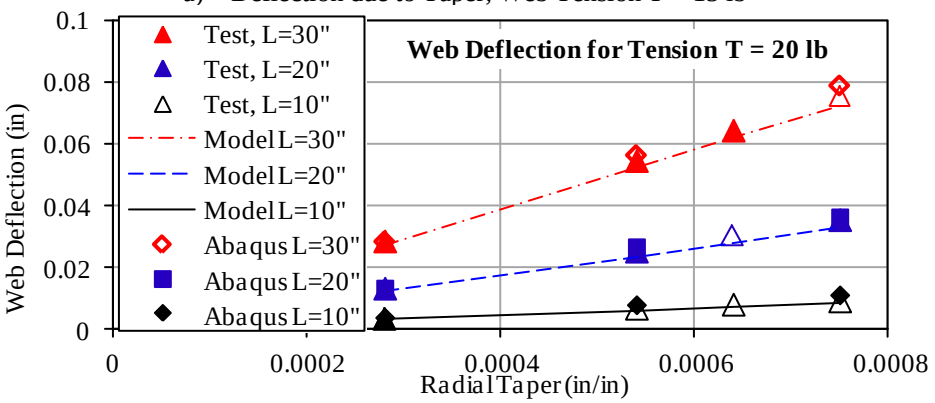

b) Deflection due to Taper, Web Tension T = 20 lb

Figure 7.3 Web Deflection due to Taper for various Web Spans and Tension at R3 Entry

The plot shown above depicts satisfactory agreement between the web deflection values on Tapered roller over various webline conditions. We see very small effect of change in webline Tension values over the web deflection on tapered roller. It appears that the disagreement

between the close form model values and Abaqus increases as the roller taper and the entering webspan increases. It also appears that the planar web deflection has better agreement than the troughed web deflection points. From Beisel's documentation [1], it was found that he recorded the deflection Test values at the downstream end of exiting span (Lb). This is nothing but the downstream roller R4 Entry. The results of Abaqus shown in Fig 7.4 are queried at the same location. While calculating the deflection for the given degree of tapered roller using the model proposed by Beisel and Good, the webspan (L) is used. This model does not calculate the deflection at the end of exiting span (Lb). For this purpose, we plot the deflection data from Abaqus and Beisel's Test data without the Model data as shown in Fig 7.4.

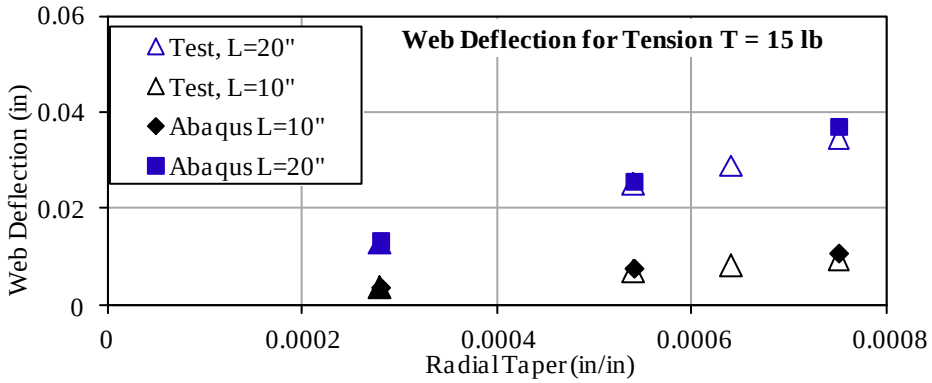

a) Deflection due to Taper, Web Tension T = 15 lb

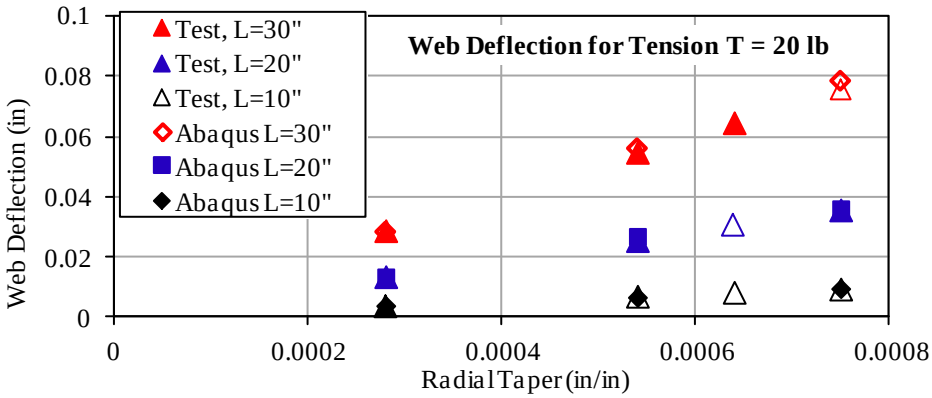

b) Deflection due to Taper, Web Tension T = 20 lb

Figure 7.4 Web Deflection due to Taper for Various Web spans and Tension at R4 Entry

Fig 7.4 represents comparison of Beisel's Test data and Abaqus deflection values obtained at the same MD location. This location is at the end of exiting span (La). The lateral behavior of web on the Tapered roller is investigated further and is discussed in Fig 7.5. It represents the centerline deformation of web. It also plots the slope of this line. Positions of all three rollers (R1, R2, & R4) along with the Tapered Roller (R3) are also marked on the plot.

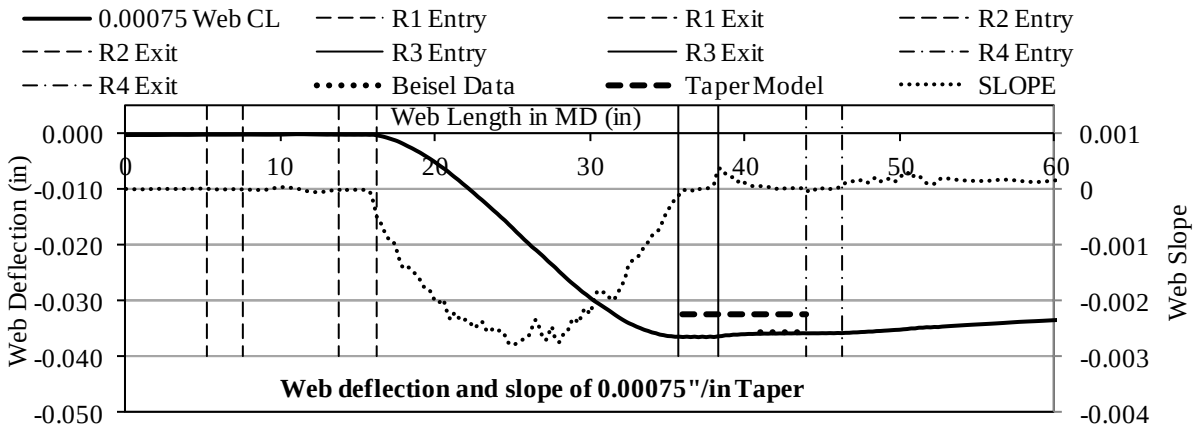

Figure 7.5 Lateral behavior of Web on 0.00075"/in Tapered Roller; L20in_T 20 lb

We compare the value of web deflection exhibited by Abaqus with test data and the close form model documented by Beisel. The test data by Beisel was recorded at the entry of R4. We compare the lateral deflection at that particular location. The close form model calculates lateral steering of the web at the end of entering span (L). It appears that there is some deflection reduction in the exit span (L_b). It might be the combined effect due to roller taper, web twist and the slippage of web at the exit of Tapered roller. The deflection model proposed by Beisel assumes that there is no slippage on the wrap of web on Tapered Roller and upstream roller R2. Both these conditions are not assumed for Abaqus simulations. Further, it was assumed in Beisel's model derivation that the friction on Tapered roller is very high. So it was assumed that the moment generated in the entering span (L) is restricted by the rollers at both the ends and does

not get transferred in either the upstream (L_a) or downstream exit (L_b) span. It is observed in the Abaqus output that the MD stress distribution (σ_{md}) is not uniform in the exit span. This moment might be the effect of slippage of web near the exit of Tapered roller. It is also observed that the MD stress distribution reverses its sign near the exit of Tapered roller to induce a moment reversal in the exit span. This moment reversal along with slippage is the prime reason for decrease, though fractional in the overall steering of web.

7.4 Troughs due to Roller Taper

Beisel's conducted experiments to test the Trough model that he proposed. He studied effect of roller taper on trough formation in given webline condition. His experiments consisted of bringing the pre decided web line tension followed by slowly reducing the Web tension until a trough was seen initiated in the webline. The decrease in tension along with the tapered roller imparted reduction in stability of webline. Web line condition and Web tension were recorded as soon as a trough was seen in the web span. The occurrence of trough in the webspan was based on the formation of a wavy pattern in the laser light incident on web. A similar procedure was followed in Abaqus simulation where we reduced the prescribed web tension in running webline. This was achieved with the help of amplitudes in abaqus. The simulation is started at high tension level and the web tension amplitude was slowly reduced across the range that is predetermined by the closed form model. Fig 7.6 shows the reduction of tension level across the total time of simulation. We let pass the web length of three times the webspan before a trough amplitude was acquired.

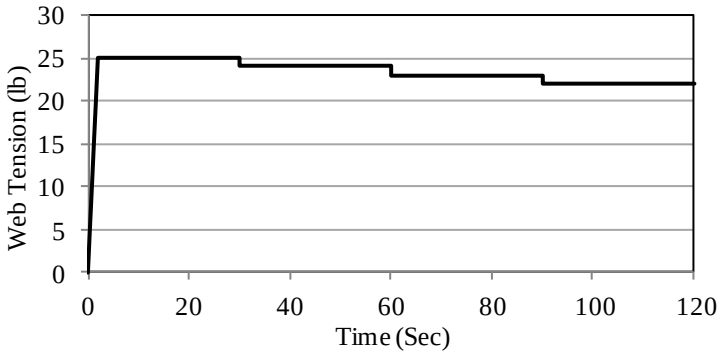

Figure 7.6 Imitation of Beisel's Trough Test for 0.00056"/in Tapered Roller, L = 10"

We see Troughs start building as we reduce Web Tension from 25lb to 21lb (where Beisel noticed troughs in his test). We see our simulations predict Troughs at higher Tension level than seen in Beisel's Test since we say a trough is formed here based on actual out of plane (U2) deformation in webspan.

With these datasets, we overlay our results on Beisel's chart. As expected we inscribe trough at higher tension level than recorded by Beisel. Beisel's data is marked with the limits of Web Tension values at which trough formation was observed. Abaqus simulation results are shown with an arrow directing towards the lower Web Tension values since we expect troughs occurring below the marked Tension for the given value of roller taper and webline conditions.

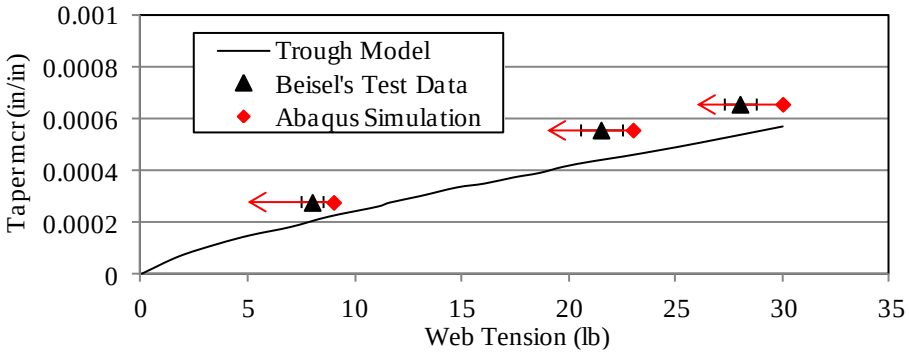

Figure 7.7 Formation of Trough due to Tapered Roller, L = 10"

CHAPTER VIII

CONCLUSION AND FUTURE WORK

Explicit finite element simulations presented in this work have ascertained the value of this type of analyses for addressing mechanics problems in web handling process machinery. The primary benefit of this technique is that only very basic assumptions in terms of boundary conditions are required for its analysis. Moreover, the interactions of web with rollers are governed entirely by forces of contact and friction that develop between the web and roller surfaces. It has also been shown that explicit method can be used effectively to study web deformations and stresses which may result in development of boundary conditions. These boundary conditions then can be employed in establishing computationally less expensive models. Additional conclusions have been drawn for the specific cases as follows:

8.1 Web Behavior on Concave Rollers

Explicit finite element modeling has been proven a useful method for the study of webs transiting concave rollers. A behavior that is evident in all the model results is a reversal in MD stress between the web entry and exit of the concave roller. MD stresses that are high at the web edges and low at the web center per expression *(5.3)* at the entry to the roller have become low at the edges and high at the web center when the web exits the roller. How this transition occurs depends entirely on the slippage which will depend case by case on roller concavity, the web to roller friction coefficient, the web thickness and modulus and web tension. For all the cases of varying roller concavity *(ρ)* studied, it was evident that the maximum spreading stress occurs as the web exits the concave roller at the web center. This behavior is the result of the MD stress near the web center rising toward the uniform stress level in the exiting span. The rise in MD tension is accompanied by a CMD contraction of the web that is resisted by friction and results in an increase in CMD spreading stress. It was shown that a concave roller can be an effective spreader locally in the entry span as the web approaches roller but can cause web instability in the form of troughs in an exit span. These behaviors described are known only as a result of this work.

For all cases studied it was found that the normal entry boundary condition is appropriate at the entry to the concave roller. The slopes at the exit of the concave roller were non-zero as a result of the slippage in the MD and CMD directions. For the wide web case the slopes at the exit of the upstream roller R2 were found to be non-zero as a result of a short entry span length. It was also found that a device which is used for spreading webs is capable of buckling the web in the exit span. As a result of this work, it is also shown that for the cases studied, that the web was observed slipping very near to the exit of concave roller, which was evident from shear force behavior compared with frictional forces in web wrap around roller.

The normal entry and no-slip boundary conditions were used to develop a static code that could be used for accurately modeling a web transiting a Concave Roller. From the Abaqus simulations, it was found that in addition to the MD stresses resulting from the parabolic profile of roller, shear stresses are also needed to be applied to bring the web to normal entry to concave roller. The Abaqus results were used to determine the form of these shear stresses. It was shown that a 5^{th} order polynomial precisely captures the form of these shear stresses. The polynomial was multiplied by a constant which is varied until the combination of MD stress and the shear stress produce normal entry over as much of the web width as possible. This method has yielded results with very less time and computational resources than compared to explicit analysis.

8.2 Web Behavior due to Roller Crown

Not unlike the concave roller, explicit finite element modeling has been proven a useful tool for the study of webs transiting crowned rollers. A behavior that was expected in all the model results is a reversal in MD stress between the web entry and exit of the crowned roller. Higher MD stresses are observed at the web center and low at the web edges. This behavior of MD stresses at the roller entry follows exactly the relation established based on strains developed due to velocity variation given in expression *(6.10).* This model accurately predicts the MD stresses at the entry of a crowned roller for different roller and webline parameters. It was shown that a crowned roller can be an effective web gatherer locally in the entry span as the web approaches roller but can cause web stretching in the form of positive CMD stresses in an exit span.

We modeled Beisel's adjustable crown roller data where in both troughs and wrinkle formation due to downstream crowned roller is studied experimentally for different convexities resulting due to levels of internal pressure for variable crown roller and various webline conditions. Modeling of trough formation due to roller crown reveals that the compressive stresses causing troughs did not extend through entire web length in entering span but forms a 'stress pocket' near crowned roller. The negative stress developed in this pocket is much more negative than expected or than the buckling criteria *(6.17).* Development of pocket of compressive stresses in web at the entry of crown roller might be one of the reason the buckling criteria for trough formation is not applicable to predict compressive stresses forming troughs in webspans. Further during all the simulations carried out, the formation of troughs was based on out of plane deformation of web in entering span. While the wavelength *(λ)* calculated by expression *(6.18)* does not exactly match with the wavelength exhibited by the simulation results, it does fall within the realm of modeling error since the element size is 0.15 in.

The formation of troughs in webspan due to crown roller has shown greater dependence on web tension *(T)* than span length *(L)*, given all other web properties are constant. A satisfactory agreement was observed with experimental study of formation of troughs on crowned roller. For Beisel's study, the realization of the trough is *initiated* at given particular tension level was based on visual appearance. Unlike the experiments, exact out of plane deformation could be plotted from Abaqus simulations. Hence the initiation point is seen at lower roller crown than compared to Beisel's value. Simulations were conducted to study formation of wrinkles due to downstream roller crown. The compressive stresses generated in the model are compared with Timoshenko's wrinkling criteria *(6.17)* which give the critical stresses required to buckle a shell in wrinkle. Based on the compressive stresses developed at the entry of crowned roller for particular web tension value and span length, we could predict the web tension at which the web should start buckling. Unlike troughs, the wrinkles forming on crown roller show greater dependence on span length *(L)* as well as tension *(T)*. Abaqus simulations enable us to gather much more information about stresses and strains responsible for wrinkles.

The procedure explained in development of static code for concave roller was followed for the modeling of web over a crowned roller. The combination of MD stress profile and the shear stresses is produced to enforce normal entry of web to crowned roller. Again, the shear stresses are multiplied by a constant that needs to be varied until normal entry is achieved for the maximum possible width of the web at the roller entry. This method is used to develop a code that can be used to predict the degree of crown required to produce trough instabilities in the entry span to a crowned roller.

8.3 Web Approaching a Tapered Roller

The study of lateral behavior of web from Abaqus simulations confirms that Swift's normal entry is a valid for web entering a tapered roller. The boundary condition derived by previous researchers for the slope of web exiting upstream roller is also found correct. It was seen that the MD stress variation induced in the web by the roller taper remains constant as the web proceeds between entry to tapered roller and its exit. Further is it also observed that a reverse moment is generated in the exit span (L_b). This moment might be the effect of slippage of web near the exit of Tapered roller. This moment reversal along with slippage is the prime reason for decrease, though fractional in the overall steering of web in exit span.

The formation of trough in webspan due to tapered roller has shown dependence on both, the web tension *(T)* and span length *(L)*. It is observed that the increased web length makes the web prone to trough for the same degree of roller taper (m) and web tension (T). A satisfactory agreement was observed with experimental study of formation of trough due to tapered roller. The exact out of plane deformation could be plotted from Abaqus simulations. Hence the trough initiation point is seen at higher web tension than compared to Beisel's test value.

8.4 Recommendation for Future Study

The work presented here is mainly concerned about the exploration of boundary conditions, web behavior and stress analysis of webs encountering the contoured rollers considered. This work has proven the usefulness of ABAQUS/Explicit® for studying details of web-Roller interaction. It could be extended further for other unexplored problems and various areas of Web Handling such as:

- The exact boundary conditions of other contoured rollers such as curved axis rollers, expanding surface rollers, flexible and rigid spiral rollers. It is already shown that computationally economical Static Finite Element codes could be employed for analysis webs on contoured rollers. It could be extended further as per the usefulness by industry and academia.

- The exact nature of slippage of web on the roller surface; may it be on the upstream roller or the contoured roller itself. The slippage might create unknown effects in the exit spans as seen in Tapered Rollers.

- The effect of slippage and additional findings thereby may be incorporated in the lateral/longitudinal behavior models and closed form solutions proposed by previous researchers.

- The effect of various webline parameters such as short/long span lengths, various concavities/crown, web tension, moment interaction and various problems of nip/wound roll mechanics for useful cases in Web Handling industries could be explored.

BIBLIOGRAPHY

1. Beisel, J.A., "Single Span Web Buckling Due to Roller Imperfections in Web Process Machinery", Ph.D. Dissertation, Oklahoma State University, Stillwater OK, October 2006.
2. Beisel, J. A. and Good, J. K., "The Instability of Web in Transport", Journal of Applied Mechanics, ASME, Vol. 78, No. 1, January 2011.
3. Brown, J.L., "Effects of Concave Rollers, Curved Axis Rollers and Web Camber on the Deformation and Translation of a Moving Web", Proceedings of the Eighth International Conference on Web Handling, Oklahoma State University, Stillwater OK, June 2005.
4. Brown, J.L., "A New Method for analyzing the Deformation and Lateral Translation of a Moving Web", Proceedings of the Eighth International Conference on Web Handling, Oklahoma State University, Stillwater OK, June 2005.
5. Brown, J.L., "What FEA Analysis Can Tell Us About Spreaders," Applied Web Handling Conference, Minneapolis, MN, May 2008.
6. Butler, T., "How Concave Rolls Can Correct Dryer Fabric Bowing", Paper Trade Journal, vol. 169, No. 3, pp. 70-72, March 1985.
7. Delahoussaye R.D. and Good J.K., "Analysis of Web Spreading Induced by the Concave Roller", Proceedings of the Second International Conference on Web Handling, Oklahoma State University, Stillwater OK, June 1993.
8. Delahoussaye R.D. and Good J.K., "Analysis of Web Spreading Induced by the Curved Axis Roller", Proceedings of the Second International Conference on Web Handling, Oklahoma State University, Stillwater OK, June 1993.
9. Feiertag, B.A., "Selection of Bow for Curved Axis Rollers", TAPPI Finishing and Converting Conference Proceedings, October 1981.
10. Fu B., Markum R., Reddy A., Vaijapurkar S. and Good J. K., "Explicit Analysis of the Lateral Mechanics of Web Spans", Proceedings of the Eleventh International Conference on Web Handling, Oklahoma State University, Stillwater OK, June 2011.
11. Gehlbach, L.S., Good J.K. and Kedl, D.M., "Prediction of Shear Wrinkles in Web Spans", TAPPI Journal, Vol. 72, No. 8, pp 129-134, August 1989.
12. Good, J.K., "Shear in Multispan Web Systems", Proceedings of the Fourth International Conference on Web Handling, Oklahoma State University, Stillwater OK, June 1997.

13. Good, J.K. and Beisel J.A., "Buckling of Orthotropic Webs in Process Machinery", Proceedings of the Seventh International Conference on Web Handling, Oklahoma State University, Stillwater OK, June 2003.
14. Good, J.K. and Beisel J.A., "Calculations Relating to Web Buckling Resulting from Roller Misalignment", TAPPI Journal, Vol. 5, No. 12, pp 9-16, December 2006.
15. Good, J. K., Beisel J. A. and Yurtcu H., "Predicting Web Wrinkles on Rollers", Proceedings of the Tenth International Conference on Web Handling, Oklahoma State University, Stillwater OK, June 2009.
16. Good, J.K., Kedl, D.M. and Shelton J.J., "Shear Wrinkling in Isolated Spans", Proceedings of the Fourth International Conference on Web Handling, Oklahoma State University, Stillwater OK, June 1997.
17. Gopal, H. and Kedl, D.M., "Using Finite Element Method to Define How Wrinkles Form in a Single Web Span Without Moment Transfer", Proceedings of the First International Conference on Web Handling, Oklahoma State University, Stillwater OK, May 1991.
18. Hawkins, W. E., The Plastic Film and Foil Web Handling Guide, CRC Press, 2003.
18a. Jacques N., Elias A., Potier-Ferry M. and Zahrouni H., "Buckling and Wrinkling during Strip Conveying in Processing Lines", Journal of Materials Processing Technology, Vol. 190, No. 1-3, pp 33-40, July 2007.
19. Kandadai, B. K. and Good, J. K., "Modeling Wound Rolls using Explicit FE Methods", Proceedings of the Ninth International Conference on Web Handling, Oklahoma State University, Stillwater OK, June 2007.
20. Kandadai, B. K., "The Development of Wound-on-Tension in Webs Wound into Rolls", PhD Dissertation, Oklahoma State University, Stillwater OK, December 2006.
21. Kliewer, G.A., "Parametric Analysis of Webs Encountering Concave Rollers", M.S. Thesis, Oklahoma State University, Stillwater OK, June 1988.
22. Leport, M. L., "The Mechanics of Webs Encountering Concave Rollers", M.S. Thesis, Oklahoma State University, Stillwater OK, December 1987.
23. Lorig, E.T., "Automatic Self-Centering Rolls and Pulleys", AISE Convention, Cleveland, OH, 1950.
24. Lynch, R., "Web Handling Seminar Notes," Web Handling Research Center, Stillwater OK, March 2011.
25. Markum, R.E. and Good, J.K., "Design of Contoured Rollers for Web Spreading", Proceedings of the Sixth International Conference on Web Handling, Oklahoma State University, Stillwater OK, June 2001.
26. Markum, R.E. and Good, J.K., "The Mechanics of Grooved Flexible Spreader Rolls", Proceedings of the Ninth International Conference on Web Handling, Oklahoma State University, Stillwater OK, June 2007.
27. Pfeiffer, J.D., "Web Guidance Concepts and Applications", TAPI, Vol. 60, No. 12, December 1977.
28. Przemieniecki, J.S., Theory of Matrix Structural Analysis, McGraw-Hill, New York, 1968.

29. Reddy, A., "Analysis of Moment Transfer in Multi-span Web Systems", M. S. Thesis, Oklahoma State University, Stillwater OK, June 2010.
30. Reddy, J.N., An Introduction to the Finite Element method, 3rd Ed, McGraw-Hill, New York, 2006.
31. Roisum, D.R., "The Mechanics of Web Spreading", Proceedings of the Second International Conference on Web Handling, Oklahoma State University, Stillwater OK, June 1993.
32. Robinson, S. W., Principles of Mechanism, 1st Ed, Wiley and Sons, New York, 1896.
33. Schwamb, S. B., Merrill S. B., Elements of Mechanism, 3rd Ed, Wiley and Sons, New York, 1921.
34. Shelton, J.J., "Buckling of Webs from Lateral Compressive Forces", Proceedings of the Second International Conference on Web Handling, Oklahoma State University, Stillwater OK, June 1993.
35. Shelton, J.J., "Lateral Dynamics of a Moving Web", PhD Dissertation, Oklahoma State University, Stillwater OK, July 1968.
36. Shelton, J.J. and Reid, K.N., "Lateral Dynamics of a Real Moving Web", ASME Journal of Dynamic Systems, measurement, and Control, Vol. 93, No. 3, pp. 180-186, 1971.
37. Shelton, J.J. and Reid, K.N., "Lateral Dynamics of an Idealized Moving Web", ASME Journal of Dynamic Systems, measurement, and Control, Vol. 93, No. 3, pp. 187-192, 1971.
38. Shelton, J.J., "Interaction Between Two Web spans Because of a Misaligned Downstream Roller", Proceedings of the Eighth International Conference on Web Handling, Oklahoma State University, Stillwater OK, June 2005.
39. Stack, K., Perconti, J., Jeans, A., LaFleche J. and Benson, R., "A Nonlinear Finite Element Model for Web Spreading", Proceedings of the Fourth International Conference on Web Handling, Oklahoma State University, Stillwater OK, June 1997.
40. Swanson, R.P., "Testing and Analysis of Web Spreading and Anti-Wrinkle Devices", Proceedings of the Fourth International Conference on Web Handling, Oklahoma State University, Stillwater OK, June1997.
41. Swift, H.W., "Camber for Belt Pulleys", Proceedings - Institute of Mechanical Engineers, June 1932.
42. Swift, H.W., "Power Transmission by Belts: An Investigation of Fundamentals", Proceedings - Institute of Mechanical Engineers, Vol. II., pp667, Nov 1928.
43. Timoshenko S. P. and Gere J. M., Theory of Elastic Stability, McGraw-Hill, New York, 1963.
44. Timoshenko S.P. and Goodier J.N., Theory of Elasticity, 3nd Ed, McGraw-Hill, New York, 1987.
45. Unwin, W. C., Elements of Machine Design, 4th Ed, Longmans Green and Co., London, 1909.
46. Vaijapurkar, S., "Explicit Finite Element Modeling of Web-Roller Interaction for Contoured Rollers in Web Process Machinery",

Preliminary Exam Report, Oklahoma State University, Stillwater OK, Apr 2010.

47. Vaijapurkar, S. and Good J. K., "Explicit Finite Element Modeling of Web-Roller Interaction for Contoured Rollers in Web Process Machinery", Proceedings of the First International Conference on Current Trends in Technology, Nirma University Institute of Technology, Stillwater OK, Dec 2010.
48. Vaijapurkar, S. and Good J. K.," Explicit Analysis of the Lateral Mechanics of Webs Transiting a Concave Roller", Proceedings of the Eleventh International Conference on Web Handling, Oklahoma State University, Stillwater OK, June 2011.
49. Webb, D.K., "Prediction of Web Wrinkles Due to Misalignment of a Downstream Roll in a Web Span", M.S. Thesis, Oklahoma State University, Stillwater OK, Dec 2004

APPENDIX A

BASICS OF WEB HANDLING

A *web* can be defined as thin material which is manufactured and processed in a continuous, flexible strip form. Web materials cover a broad spectrum from extremely thin plastics to papers, textiles, metals, and composites. *Web Handling* may be defined as the transport of continuous thin materials (*webs*) through process machinery. Almost 5000 years ago web materials such as papyrus were being made, cast and pressed into sheets. Today's webs are produced in continuous processes. Some common examples of web handling processes include; casting, cleaning, coating, cooling, drying, dyeing, embossing, extruding, folding, printing, slitting or laminating.

Being the most convenient form of storage and other related processes, webs are often stored in wound rolls. Webs are unwound from a roll and made to travel over rollers or air bars through a process machine-line, often called web line. After the web is processed it is again wound into a roll for storage or cut into other desired geometries for its final application. During this course of transport through a web line the web may experience forces resulting in inducing stresses. These stresses may cause instability in the web that is traveling. Troughs and Wrinkles are the two levels of instabilities. *Troughs* are defined as an out-of-plane instability of a web *in a free span*. A free span is a tensioned section of web between two rollers. A *wrinkle* is defined as an out-of-plane instability of a web *crossing a roller*. Formation of troughs and wrinkles has been a source of concern for the web handling industry. Troughs in sections of a process machine are usually tolerated depending on whether the process requires web to be flat. Wrinkles are not acceptable under any conditions, as they typically cause permanent damage or breakage to the web. Wrinkling may cause devastating effects to downstream rolls and other intermittent processes as well.

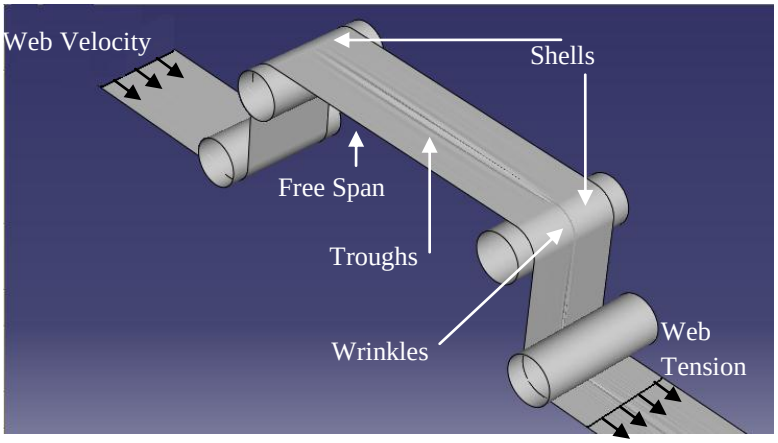

Figure A1: Web in Transport through Process Machine.

Web tension and web velocity are independent machine parameters. Driven rollers cause webs to travel through machines along the direction of its length. This direction is called as Machine Direction, hence forth is termed as MD. Changes in velocity from one driven roller to the next results in web tension change. As a result of Poisson's contraction, MD tension may induce some changes in width. The normal direction to MD is known as Cross Machine Direction and will be referred as CMD in this document. For analysis and design, webs are usually considered as a series of plate and shell structures, as shown in Figure A1. The MD tension is responsible for forcing the web to conform to the rollers in form of shape of a sector of a cylindrical shell. The tension causes web-shells to induce normal contact forces with the surface of roller. It is assumed, if the tension and friction are sufficient that the tangential velocities of the web-shell/plate and the roller surface must be the same.

VITA

Siddharth Shriram Vaijapurkar

Candidate for the Degree of

Doctor of Philosophy

Thesis: EXPLICIT FINITE ELEMENT ANALYSIS OF WEB-ROLLER INTERACTION IN WEB PROCESS MACHINERY

Major Field: Mechanical and Aerospace Engineering

Biographical:

Education:

Received the Bachelor of Engineering in Civil Engineering at University of Pune, Maharashtra, India in 2003; completed the requirements of the Master of Technology in Structural Engineering at National Institute of Technology, Surat, Gujarat, India in 2005. Completed the requirements for the Doctor of Philosophy in Mechanical and Aerospace Engineering at Oklahoma State University, Stillwater, Oklahoma in May 2013.

Experience:

As a Field Design Engineer for Essar Oil Ltd (Essar Group) Mumbai, India in 2005 - 06, designed high capacity storage tanks, industrial roof and facility structures. Taught Design of Structures to graduating class of Civil Engineering and conducted lab sessions of Engineering Mechanics for freshman students of Pune University in 2006 - 07. Analyzed the web-roller interaction using finite element while working as a Research Associate under the supervision of Dr. J. K. Good at the Mechanical and Aerospace Engineering Department of Oklahoma State University from 2007-2012.

Professional Memberships:

Student Member of American Society of Mechanical Engineers (ASME)